Research & Technology Transfer

Alaska Department of Transportation & Public Facilities

Pile Length Determination at Unknown Bridge Foundations

Final Report

Prepared by: **Vivek Samu and Murthy Guddati**
North Carolina State University
Department of Civil, Construction and Environmental Engineering
Raleigh, NC 27695-7908

Date: September 30, 2019

Prepared for:
Alaska Department of Transportation & Public Facilities
Statewide Research Office
3132 Channel Drive
Juneau, AK 99801-7898
Report #: FHWA-AK-RD-000S(875), HFHWY00009

REPORT DOCUMENTATION PAGE	Form approved OMB No.

Public reporting for this collection of information is estimated to average 1 hour per response, including the time for reviewing instructions, searching existing data sources, gathering and maintaining the data needed, and completing and reviewing the collection of information. Send comments regarding this burden estimate or any other aspect of this collection of information, including suggestion for reducing this burden to Washington Headquarters Services, Directorate for Information Operations and Reports, 1215 Jefferson Davis Highway, Suite 1204, Arlington, VA 22202-4302, and to the Office of Management and Budget, Paperwork Reduction Project (0704-1833), Washington, DC 20503

1. AGENCY USE ONLY (LEAVE BLANK) FHWA-AK-RD-000S(875)	2. REPORT DATE September 30, 2019	3. REPORT TYPE AND DATES COVERED Final, September 2015 – September 2019

4. TITLE AND SUBTITLE Pile Length Determination at Unknown Bridge Foundations	5. FUNDING NUMBERS Federal #: 000S(875) IRIS #: HFHWY00009
6. AUTHOR(S) Vivek Samu and Murthy Guddati	
7. PERFORMING ORGANIZATION NAME(S) AND ADDRESS(ES) North Carolina State University Department of Civil, Construction and Environmental Engineering Raleigh, NC 27695	8. PERFORMING ORGANIZATION REPORT NUMBER
9. SPONSORING/MONITORING AGENCY NAME(S) AND ADDRESS(ES) State of Alaska, Alaska Dept. of Transportation and Public Facilities Research and Technology Transfer 3132 Channel Drive Juneau, AK 99801-7898	10. SPONSORING/MONITORING AGENCY REPORT NUMBER HFHWY00009
11. SUPPLEMENTARY NOTES	
12a. DISTRIBUTION / AVAILABILITY STATEMENT Copies available online at http://www.dot.alaska.gov/stwddes/research/search_lib.shtml	12b. DISTRIBUTION CODE

13. ABSTRACT (Maximum 200 words)

A new methodology to estimate unknown pile length called Effective Dispersion of Reflections (EDAR) was developed. A software package was also developed for seamless application of the methodology. EDAR software facilitates data acquisition in the field and the subsequent analysis of the data to estimate pile length. In addition to providing length estimates, EDAR has the ability to estimate some of the material property of the pile. EDAR was validated successfully for Concrete Filled Steel Tube (CFST) piles at various locations in Alaska. This report contains the details of EDAR methodology, testing, step-by-step instructions for the software, as well as the details of the testing equipment and the underlying theory.

14. KEYWORDS: Unknown foundations, length estimation, hammer impact, pile foundation, reflection, lateral impact, attenuation	15. NUMBER OF PAGES 92
	16. PRICE CODE N/A

17. SECURITY CLASSIFICATION OF REPORT	18. SECURITY CLASSIFICATION OF THIS PAGE	19. SECURITY CLASSIFICATION OF ABSTRACT	20. LIMITATION OF ABSTRACT
Unclassified	Unclassified	Unclassified	N/A

Notice

This document is disseminated under the sponsorship of the U.S. Department of Transportation in the interest of information exchange. The U.S. Government assumes no liability for the use of the information contained in this document. The U.S. Government does not endorse products or manufacturers. Trademarks or manufacturers' names appear in this report only because they are considered essential to the objective of the document.

Funding for this project is provided by the US DOT Federal Highway Administration (FHWA, project 000S875) and administered by the Alaska Department of Transportation and Public Facilities (DOT&PF, project # HFHWY00009

Quality Assurance Statement

The Federal Highway Administration (FHWA) provides high-quality information to serve Government, industry, and the public in a manner that promotes public understanding. Standards and policies are used to ensure and maximize the quality, objectivity, utility, and integrity of its information. FHWA periodically reviews quality issues and adjusts its programs and processes to ensure continuous quality improvement.

Author's Disclaimer

Opinions and conclusions expressed or implied in the report are those of the author. They are not necessarily those of the Alaska DOT&PF or funding agencies.

METRIC (SI*) CONVERSION FACTORS

APPROXIMATE CONVERSIONS TO SI UNITS

Symbol	When You Know	Multiply By	To Find	Symbol
		LENGTH		
in	inches	25.4		mm
ft	feet	0.3048		m
yd	yards	0.914		m
mi	Miles (statute)	1.61		km
		AREA		
in^2	square inches	645.2	millimeters squared	cm^2
ft^2	square feet	0.0929	meters squared	m^2
yd^2	square yards	0.836	meters squared	m^2
mi^2	square miles	2.59	kilometers squared	km^2
ac	acres	0.4046	hectares	ha
		MASS (weight)		
oz	Ounces (avdp)	28.35	grams	g
lb	Pounds (avdp)	0.454	kilograms	kg
T	Short tons (2000 lb)	0.907	megagrams	mg
		VOLUME		
fl oz	fluid ounces (US)	29.57	milliliters	mL
gal	Gallons (liq)	3.785	liters	liters
ft^3	cubic feet	0.0283	meters cubed	m^3
yd^3	cubic yards	0.765	meters cubed	m^3
		TEMPERATURE (exact)		
ºF	Fahrenheit temperature	5/9 (ºF-32)	Celsius temperature	ºC
		ILLUMINATION		
fc	Foot-candles	10.76	lux	lx
fl	foot-lamberts	3.426	candela/m^2	cd/cm^2
		FORCE and PRESSURE or STRESS		
lbf	pound-force	4.45	newtons	N
psi	pound-force per square inch	6.89	kilopascals	kPa

Note: Volumes greater than 1000 L shall be shown in m^3

These factors conform to the requirement of FHWA Order 5190.1A *SI is the symbol for the International System of Measurements

APPROXIMATE CONVERSIONS FROM SI UNITS

Symbol	When You Know	Multiply By	To Find	Symbol
		LENGTH		
mm	millimeters	0.039	inches	in
m	meters	3.28	feet	ft
m	meters	1.09	yards	yd
km	kilometers	0.621	Miles (statute)	mi
		AREA		
mm^2	millimeters squared	0.0016	square inches	in^2
m^2	meters squared	10.764	square feet	ft^2
km^2	kilometers squared	0.39	square miles	mi^2
ha	hectares (10,000 m^2)	2.471	acres	ac
		MASS (weight)		
g	grams	0.0353	Ounces (avdp)	oz
kg	kilograms	2.205	Pounds (avdp)	lb
mg	megagrams (1000 kg)	1.103	short tons	T
		VOLUME		
mL	milliliters	0.034	fluid ounces (US)	fl oz
liters	liters	0.264	Gallons (liq)	gal
m^3	meters cubed	35.315	cubic feet	ft^3
m^3	meters cubed	1.308	cubic yards	yd^3
		TEMPERATURE (exact)		
ºC	Celsius temperature	9/5 ºC+32	Fahrenheit temperature	ºF
		ILLUMINATION		
lx	lux	0.0929	foot-candles	fc
cd/cm^2	candela/m^2	0.2919	foot-lamberts	fl
		FORCE and PRESSURE or STRESS		
N	newtons	0.225	pound-force	lbf
kPa	kilopascals	0.145	pound-force per square inch	psi

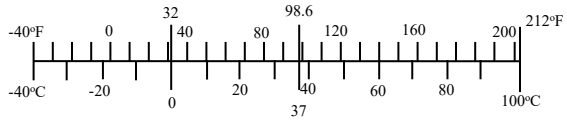

Table of Contents

List of Figures

List of Tables

Acknowledgements

Financial support from Alaska Department of Transportation and Public Facilities (DOT&PF) has been crucial for the success of this work. We would like to thank Mike Knapp, Hiram Henry, Dave Hemstreet, Elmer Marx, Janelle White and Anna Bosin for their support and valuable suggestions throughout the project duration. The field testing would not have been possible without the extensive help from Hiram Henry, Mike Knapp, Dave Hemstreet, Andrew wells, Sara Manning, Ben Still, Benjamin Fetterhoff and Nicholas Murray.

A parallel ongoing project from NCDOT on field testing in North Carolina is also crucial for the success of the EDAR development. We would like to thank Mohammed Mulla and Chris Chen for supporting and managing the project. Mohammed Mulla, Chris Kreider and Tom Santee have been instrumental in identifying potential sites in NC and with field testing. Given the geographical proximity, this was essential for more immediate field validation of our methodology.

Drs. Mervyn Kowalsky and Shamin Rahman served as senior investigators on the project and provide valuable support. Specifically, Dr. Kowalsky and his former student Dr. Diego Aguirre Realpe helped us with initial laboratory testing; this helped us validate the methodology for the first time and was the early catalyst for the eventual success of EDAR. Discussions with Drs. Mo Gabr and Ashly Cabas were helpful in understanding field conditions in North Carolina. Sriram Guddati contributed to various aspects of data acquisition, signal processing and software development. Tuhin Roy helped with his expertise in MATLAB app development that contributed to the final form of the EDAR software. Abdelrahman Elmeleigy, Abhinab Bhattacharjee and David Zabel helped with field testing in North Carolina.

Chapter 1: Introduction

Executive Summary

Bridge foundations with undocumented pile length are regarded as unknown foundations and present a long-standing challenge in managing bridge safety and stability. In the context of river and stream erosion, unknown pile length compounds the uncertainty in determining bridge vulnerability to scour. Motivated by this, a new and reliable nondestructive testing method is developed to estimate pile length. Named Effective Dispersion Analysis of Reflections (EDAR), the methodology combines wave physics and signal processing to estimate the length of the pile by examining the reflection of dispersive waves from the pile tip (detailed in Appendix B).

EDAR Testing: Pile foundations are made of various materials, such as timber, concrete, steel, or a combination thereof, and are either cast in place or driven deep into the soil. Many bridges have part of the pile exposed above the soil, terminating in the pile cap. EDAR requires the pile foundation to be excited by imparting a sharp strike using a hand-held hammer, and the response be measured at a minimum of two locations on the foundation using sensors such as accelerometers. Figure 1 presents a typical pile subjected to lateral impact, which is also the experimental set-up used in this study.

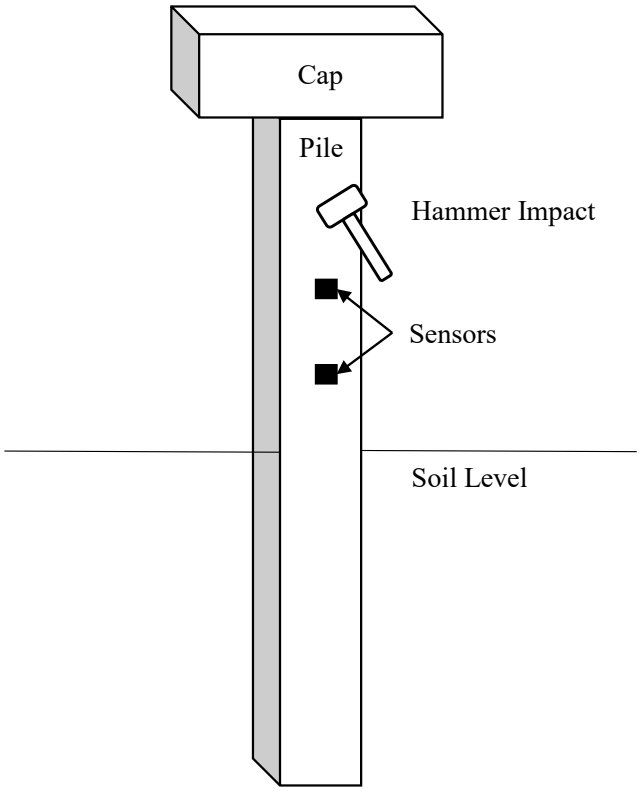

Figure 1: Pile and experimental set-up schematic

EDAR Processing: The major difference from the existing methods is how EDAR processes the data recorded at the sensors; EDAR carefully combines the physics of wave propagation with signal processing techniques to result in accurate estimates of pile depth. Response measured at two sensor locations are processed in the frequency domain by explicitly incorporating the dispersion properties of the waves generated to estimate the pile length (both frequency domain processing and incorporation of dispersion properties are novel to EDAR methodology). Depending on the location and type of excitation imparted to the pile, several types of waves exist, such as longitudinal, flexural, and high order guided waves, and EDAR processing has the ability to consider various types of waves.

EDAR Software: EDAR testing and processing is made seamless through a stand-alone software package meant for research use. The software not only facilitates data acquisition, but also predicts, with some intervention from the user, the final pile depth by processing the signals from the accelerometer.

EDAR Validation: The methodology is first validated in the laboratory for concrete filled steel tubes (CFST), resulting in less than 5% error. The method is applied in the field and the resulting data is processed through EDAR software. In field conditions, the length estimates are often within 10% error margins, whenever good data was recorded. Predominantly CFST's were tested in field conditions with a few concrete piles tested in North Carolina (presented in Appendix C). Other pile types such as timber and H-piles were not investigated in detail in this project. Further research is needed before the current methodology can be employed on other pile types.

Report Organization

At the request of AKDOT&PF, the report places predominant emphasis on the implementation of the EDAR methodology. The remainder of this chapter consists of software installation instructions. Chapter 2 details all the necessary steps for successful EDAR testing and analysis. Chapter 3 contains examples of pile tests and associated data analysis with EDAR software. This is followed by summary and conclusions in Chapter 4. Equipment specifications are detailed in Appendix A, while theoretical considerations, underlying mathematical formulation as well as laboratory and preliminary field validation are detailed in Appendices B and C.

Software Installation

Follow these steps to run the EDAR application:

1. For the data acquisition, use the following link to download and install the National Instrument Driver to the laptop computer that will be used in the field for testing.
   https://www.ni.com/en-us/support/downloads/drivers/download.ni-daqmx.html#311818

2. Once the above driver is installed, use the following steps to install the EDAR program:
   a. Run EDAR_mcr.exe file, in the EDAR software folder provided to AKDOT. This will install the MATLAB runtime application necessary to run EDAR software.

While installing the MCR file, you can select the checkbox option for desktop shortcut and follow the instructions.

b. After installing the MCR file, run EDAR.exe. You will find this file on your desktop if you checked the desktop-shortcut option, else you will find it in the EDAR software folder provided to AKDOT.
c. EDAR.exe will open the application containing both parts of the application: data acquisition and data analysis. The time taken for the application to open depends on the configuration of the computer being used and, in some cases, this can take a significant amount of time.

Chapter 2: Implementation of EDAR Methodology

EDAR Methodology is a two-step process, which involves data collection and data analysis:

- Data collection involves performing EDAR experiments in the field where the pile foundation is excited by a hammer impact and its response is measured in a set of two or more sensors attached to the pile.
- Data analysis involves processing the data collected using the EDAR algorithm and obtaining the cycle and wiggle periods from the EDAR plots. Cycle and wiggle values are processed to obtain length estimate.

Testing and Data Acquisition

The main components required for the accurate measurement of pile response are accelerometers, data acquisition system (DAQ), processing center (computer or tablet), accessories to connect the systems and a hammer to impact the pile to generate a response in the desired frequency range. Further details and specifications of the equipment can be found in Appendix A.

Test Preparation

1. Field reconnaissance

On reaching the bridge site, piles are identified for testing based on access, ease of impacting and exposed length available for testing. EDAR requires a minimum of two sensors but the current DAQ can support up to four sensors. It is recommended to have a minimum of four feet of exposed length when using all four sensors to provide sufficient space for impacting the pile. Figure 2(a) shows a schematic of a typical sensor arrangement. In case of insufficient exposed length, the number of sensors can be reduced to three to accommodate sufficient space for impact.

Piles should be evaluated for areas of debonding between steel and concrete, which pollute signal with ringing which makes it difficult to identify the reflection from the pile tip. A steel tip hammer can be lightly tapped throughout the piles surface, while listening to the audible response. Well-bonded areas respond with a bright “ping” sound, whereas poorly bonded areas have a hollow “flat” sound. Poorly bonded locations (and faces of pile) should be avoided for both sensor installation as well as impact locations. Once the best locations on the pile surface is identified, a centerline is made using a tape measure and tentative sensor locations are marked as shown in Figure 2(b).

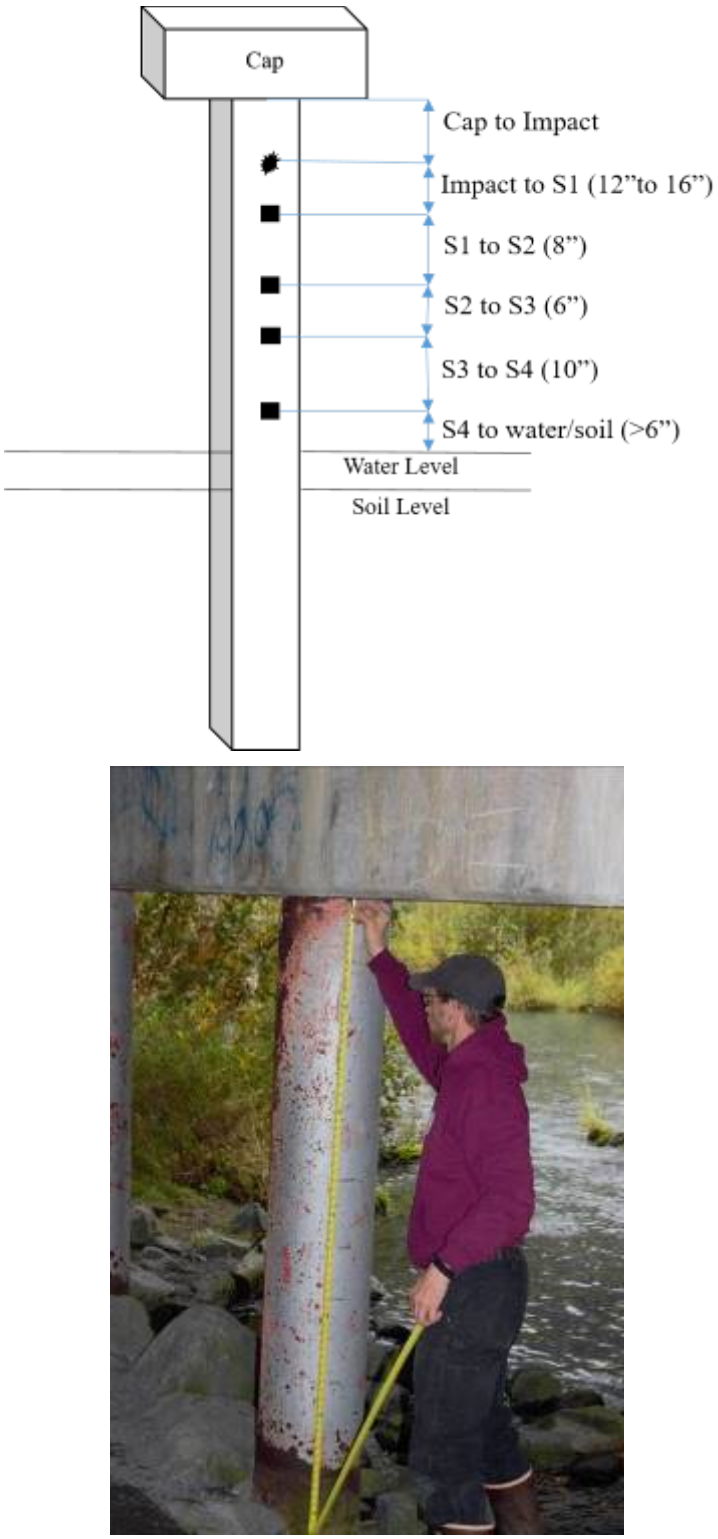

Figure 2: (a) Schematic of typical pile with sensor spacing details (b) Pile preparation

2. Surface preparation

Prior to installation of sensors, depending on the pile condition, surface preparation may be required. Concrete filled steel tubes often have a layer of rust on the outer surface of the steel, which might prevent a good connection between the sensors and the pile. In such cases, it is necessary to grind the outer layer of rust exposing the steel surface on which the studs are mounted. A small (one-inch) square area is sufficient for mounting the studs. Concrete surface typically does not require any grinding but removing surface irregularities using a scrapper might be required before installation of sensor studs to ensure good connection. After testing, the grinded locations can be re-painted to prevent rusting, using a cold-galvanizing or anti-corrosion, zinc-rich paint.

Figure 3: Surface Preparation

3. Sensor and DAQ Mounting

The sensors used for current EDAR testing are mostly PCB 352C33 stud-mounted accelerometers. The studs are attached to the pile using regular super glue at prepared locations from the previous step. It is recommended to wait for ten minutes for the super glue to set fully before mounting the sensors. It is important to take additional care while installing the sensors on the studs to make sure they are not dropped, which would damage the sensitive sensors.

The DAQ is mounted onto the pile using a pouch that can be tied around the pile using a bungee cord. Once all the equipment is mounted, the sensors need to be connected to the DAQ using coaxial cables. The DAQ is connected using USB to the tablet computer and this completes the installation process.

Figure 4: (a) Stud mounts for sensors (b) Sensor and DAQ Mounting (c) Connecting equipment

Data Acquisition

The Data Acquisition tab in the EDAR software (shown in Figure 5) is used to collect and store data with all the necessary information about the pile and the test. The current methodology requires two people to conduct the test with one person handling the computer and the other person handling the impacts with the hammer. Since testing involves several impact scenarios that include different hammer types and impact locations, it is critical to keep track of the conditions under which the data is collected. The major categories that frequently change on field are the hammer and impact characteristics. A convention for naming the file is shown in Figure 6. For example, a file name SAL_P01_LH_111_004 refers to Salmon creek (SAL) bridge pile 1 (P01) impacted using a large hammer hard tip (LH) with

the impact on top of the sensors on the same side of sensors (1) at a distance of 1 ft from the top sensor (average of 1 and 1) and the fourth repetition of the same scenario (004). Note that all the information is coded into the filename, which changes as needed during data collection.

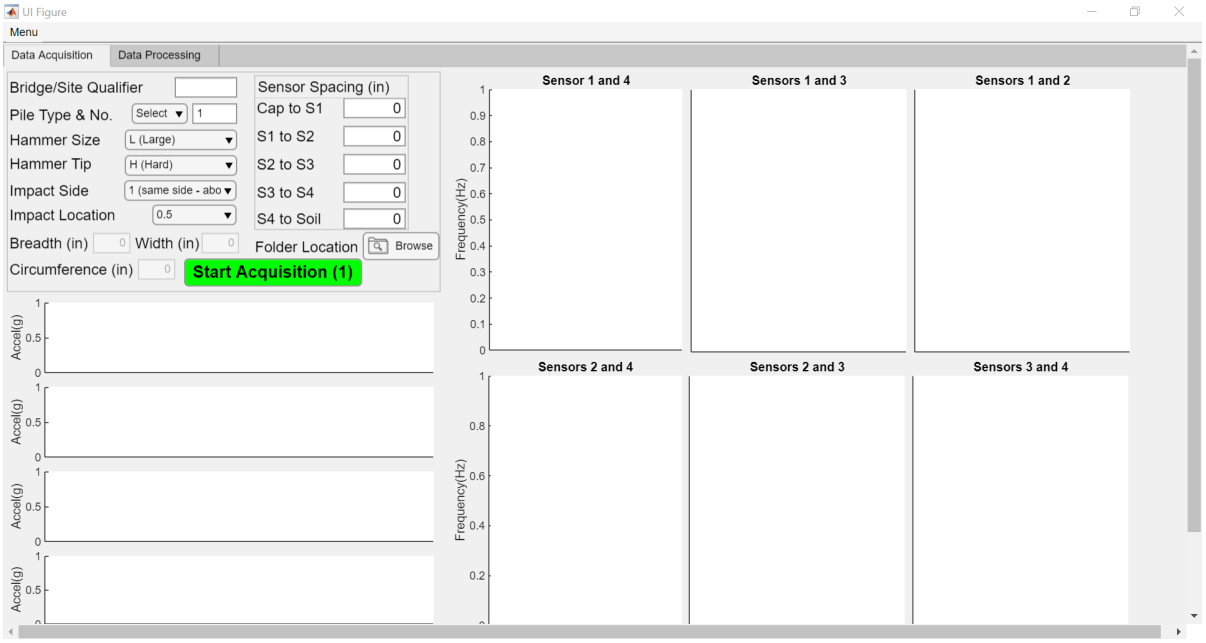

Figure 5: Data Acquisition tab of EDAR application

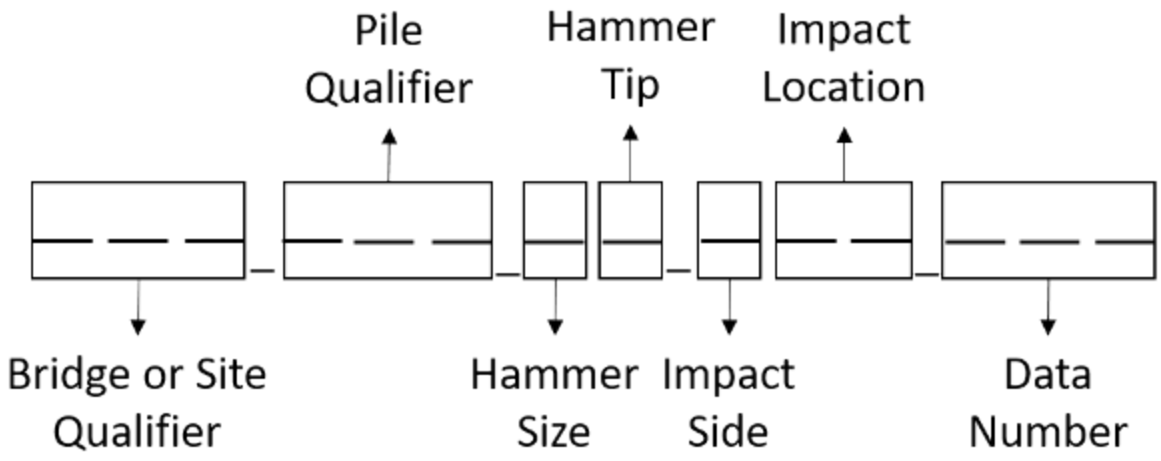

Figure 6: File naming convention

The bridge/site qualifier used to keep track of the bridge site where the test is conducted. Bridge or site qualifier is a 3-character string containing an abbreviated version of the bridge site location as shown in Table 1. A modification with two characters and pier number as the

third character can be used in situation that need more information added to the file name for better identification. Pile qualifier is a three-character qualifier specifying the pile number. For example, the qualifier for the third pile is P03, and for the15th pile is P15. Hammer size code specifies the size of the hammer as shown in Table 3. An additional option of N (noise) is added to note other scenarios that may arise in the field during testing (this information is not used at this time, but may be beneficial for future investigations). Hammer tip code specifies the hardness of the tip used as shown in Table 4. Impact side and location specify details about the impact characteristics as shown in Table 5 and Table 6. Impact location is specified using two-digit number: average of the two numbers provides the actual impact location relative to the nearest sensor.

Table 1: Bridge or Site Qualifier

Code (Examples)	Bridge or Site Details
OB1	Outer Banks
KIN	Kinston Piles without cap
SAL	Salmon Ck
POR	Portage Ck
GOL	Gold Ck
LMN	Lemon Ck
LAK	Lake Ck

Table 2: Hammer Size Code

Code	Name
L	Large
S	Small
N	Noise

Table 3: Hammer Tip Code

Code	Name
H	Hard
S	Soft
C	Medium Hard
M	Medium
G	Super Soft
T	Tough

Table 4: Impact Side Code

Code	Condition
1	Same side – Above sensors
2	Opposite side – Above sensors
3	Same side – Below sensors
4	Opposite side – Below Sensors

Table 5: Impact Location

Code	Impact location details
1	1 ft

2	2 ft
3	3 ft
4	4 ft
5	5 ft

The naming is automatic based on the inputs provided by the user during the process of data collection in the data acquisition control panel shown in Figure 7. Starting with the bridge site qualifier the user needs to specify a three-character identifier like POR for Portage Creek bridge. The cross section of the pile can be chosen from the pile type drop-down list. The software currently supports cylindrical and rectangular cross section. Based on the pile numbering conventions, the number of the pile tested is given as an input. Depending on the cross section, the either the diameter for the cylinder or the breadth and width for a rectangular cross section needs to be measured on field. On-field measurements need to be made to accurately to measure both the cross-sectional properties as well as sensor spacing. Distances between bottom of the pile cap and top sensor, and between each of the sensors and between bottom sensor and the ground level should be measured with a maximum tolerance of 1/16th of an inch. All distances measured between the sensors are center to center distances. Since the method is sensitive to these measurements, utmost care must be taken to obtain the sensor spacing details. Before starting the testing, a folder location on the tablet computer needs to be selected to store all the collected data.

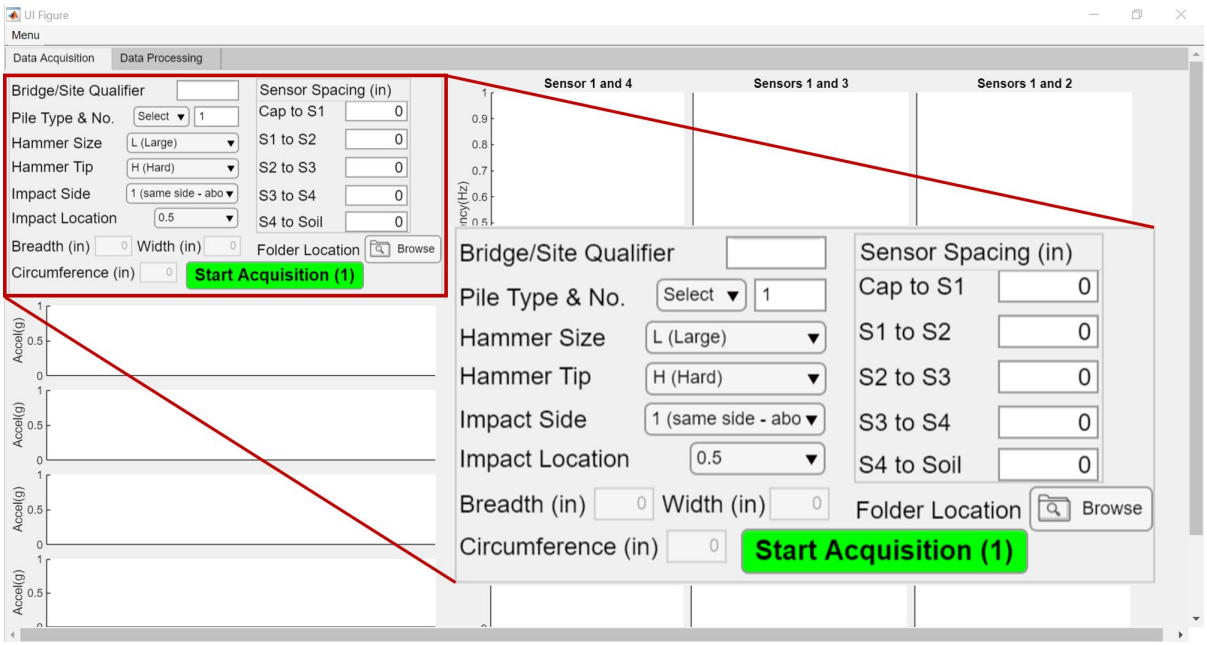

Figure 7: Data Acquisition Control Panel

Hammer and impact characteristics are important to obtain good data and determine the quality of resulting EDAR plots and frequency of occurrence of wiggles that are critical to pile length estimation. Depending on the hammer size and tip, the impact duration can be varied which in turn results in different frequency content of excitation. Generally, softer tips result in longer impacts and harder tips result in sharper impulse with shorter impact

durations. The smaller hammers are in general easier to operate with a more precise control on the impact application. In contrast, the larger hammers are capable of imparting higher energy due to their weight but are harder to control. Six hammer tips are utilized to date for EDAR testing and are shown in Figure 8They include large sledge hammer with hard (LH) and soft (LS) tips and small hammer with Hard (SH), Medium Hard (SMH), Medium (SM) and Tough (ST) tips. Specifications about all the hammers can be found in Appendix B.

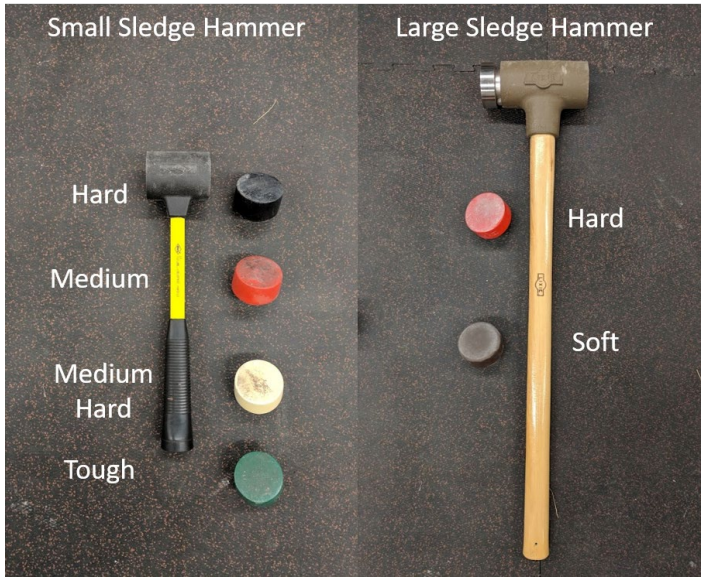

Figure 8: Different hammers and tips used for testing

Based on the observations so far with various hammer sizes and tips, it is recommended that the hammers are used in the following order for CFST piles for maximized rate of success: large hammer hard tip, small hammer hard tip, large hammer soft tip, small hammer medium tip, small hammer medium hard tip and small hammer tough tip.

Impact locations are also varied to identify the best locations for impact that lead to most usable data for EDAR procedure. Impact locations are varied between one and two feet from the top sensor. A minimum distance of one foot is required to have a strong impact yet does not overload the top sensors (overloading beyond specified range of acceleration leads to unusable data). If the sensors are overloaded, then the time domain signal will look something similar to the Figure 9 and this situation should be corrected by either reducing the impact force or impacting farther from the sensors. It is recommended to start with an impact at 1.5 ft from the top sensors and depending on the observations this impact location can be varied to avoid sensor overloading. The user can impact the pile with varying levels of energy in the beginning to understand the pile behavior and find the hardest level they can impact before overloading the sensor and use this level of energy for the remaining impacts.

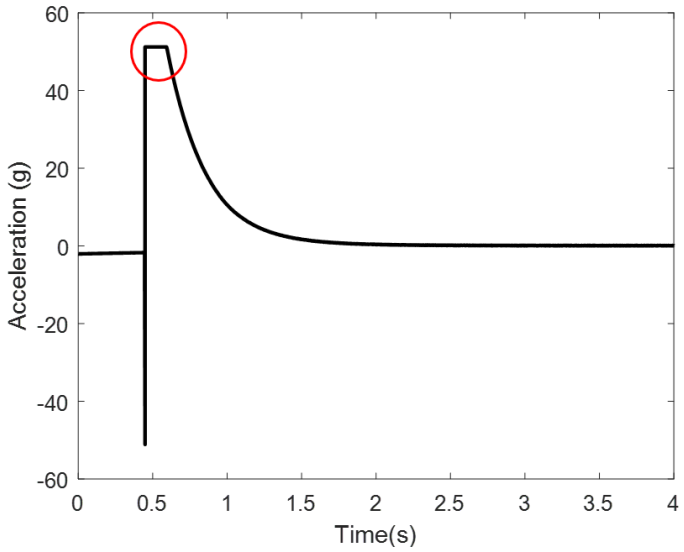

Figure 9: Sensor Overload

Once the hammer size, tip, impact side and location are chosen, the user can start collecting data. The person holding the tablet needs to press the *Start Acquisition* button and signal the person holding the hammer to impact the pile. Check if the Data acquisition system is connected to the computer before pressing the Start Acquisition button the very first time. The application acquires only four seconds of data from the sensors once the button is clicked so it is important for the person impacting to coordinate with the other person to impact the pile right after clicking the button. The click of the button and the impact are sequential events and should not happen at the same time. The software may take a longer time to complete the acquisition for the first time Start acquisitions is pressed. The pile is impacted in line with the sensors on the same side of the pile as well as on the opposite face of the pile for the same distances from the top sensors as the previous case as shown in Figure 10. The four time-domain plots in the bottom left of the screen and the EDAR plots on the right will be populated after each instance of acquisition for the user to review the data collected. The time domain plots can be used to check sensor overload and the EDAR plots are evaluated for existence of wiggles which will be later used for estimating the pile length.

For a given set of hammer and impact characteristics it is recommended to obtain *at least five sets* of valid data files. If a particular situation is found to produce wiggles, recording more data for that scenario will be useful during data analysis. Identifying wiggles is discussed in Data Organization and Analysis section below.

The sensor data is automatically saved to the destination folder with a '*.lvm' extension. Each file corresponds to a single impact. In addition to the impact data file a excel spreadsheet is also generated with all the information about the pile cross section and the sensor spacing details which will be used during the data processing step. This process is repeated for each hammer tip in the order recommended previously, and all the data files generated will be saved in the destination folder.

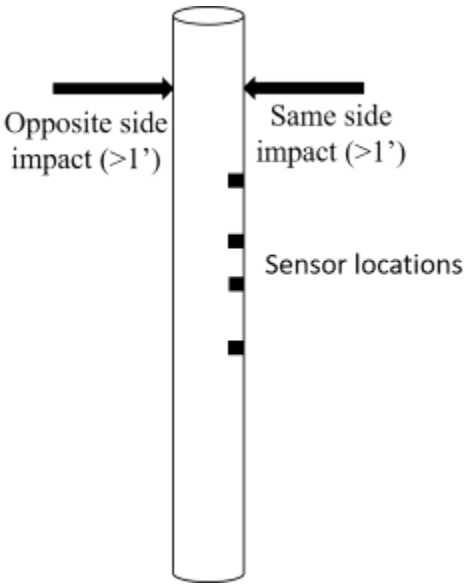

Figure 10: Impact Locations

Summary of the data acquisition procedure

1. Field reconnaissance
    a. Identify the piles on site for testing based on access, ease of impacting and exposed length (recommended minimum of 4 feet) available.
    b. Evaluate locations on the pile for debonding using a steel tip hammer. Avoid these locations.
2. Surface preparation
    a. Mark the locations of the sensors (recommended spacing 8, 6 and 10 inches between sensors).
    b. Grind any surface impurities such as rust to attach the stud onto the pile.
3. Sensor mounting
    a. Mount the studs using superglue. Screw the sensors onto the studs.
    b. Mount the data acquisition system into its sleeve and wrap around the pile using a bungee cord.
    c. Connect the sensors to the data acquisition system.
4. Data acquisition
    a. Input all the pile and test details into the data acquisition control panel.
    b. Select the destination folder where the test data will be stored.
    c. Identify impact locations with a minimum distance of 1 ft from the top sensor to avoid sensor overloading. It is recommended to start with 1.5 ft and move closer or farther based on the maximum amplitude of the acceleration in the nearest sensors (top sensors).
    d. With one person holding the tablet and other person holding the hammer, coordinate to press the Start Acquisition button about one second before hammer impact to the pile

e. Whenever hammer or impact characteristics change, the input panel must be updated accordingly.
f. Continue the process until at least five good data sets are recorded for each of the conditions used.

A representative *Data Acquisition* tab at the end of each impact is shown in Figure 11.

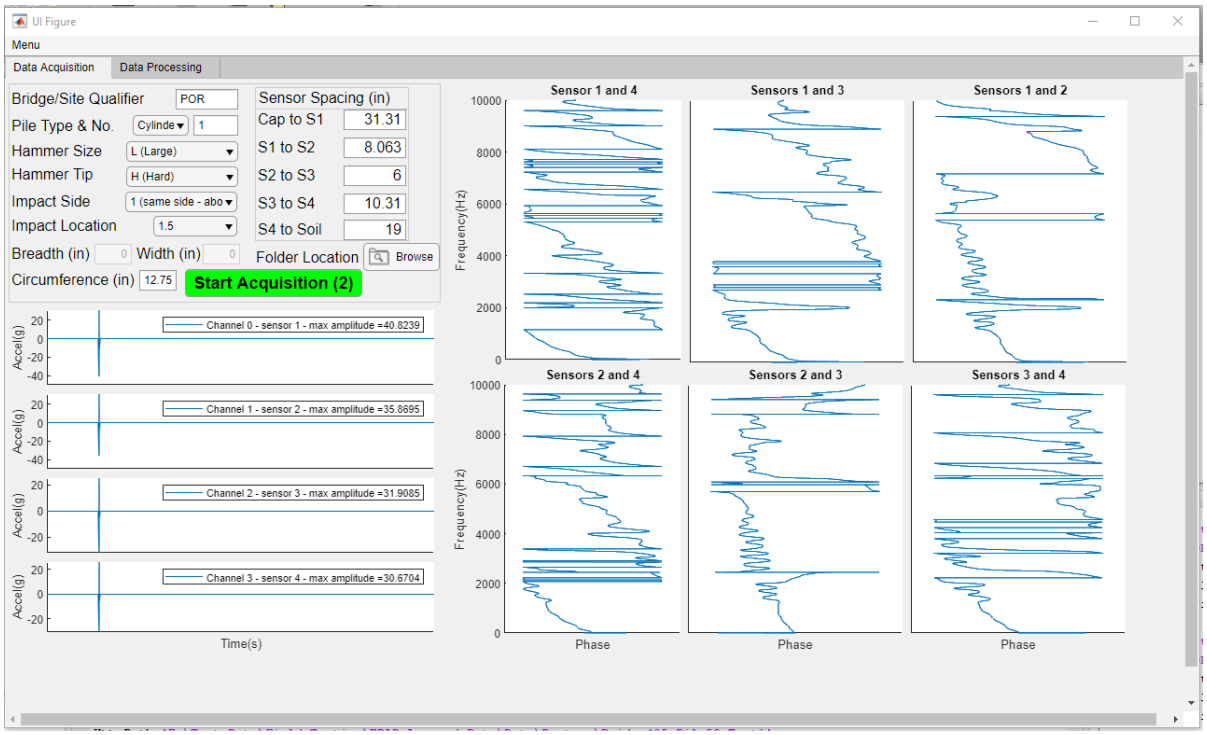

Figure 11: Typical *Data Acquistion* tab during data collection

Data Organization and Analysis

The data collected on field is stored on the tablet computer in specific folders corresponding to the test and pile. The data processing tab in EDAR software is shown in Figure 12, which not only contains the main EDAR methodology of length estimation, but also the intermediate step of material property estimation.

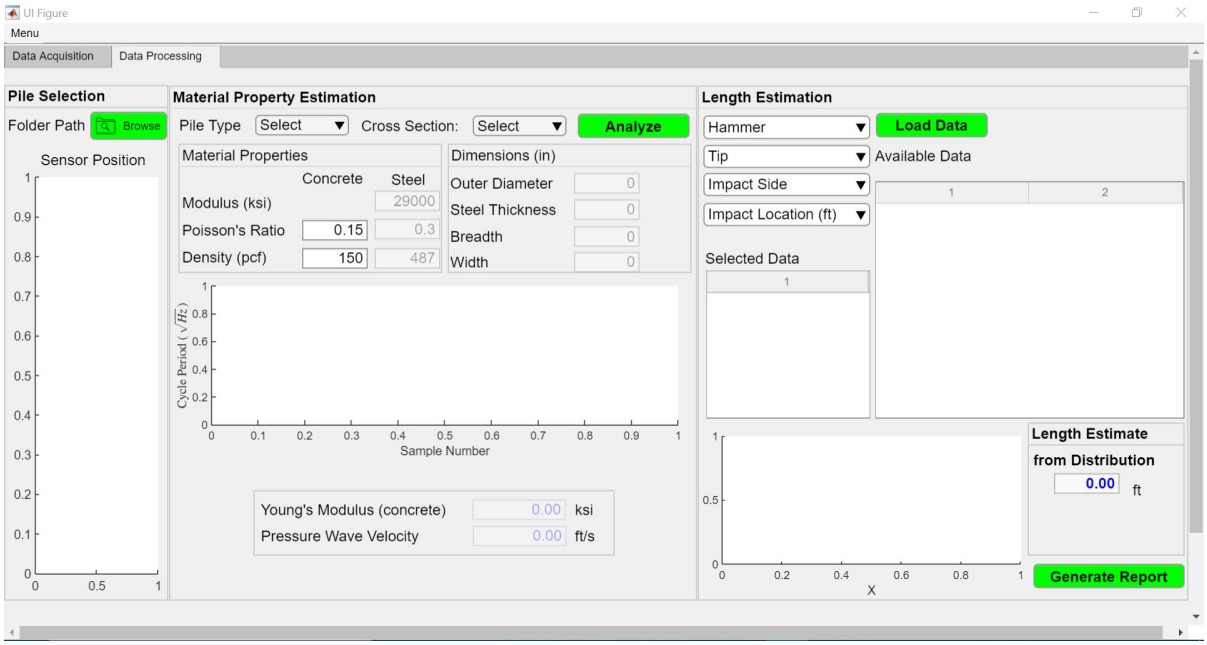

Figure 12: Data Processing tab of EDAR application

The Data Processing tab is divided into three panels namely: *Pile Selection*, *Material Property Estimation* and *Length Estimation*. Pile selection is the first step of the process where the user needs to select the folder containing all the data for a particular test conducted on field by clicking the *Browse* button. This will read all the information about the test using the Excel spreadsheet, and plots the sensor spacing details to the *Sensor Position* plot on the left. Also, the file names contained within the folder are processed and all the available data from the test is summarized in the *Available Data* table in the far right panel.

The second step of the process is the *Material Property Estimation* in which the cycle period estimates from the data are used to optimize for the concrete modulus which in turn will provide the user the *Pressure Wave Velocity* needed for length estimation (see Appendix B for more details on cycle period). The user needs to select the *pile type* and *cross-section* type from the drop-down menus. Currently, EDAR software supports only cylindrical cross sections for CFST piles but both cylindrical and rectangular cross-sections for solid concrete piles. Other material properties required for Timoshenko beam modeling of the pile are automatically populated by their default values, but the user can change these values if needed. The cross-sectional details are loaded from the excel sheet which includes the diameter for cylindrical piles, or breadth and width for rectangular piles. In case of CFST pile, the user needs to input an additional information on the steel thickness before the concrete modulus can be calculated. The best estimate of the thickness is to be used either

from as-builts or from other knowledge. Once all the values are populated, click the *Analyze* button. The application automatically analyzes the sensor signals from all the available data files to compute the cycle period for the longest sensor combination along with the average value which will be shown in the plot. The software then uses the average cycle period along with the other material and cross-sectional properties to optimize for the concrete modulus and the pressure wave velocity. The example appearance of the tab after the completion of the first two steps in shown in Figure 13.

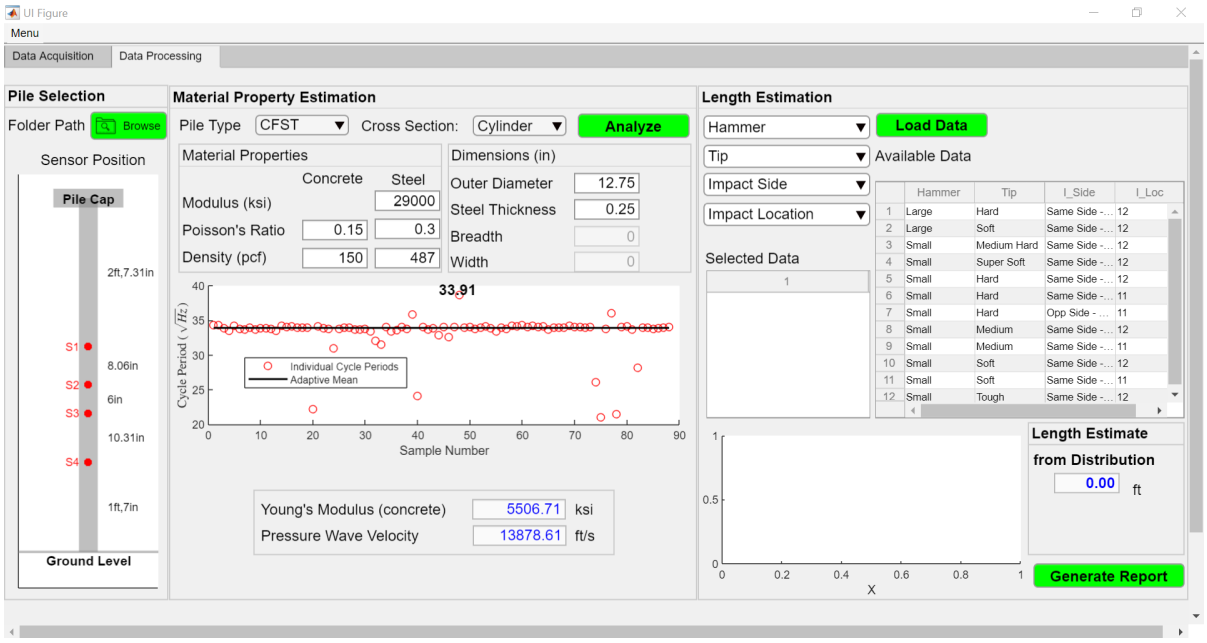

Figure 13: Data Processing after Pile Selection and Material Property Estimation

The third step involves estimating the wiggle period from the EDAR plots and subsequently the length of the pile. The *Length Estimation* panel contains four drop down lists to segregate the data based on different conditions. The drop-down lists are auto populated hierarchically from left to right. These are the same hammer and impact characteristics that were used during the data acquisition process. Since the folder contains large amount of data, is it best to segregate the data based on the hammer and impact conditions to identify and analyze the good data to obtain wiggle periods from the EDAR plot. Once the hammer size, tip, impact side and location are selected, the *Selected Data* table is updated to reflect the number of impacts available for the chosen scenario. It is not necessary to choose all the hammer and impact characteristics but at least the hammer size needs to be selected before the next step. It is recommended that the user select an available option for each of the four drop-down lists whenever possible so that the number of selected data files are manageable. The *Load Data* button analyzes this data and produces separate figures for all the sensor combinations and all different impacts as shown in Figure 14. This figure can show information from a maximum of ten different impacts which are arranged in descending order of their absolute maximum acceleration from top left to bottom right. If there are more than ten impacts, additional plots are accordingly generated, each containing up to ten sub plots. In addition to ten sub plots on each tab there are ten different tabs for the all the combination of the sensors (all one sensor

phase plots for each of the four sensors, and one phase-difference plot for each of the six sensor pairs). Each plot has a title with five numbers. The first four numbers within square brackets correspond to the maximum absolute acceleration recorded in each sensor starting from the top sensor. The fifth value (after the comma) specifies the data index.

These figure plots have the option of varying the y axis format among *Linear*, *Sqrt (square-root)* and *Linear Peak*. The *Linear* option is used for the wiggle analysis and the *Linear Peak* option can be used if the user would like to see the values of peaks for manually picking the wiggle period. This is intended only to be used by advanced users as a check after the automated process is complete. Similarly, the S*qrt* option changes the y axis to square-root frequency and is also intended to be used only as a check by advanced users for the value of the cycle period obtained automatically by EDAR software (see the theory in Appendix B for the motivation behind using the square-root of frequency). Options to zoom and pan each plot can be activated by hovering the mouse over the plot area.

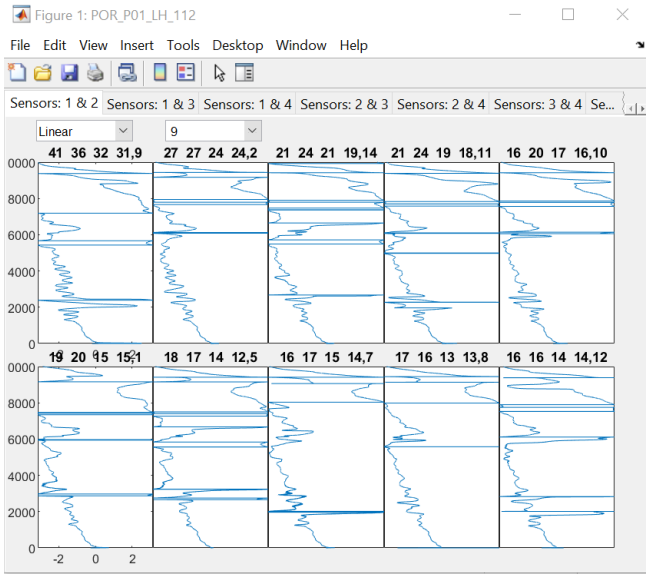

Figure 14: EDAR plots generated on presing *Load Data*

Identifying good data: Theoretical EDAR plots are shown in Appendix B Section 3 (Effective Dispersion Analysis of Reflections (EDAR): Theory) which clearly show the difference between cycle and wiggles in the EDAR plot. EDAR plot from actual field tests contain several sources of noises and other effects leading which interfere with the wiggles in the EDAR plots. Good EDAR data is defined by EDAR plots containing clear and consistent wiggles. Several instances of good EDAR plots from laboratory and field experiments are detailed in Appendices B and C. Wiggles may be seen in more than one EDAR plot, and choosing the better ones leads to a better estimate of the pile length. The process of identifying good data based on visually examining the wiggles, thus currently requires user experience refined through sometime choosing the wrong wiggles that result in inaccurate pile length estimates. Users are strongly recommended to read, at a minimum, Section 3 and 4 in Appendix B to understand the basics of the EDAR methodology to be better equipped in identifying the wiggles in the EDAR plot, followed by practicing the use of EDAR software

with the already existing data. Throughout this document, examples of good and bad EDAR plots are shown for different piles with different conditions. Figure 15 shows an example extracted from Portage pile data using a large hammer with hard tip. As seen in the figure, good EDAR plot contains clear and continuous oscillations (wiggles) in specific regions in comparison to the bad EDAR plot. Portage pile had a relatively short exposed length of about six feet and thus the effects of the reflections coming from the pile cap do not significantly interfere with the reflection from the pile tip. This might not be the case for longer exposed length as seen later for other piles. This process of identifying good EDAR plots is further detailed in the next chapter for each pile test results presented based on examples to help the user understand the process. In addition to the theory, the user is encouraged to go through those examples to train himself/herself for practical use of EDAR software.

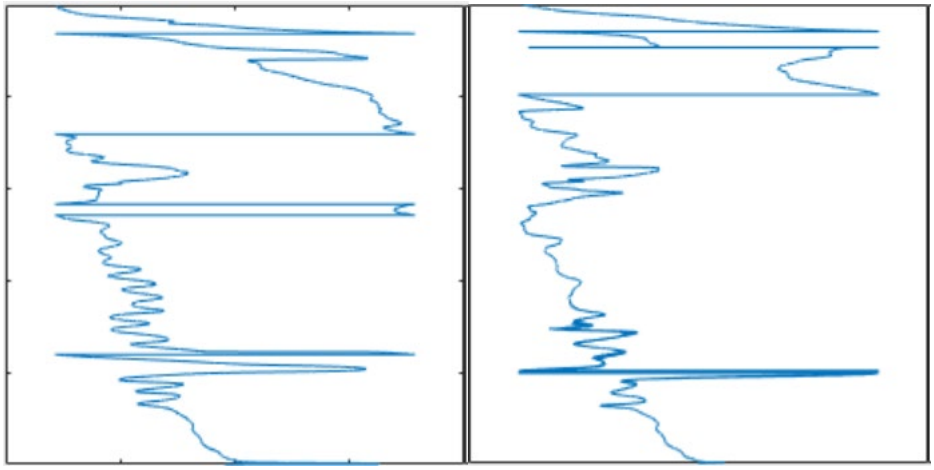

(a) (b)

Figure 15: Portage example plots (a) Good EDAR plot (b) Bad EDAR plot

Once a good data set is identified, the second drop down list is used to select that particular data set, based on the data index from the plot title, for further detailed analysis. This opens a new interactive figure as shown in Figure 16, which contains a further processed version of the ten EDAR plots corresponding to the impact data selected in two tabs. The first tab contains six EDAR plots from phase difference from sensor pairs and second tab contains four EDAR plots from the absolute phase from four sensors. As mentioned earlier EDAR plot contains wiggles at specific locations and not through the plot. The aim is to use only the effect from the bottom reflections and ignore the other effects. This is done by selecting specific parts of the EDAR plot using the interactive lines in green and red to specify the upper and lower limits respectively. The lines can be moved up or down by holding down left button of the mouse on the line. Only the regions with wiggles should be chosen, and it is recommended to avoid sudden jumps (phase change between $+\pi$ and $-\pi$) in the plot as much as possible without compromising on the wiggle region selection. Generally, based on the experience gained thus far, wiggles are expected to fall in the medium (roughly 2000 to 4000 Hz) to high (roughly 4000 to 8000 Hz) frequency ranges and whichever region of the EDAR plot contains clean, consistent and repeatable wiggles is selected. It is not necessary that all

the EDAR plots contain wiggles to the same degree as it depends on the data recorded at that location of the sensors. This is one of the main reasons for using four sensors and adding more redundancy so that the user has the option of choosing from multiple combinations as opposed to relying on a single combination from two sensors. In case of a particular plot not containing sufficiently good wiggles, it can be excluded by unchecking the box on the left corresponding to its title.

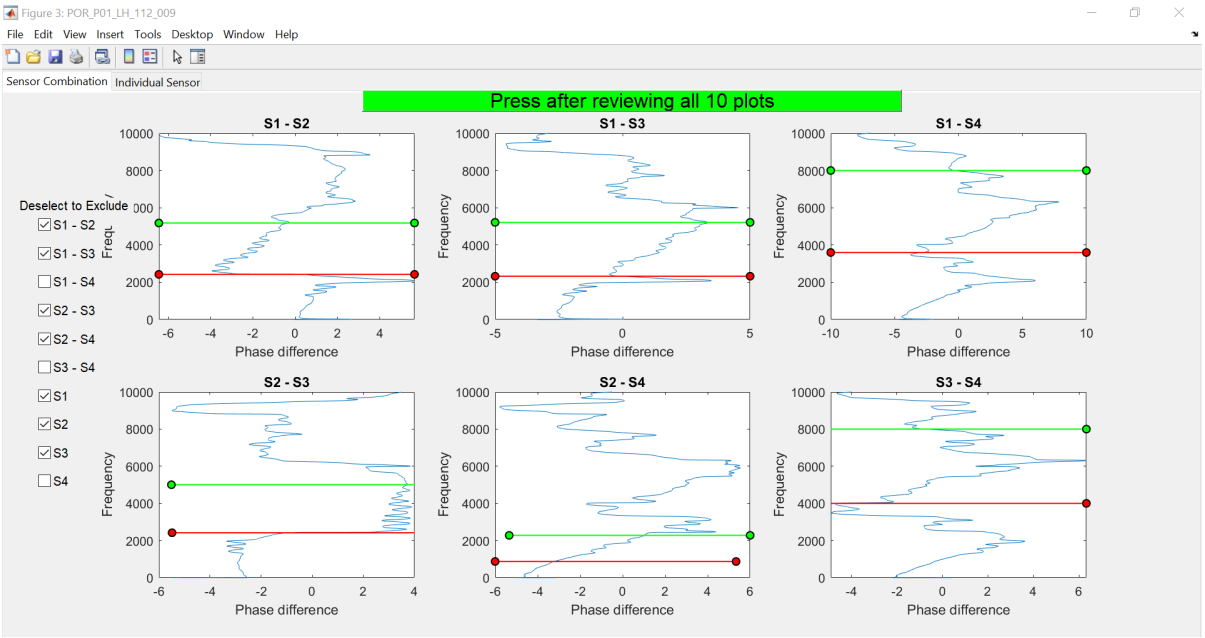

Figure 16: Interactive plot on selecting single data for wiggle analysis

After reviewing all the ten plots and choosing specific regions of the EDAR plot, press the *green button* on the top. All the regions on the plots which were selected by the user are processed automatically to obtain wiggle period estimates. Clustering algorithms are employed to obtain a best estimate for the wiggle period from all the observed wiggles. Probability distribution of the wiggle periods is shown in the plot in the *Length Estimation* panel. This process can be repeated for multiple impacts with good EDAR plots and all the values obtained accumulate in the software to provide a probability density based final length estimate. The final length is estimated from the wiggle period distribution and the pressure wave velocity estimation from the previous step, and is displayed in the Length Estimation panel. Since the length estimate is based on probability distribution, using the good regions of the EDAR plot from multiple impacts increases the chances of obtaining a better length estimate. Lack of care in the selection of the good regions of the EDAR plot will lead to a wrong length estimate. Several example are provided in the next chapter to orient the user to several situations that might arise while picking the regions for wiggle analysis.

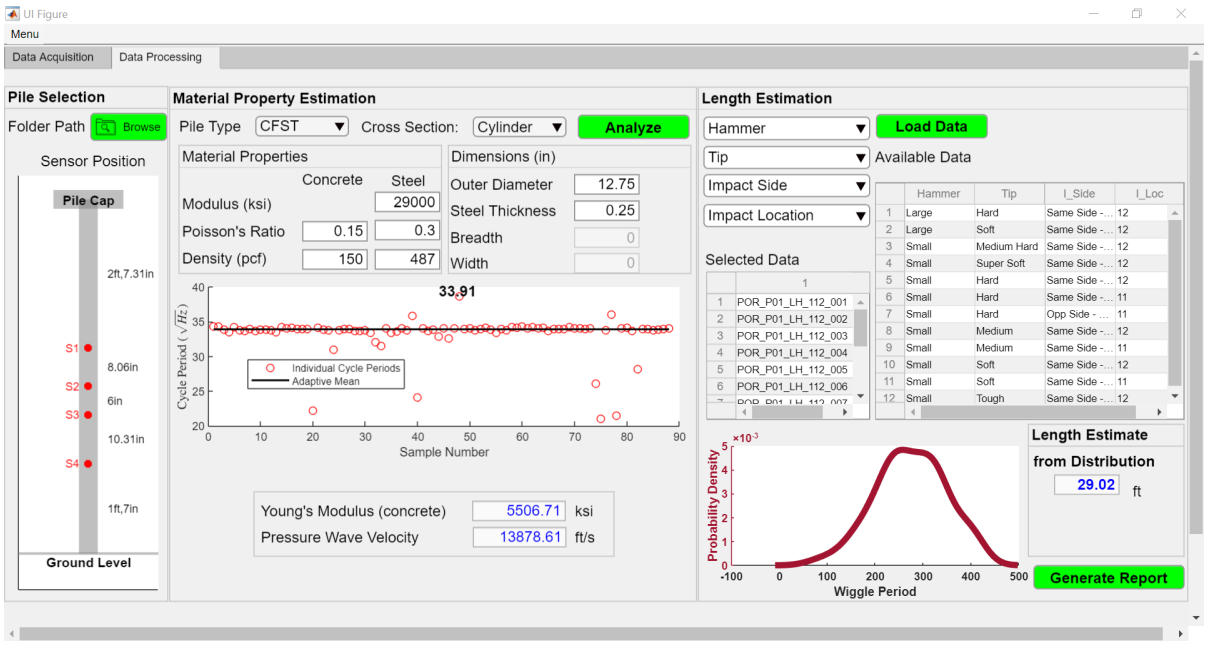

Figure 17: Length estimates updated in the application

After the entire analysis is completed from the good EDAR plots obtained from multiple hammers, the *Generate Report* button can be used to obtain a summary of the analysis conducted. This creates a pdf file in the same folder as the data specified in the first step. Additionally, the menu on the top left corner of the software has two options: *Documentation* and *Reset EDAR*. The documentation option opens a pdf file containing summary of data acquisition and data processing steps. The reset button can be used to clear the software memory and plots to start fresh and clears both the data acquisition as well as the data processing tab.

Summary of Data Processing:

1. Step 1 – Pile Selection
    a. Select the folder containing the data files corresponding to the pile.
2. Step 2 – Material Property Estimation
    a. Select the pile type and cross section type from the drop-down lists.
    b. In case of CFST pile, input the additional information, i.e. steel thickness.
    c. Click *Analyze* to estimate the material properties.
3. Step 3 – Length Estimation
    a. Select the hammer size and tip, impact side and location options.
    b. Select *Load Data* to plot all the EDAR plot combination for the selected data in a separate pop up figure.
    c. Select the impact data with good EDAR plots from the drop-down list for further detailed analysis of the data. This pops up an interactive matlab figure with all processed EDAR plots for the specific impact.

d. Move the green and red line to adjust the regions of the EDAR plots for wiggle analysis (green line for the upper limit and red line for the lower limit). Deselect specific EDAR plots if needed and press the green button on the top after reviewing all the ten plots presented.
e. Go back to the main window to see the probability density of wiggle periods calculated and the updated length estimate from the wiggle analysis.
f. Repeat steps (a) to (e) as many times needed for the data available to obtain the final length estimate from the application window.
g. Once the data analysis is complete, click *Generate Report* button to generate a pdf report of the analysis. The pdf report is stored in the same folder as the data.

Chapter 3: Field Testing Results

Testing was performed at several bridge sites in Alaska with different pile characteristics. This included Portage creek, Lemon creek, Salmon creek, Gold creek, Lake creek and Chester Creek piles. In addition, a cylindrical concrete pile at Kowee ck and H-piles at Sheep creek were tested. Results for the Kowee ck and Sheep creek piles are not presented in this report; currently EDAR is confirmed to work for CFST and the results from five of the six concrete filled steel tube piles are detailed in this chapter. Results from Chester ck pile test are not presented due to significant amount of data containing effects of ringing and overloading of the sensors even for a soft impact.

Data processing is detailed in this chapter through a step by step procedure using the EDAR software (in addition being a validation document, this chapter can thus be used as a tutorial for the users of EDAR software). Portage Creek testing resulted in good data with consistent and repeatable wiggles and is presented first. This is followed by Lake Creek pile which resulted in data containing no significant wiggles and thus the analysis was inconclusive. This is followed by piles tested in Salmon, Lemon and Gold creeks which resulted in mixed data but the EDAR software was able to extract the length.

Portage Creek

Pile 59 of bridge 405 of Portage creek, was tested and analyzed to estimate its length. It had an outer diameter of 12.75 inches and an expected embedment of 24 feet. This is relatively a smaller cross section pile with shorter embedment compared to the other piles tested. Pictures of the site and the instrumented pile are shown in Figure 18.

(a) (b)

Figure 18: (a) Portage creek (b) Instrumented pile

As detailed in the previous chapter, the data processing is done in three steps as follows.

1. Step 1. Pile Selection: The folder containing the files from the pile test is selected after clicking *Browse.* The updated screen is shown in Figure 19. The sensor configurations are shown on the left and the table of the available data is updated on the right.

2. Step 2. Material Property Estimation: Pile type is selected from the drop-down list as CFST. Since the software supports only cylindrical CFST cross section, it is automatically updated to cylinder. Default values of concrete density and Poisson's ratio, as well as steel modulus, density and Poisson's ratio are provided (these can be modified if needed). The outer diameter field is updated based on the information from the excel sheet in the same folder. The user needs to provide the steel thickness. In case of the Portage pile, the steel thickness was obtained from the as-builts. Even though as-builts do not contain the exact thickness of the steel tube used, the recommended value is provided in most cases. The recommended value for the Portage pile was specified as a maximum of 0.25 inches, which is used for the cycle period analysis. After specifying all inputs, pressing the *Analyze* button automatically reads all the data available to estimate the cycle period and subsequently the pressure wave velocity. The application widow after completion of the second step is shown in Figure 20.

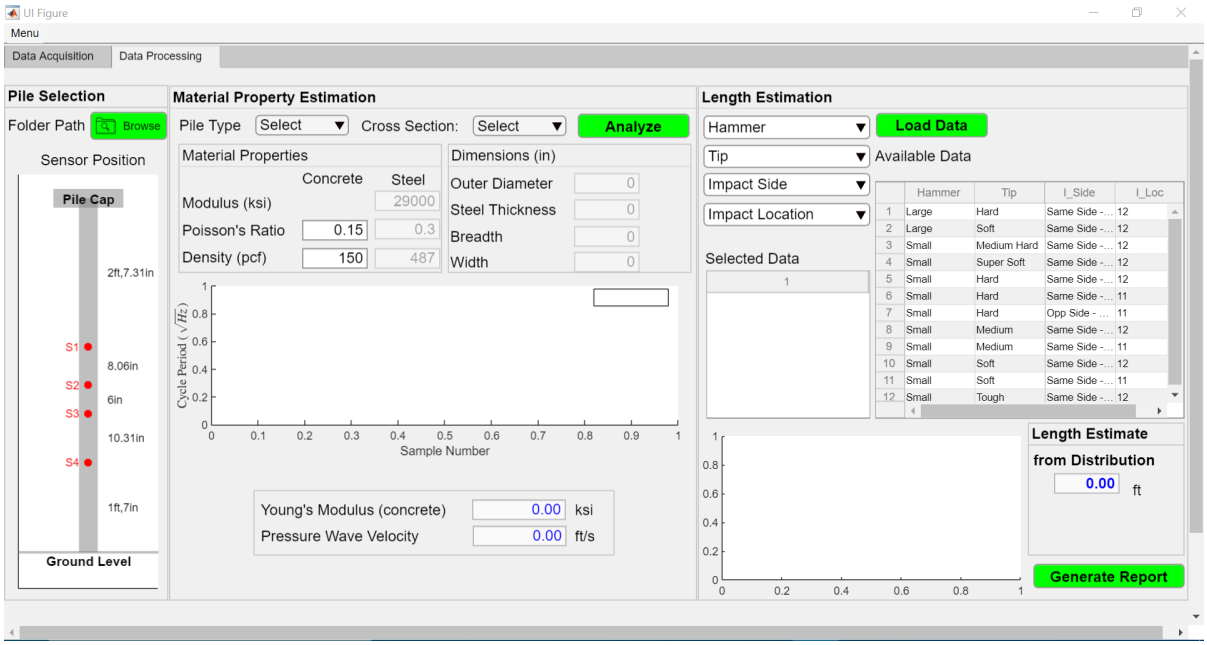

Figure 19: Portage pile analysis step 1

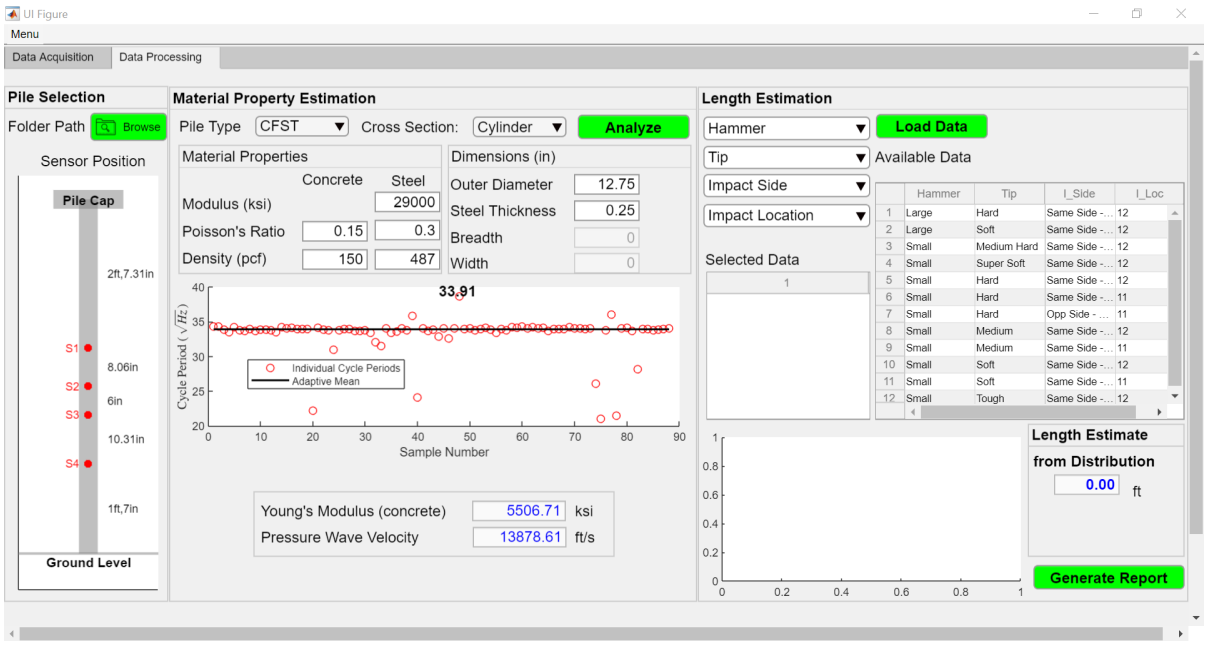

Figure 20: Portage pile analysis step 2

3. Step 3. Length Estimation: Firstly, hammer and impact characteristics are selected to narrow down the selected data. Starting with the large hammer hard tip with same side impact at 1.5 feet from the top sensor, the selected data table is updated with 14 rows corresponding to 14 available impacts. Clicking the *Load Data* pops up two different figures with 10 and 4 impacts as shown in Figure 21. The EDAR plots are reviewed for the best-looking data based on observing the wiggles as shown in Figure 15. Since the data collected for the Portage pile are generally good, the top five plots in the first figure are chosen for further analysis. Each impact is chosen sequentially from the second drop down list with the data numbers. Selecting each data (for example data index 9) pops up another plot as shown in Figure 22. This figure is interactive with a green and red line on each of the plots to select the regions of EDAR, which will be considered for the wiggle analysis. EDAR plots which do not exhibit proper wiggle like characteristics are deselected. It is recommended that maximum number of EDAR plots are used at least at the beginning of the analysis procedure in order for the wiggle analysis algorithm to have sufficient number of points to perform clustering. Otherwise this can result in an error message which will be shown in the command window in the background. Pressing the green button on the top of the plot analyzes the selected regions of the EDAR plot and the resulting probability density is plotted in the length estimation panel along with the estimated length (see Figure 23 (a)). This process is repeated for multiple impacts and the resulting length estimate after analyzing top five impacts in Figure 21 is shown in Figure 23 (b). The resulting length estimate can be seen as 29 ft which is within 3% of the actual length of 29.92 ft.

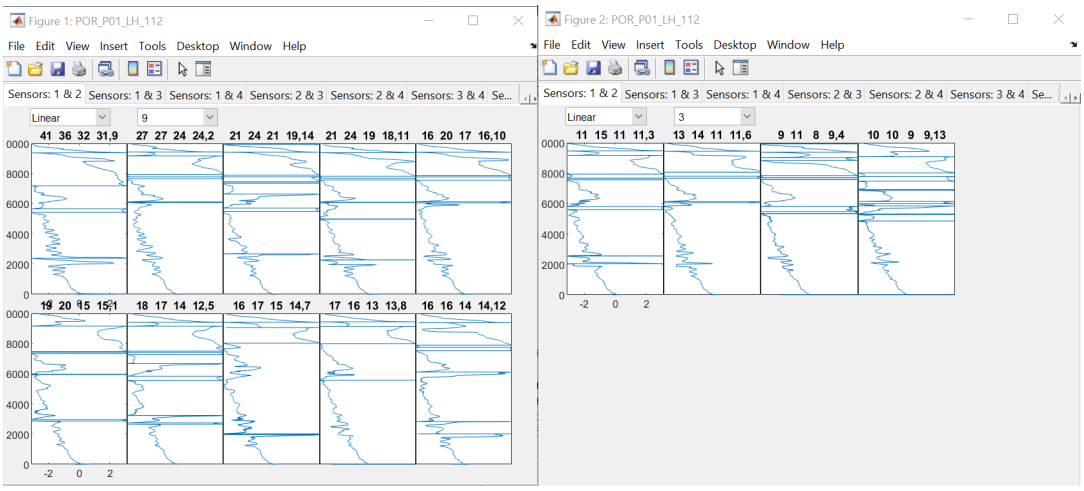

Figure 21: Portage pile EDAR plots: Large hammer hard tip with same side impact at 1.5 feet

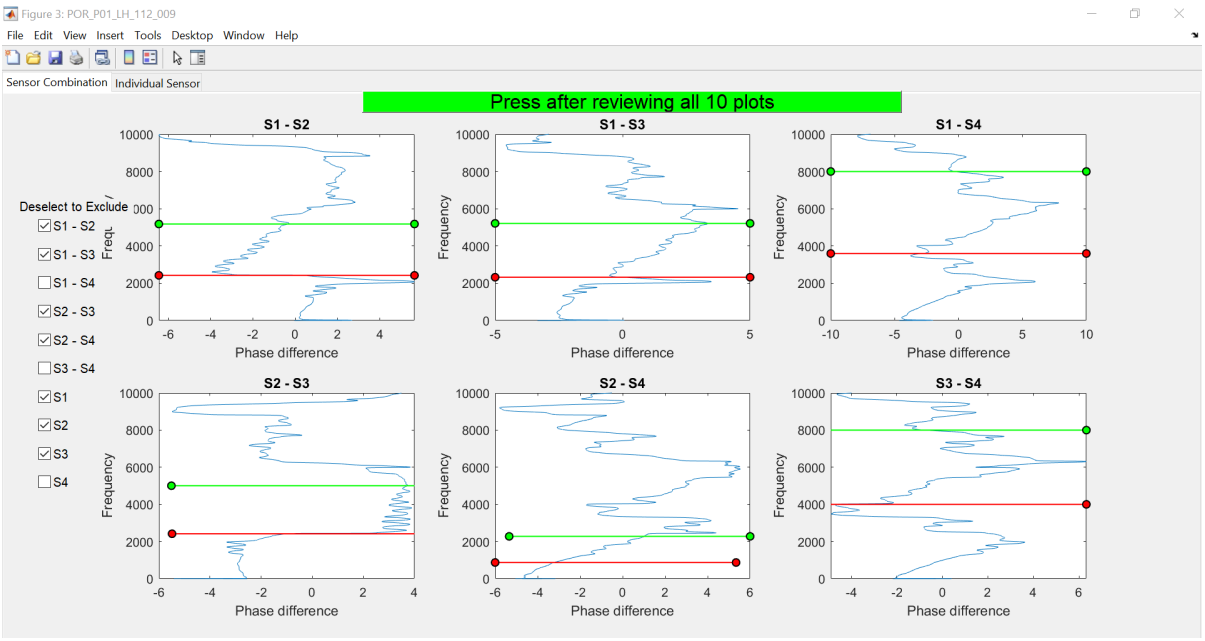

(a)

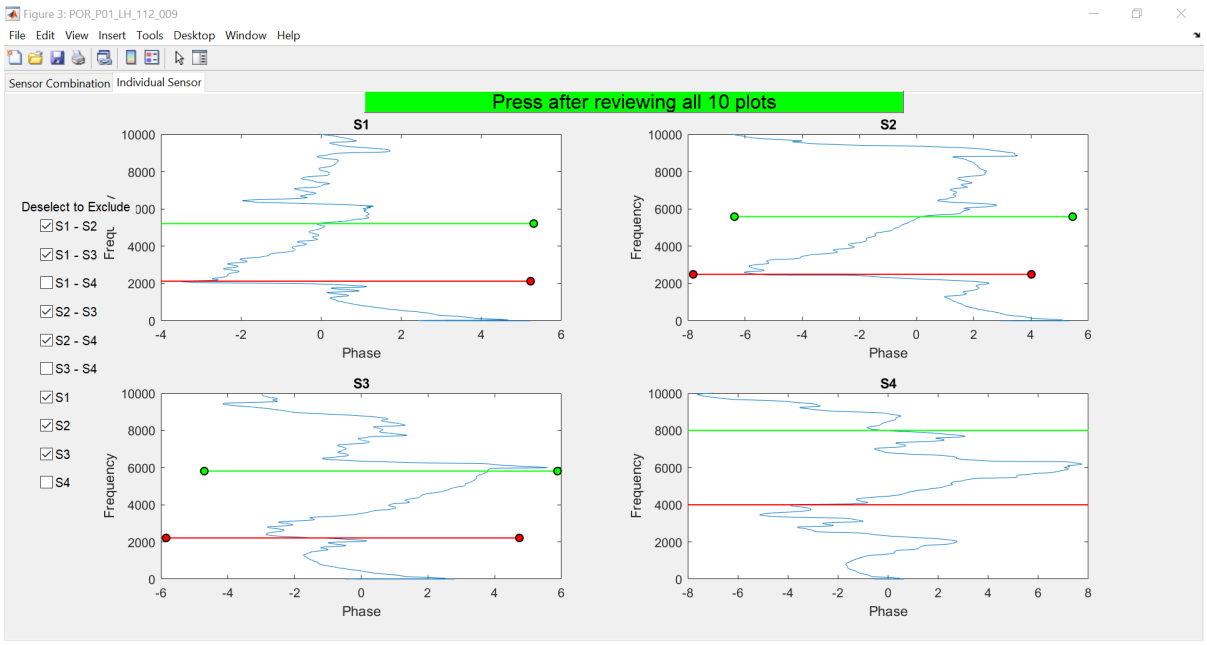

(b)

Figure 22: Portage pile: EDAR plots for data with filename POR_P01_LH_112_009 (a) Sensor combination (b) Indivdual sensors

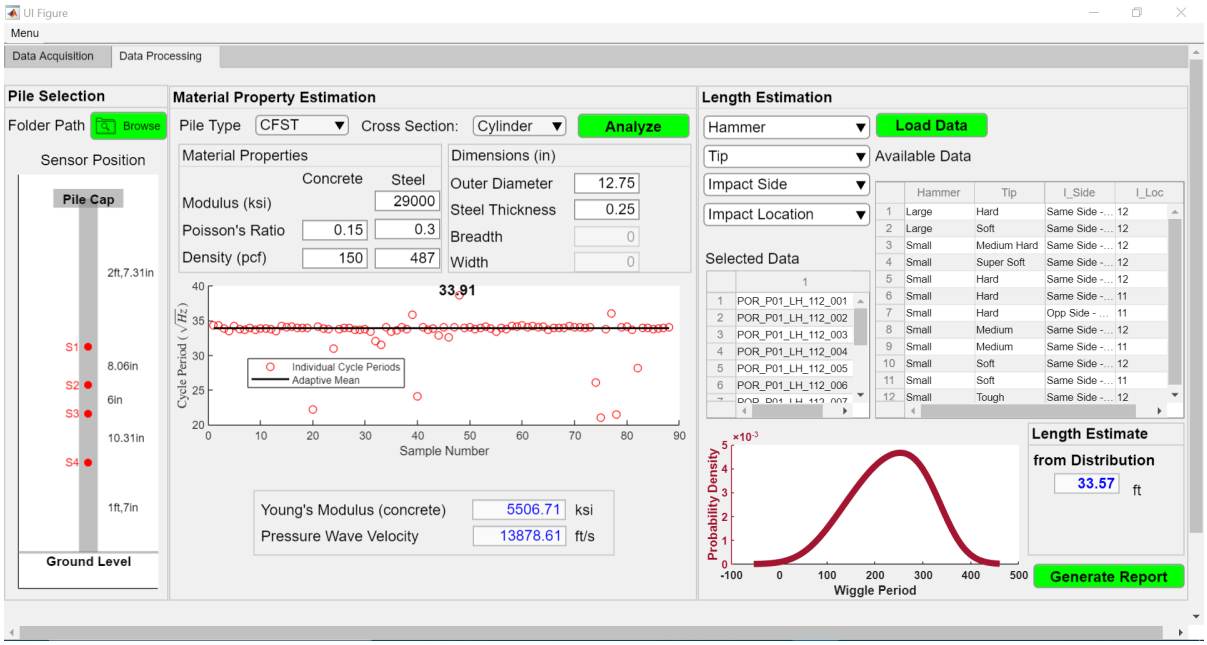

(a)

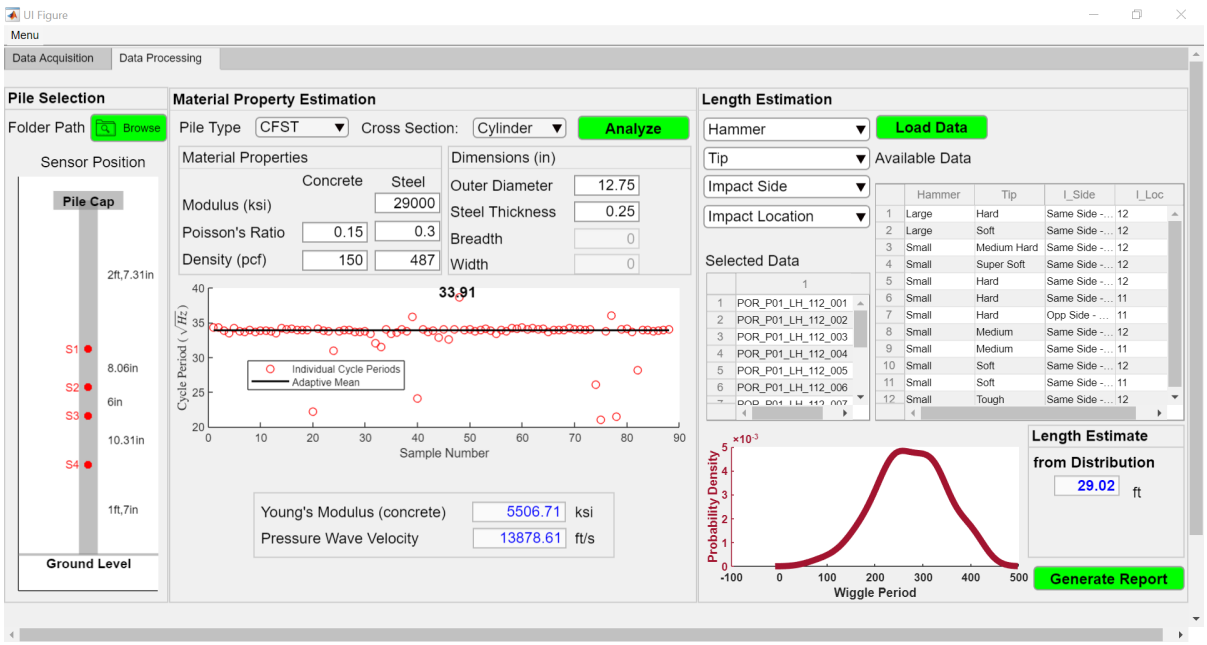

(b)

Figure 23: Portage pile (a) Wiggle analysis and length estimate after analyzing one impact data (b) Wiggle analysis and length estimate after analyzing five impacts for large hammer hard tip same side impact at 1.5 feet

Lake Creek

Lake Creek piles are 12-inch CFST and shown in Figure 24. Three-step processing similar to Portage pile was conducted. Results from steps 1 and 2 are shown in Figure 25.

Figure 24: Lake creek pile

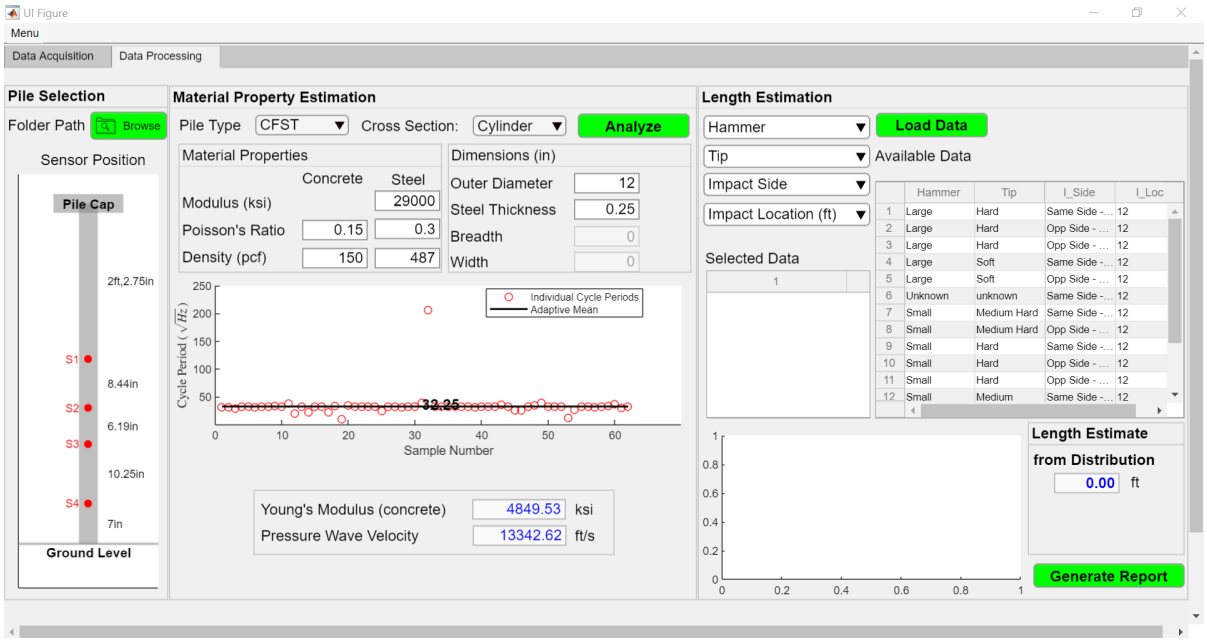

Figure 25: Lake creek data processing steps 1 and 2

Hammer and impact characteristics are chosen from the length estimation panel to generate the corresponding EDAR plots as shown in Figure 26. Very few wiggles with faint oscillations are observed and not repeatable across multiple hammer size and tips. Thus, further analysis of EDAR plots is not expected to provide an accurate estimate of the pile length. Nevertheless, a particular EDAR plot shown in Figure 27 (a) was analyzed for wiggles, which resulted in a length estimate of 25.6 ft (shown in Figure 27 (b)). It is important to note here that the software analyzes the parts of the EDAR plot selected irrespective of existence of wiggles and outputs a length estimate which does not correspond to the actual length of the pile. Paying attention to the repeatability and consistency of the wiggles across multiple impacts is critical for successful length estimation using the EDAR software.

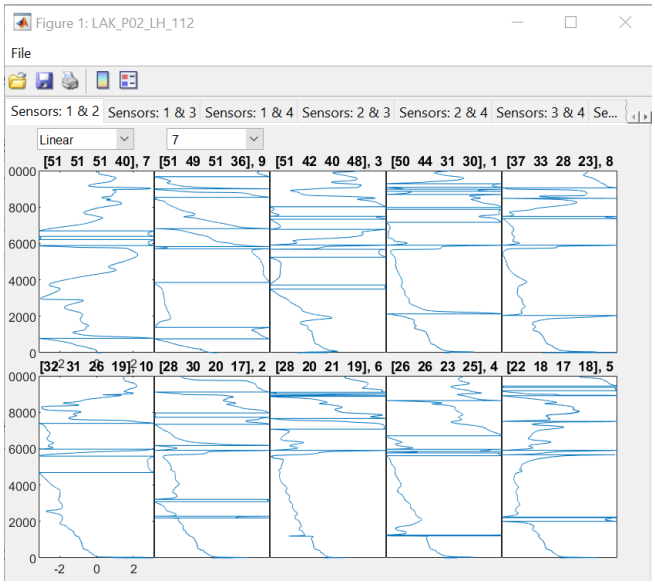

Figure 26: Lake creek EDAR plot

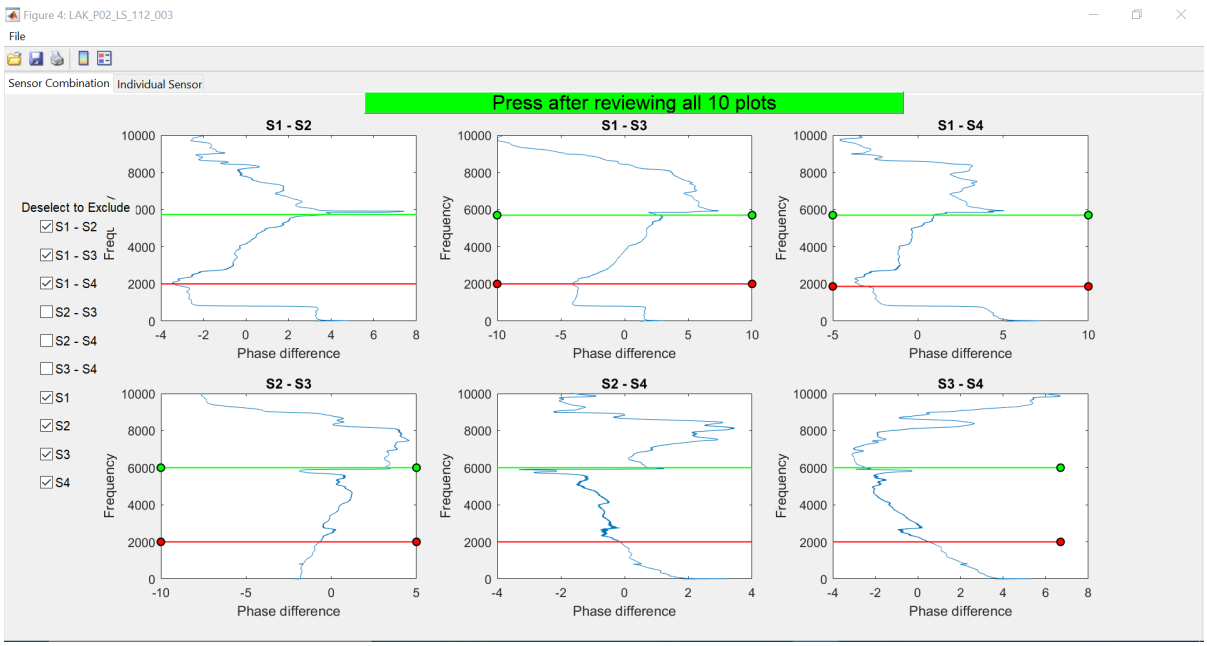

(a)

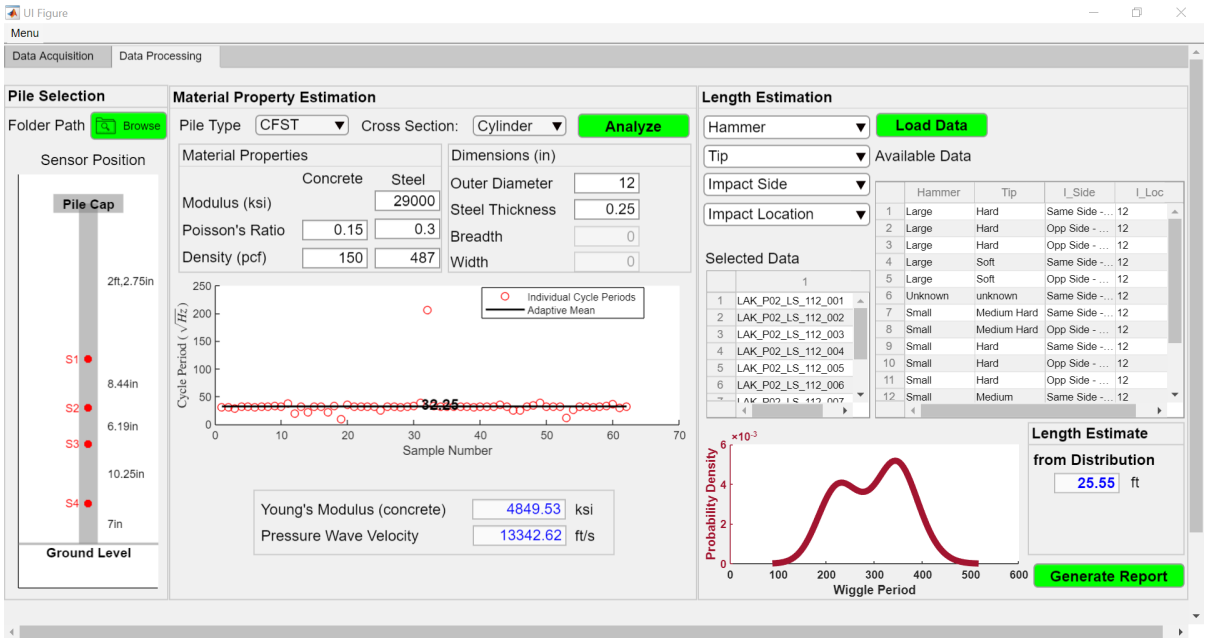

(b)

Figure 27: Lake creek (a) Wiggle analysis (b) Length estimate

Lemon Creek

Lemon creek piles were 18-inch CFST and are shown in Figure 28. A similar procedure as that of the Portage pile is followed for the analysis. Data processing steps 1 and 2 are shown in Figure 29. The steel thickness was assumed to be 0.375 inches for the material property analysis based on information from the as-builts.

(a) (b)

Figure 28: Lemon Ck (a) site (b) pile test

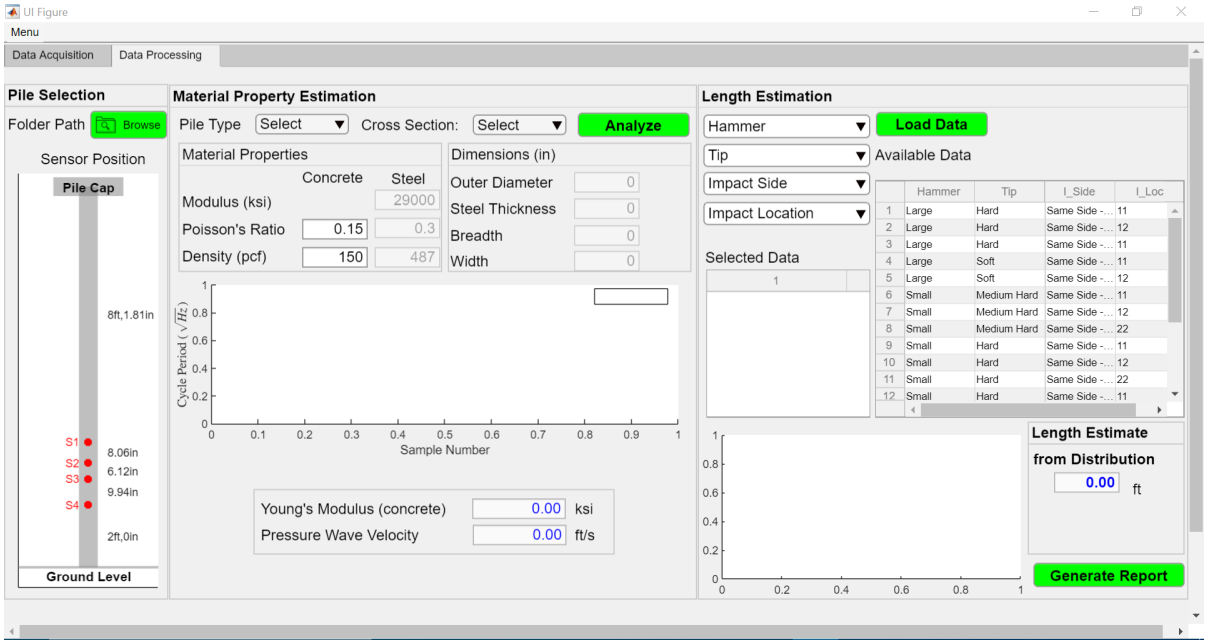

(a)

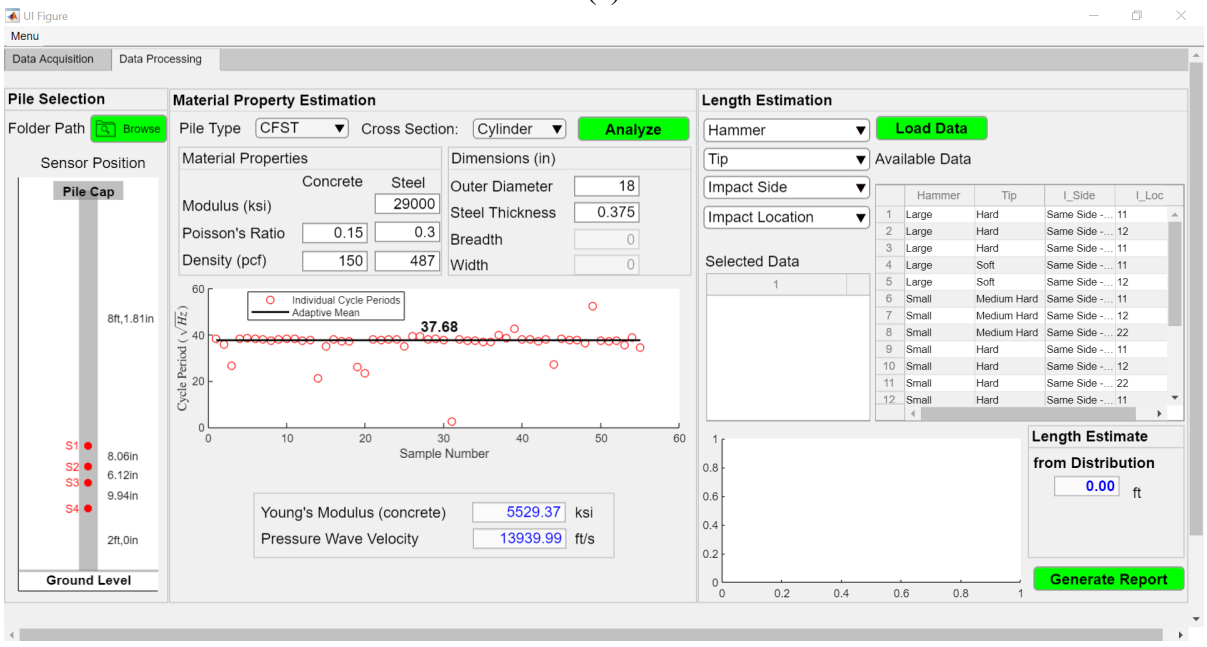

(b)

Figure 29: Lemon creek pile data processing (a) Step 1 (b) Step 2

Wiggle analysis is performed from the Length Estimation panel. Lemon creek pile has a longer exposed length and results in the top reflections interfering with the reflection from the bottom. The top reflections also show up as wiggles in the EDAR plot but with a different signature and their period is related to the exposed length (Further details and theory can be found in Appendix B Section 3). In this particular case, due to the longer exposed lengths EDAR plot contains two distinct periods superimposed on each other. This can be clearly seen in the EDAR plots shown in Figure 30. This behavior in the EDAR plot can be expected

whenever the exposed length is long (typically more than 6ft of pile above the top sensor). It is advisable for the user to be aware of this superimposed oscillations when picking the ranges in the EDAR plot containing wiggles; if EDAR plot indicates that a particular frequency range shows cleaner non-superimposed wiggles, it may be more advisable to pick this range over other ranges. At the end however, the wiggles from the top reflections are expected to be automatically filtered out by the EDAR software, with an assumption that the exposed length is shorter than the embedded length of the pile.

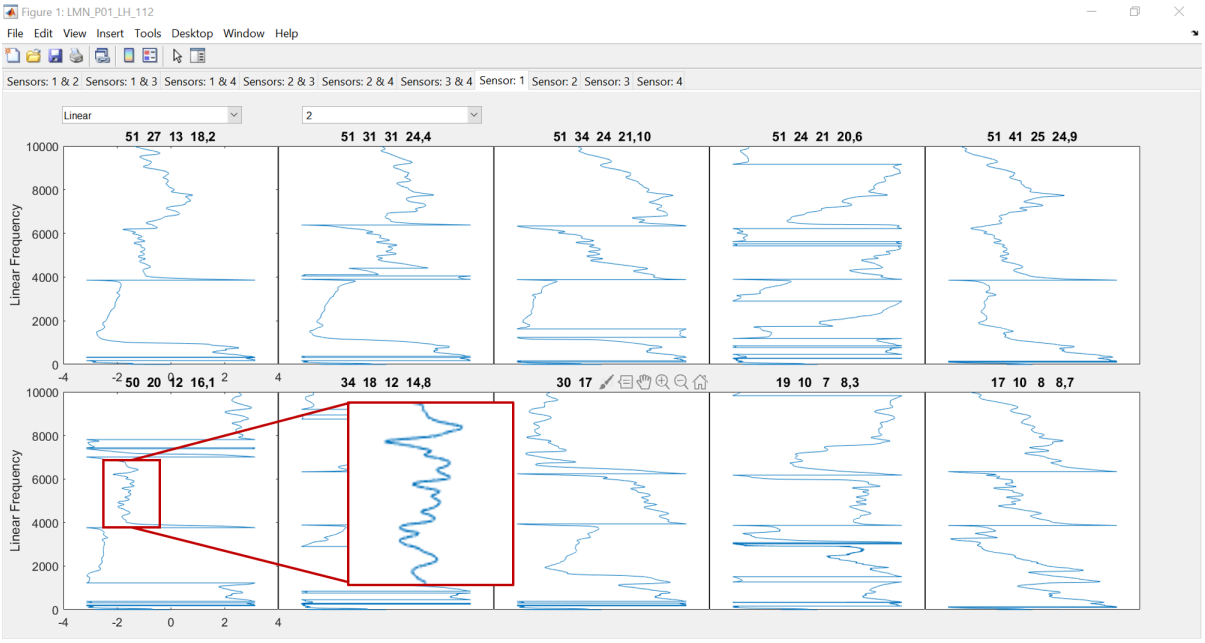

Figure 30: Lemon creek EDAR plot: Two wiggle periods superimposed due to interference from the top reflection

Nevertheless, good EDAR plots that exhibit characteristics of the wiggle are selected for further analysis. Ranges within which clear wiggles can be observed with minimal jumps between $-\pi$ and $+\pi$ are selected for multiple impact scenarios. The wiggle periods get accumulated after analysis of each data and the length estimate is updated. The length estimate obtained from the analysis after analyzing four and five different impacts is 67.3 ft, as shown in Figure 31.

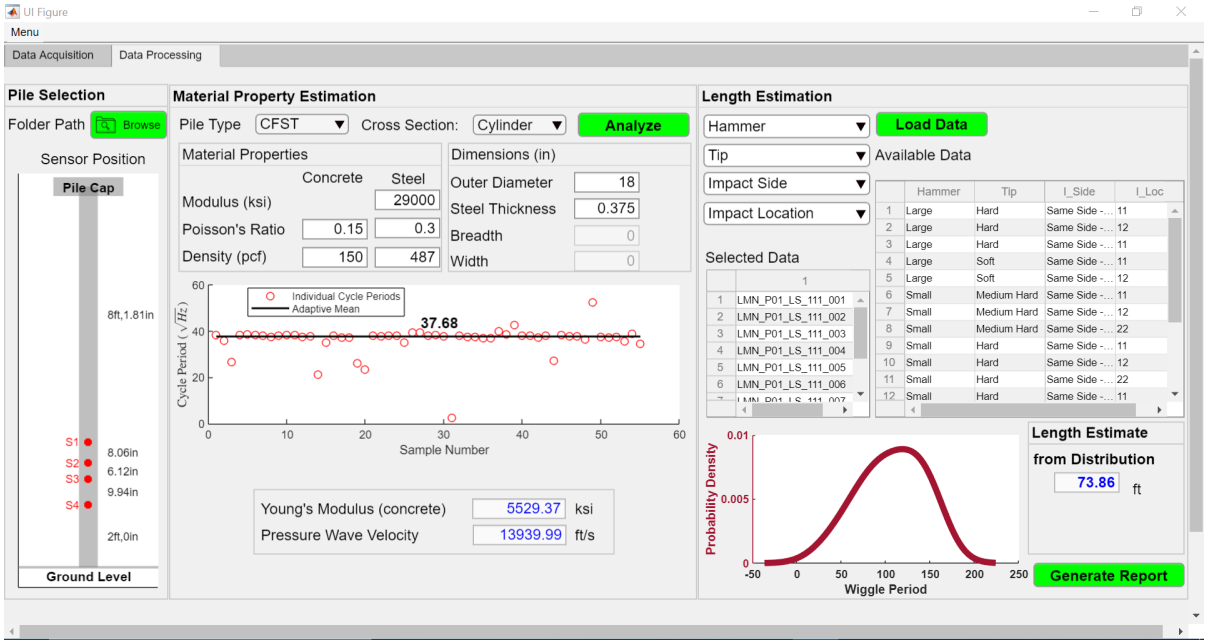

(a)

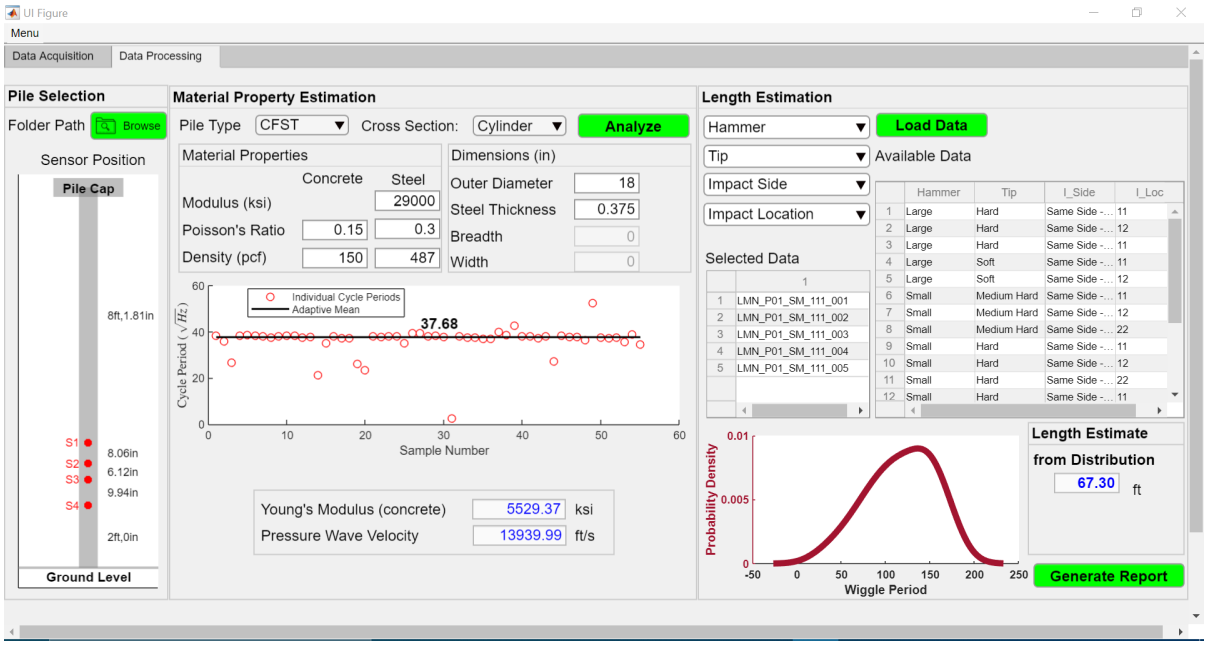

(b)

Figure 31: Lemon Creek length estimate after considering (a) 4 impacts (b) 5 impacts

The length estimate value changes every time an additional data set is analyzed. If sufficiently high number of data sets are analyzed with good EDAR plots, the length estimate is expected to converge to the actual length. The actual length of this pile obtained from pile driving logs was 68.89 ft.

Salmon Creek

Salmon Creek piles are 18 in CFST and shown in Figure 32. Data processing steps 1 and 2 are shown in Figure 33. Data with proper wiggles were not very common for this bridge site. One particular set of data obtained with very strong impacts showed more consistent wiggle like oscillations. Similar to Lemon creek this pile has a longer exposed length and thus a pattern of superimposed wiggles are expected. Based on this observation, wiggles are identified in specific frequency ranges and once identified this frequency range is scrutinized for other impacts. Length estimate obtained after wiggle analysis is shown in Figure 34.

Figure 32: Salmon Creek

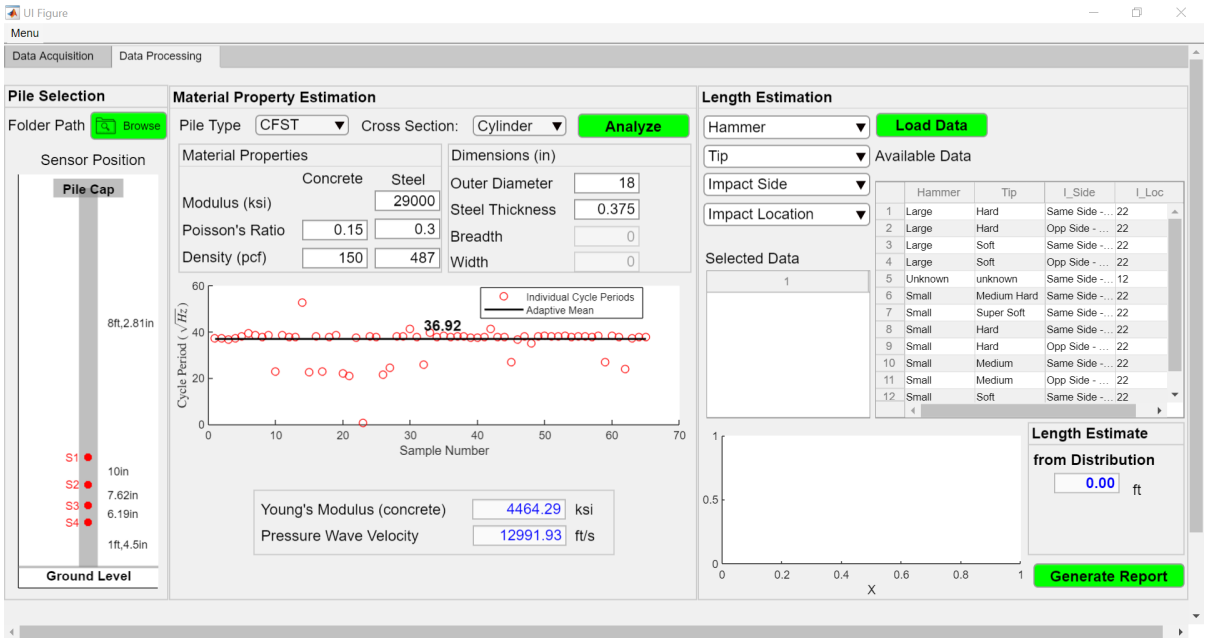

Figure 33: Salmon creek data processing steps 1 and 2

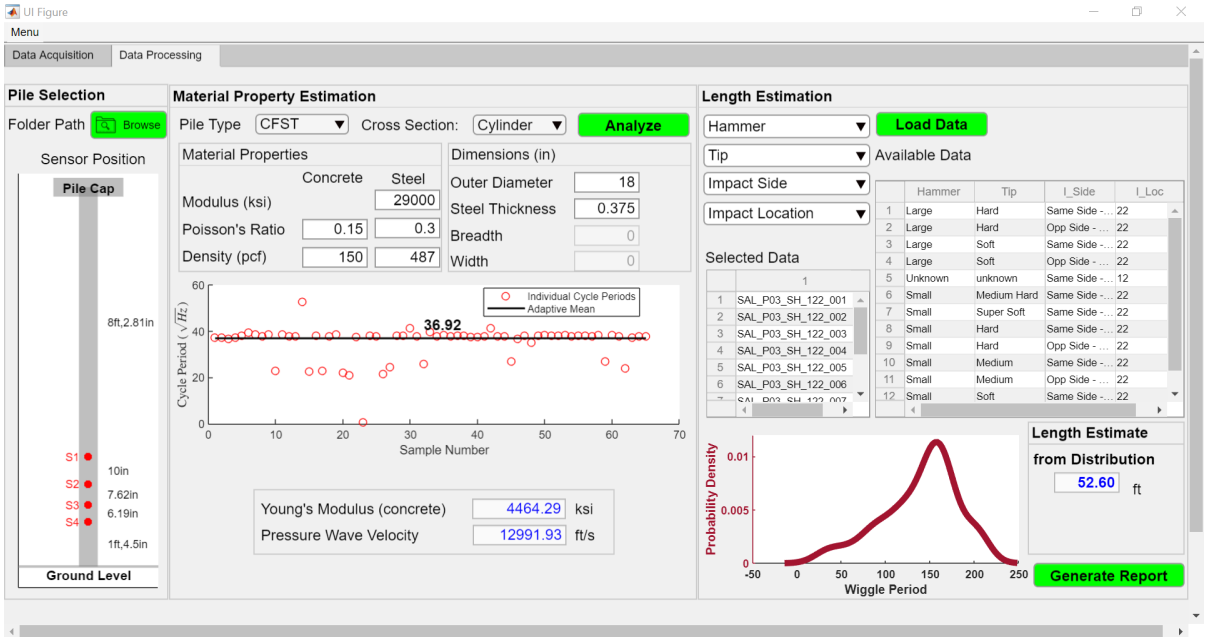

Figure 34: Salmon creek length estimate

Gold Creek

Gold Creek piles were similar in cross section to the Lemon and Salmon Creek piles with an outer diameter of 18 in and is shown in Figure 35. This site had a large influence of tidal cycles and significant amount of barnacles on the pile. The barnacles had to be scraped off

the pile surface before grinding and installing the sensors for data acquisition. Data processing steps 1 and 2 are shown in Figure 36. The main difference between the other piles tested was the significantly longer exposed length (almost 18 ft). This longer exposed length leads to more interference with the top reflections as the period oscillation from top reflection are smaller and comparable to the wiggle period from the bottom. Nevertheless, the EDAR plots obtained showed visible difference from the other piles with significant activity in the EDAR plots. The pile length is estimated to be large, 86 ft, as shown in Figure 37.

(a)

(b)

Figure 35: Gold creek bridge (a) site and (b) pile tested

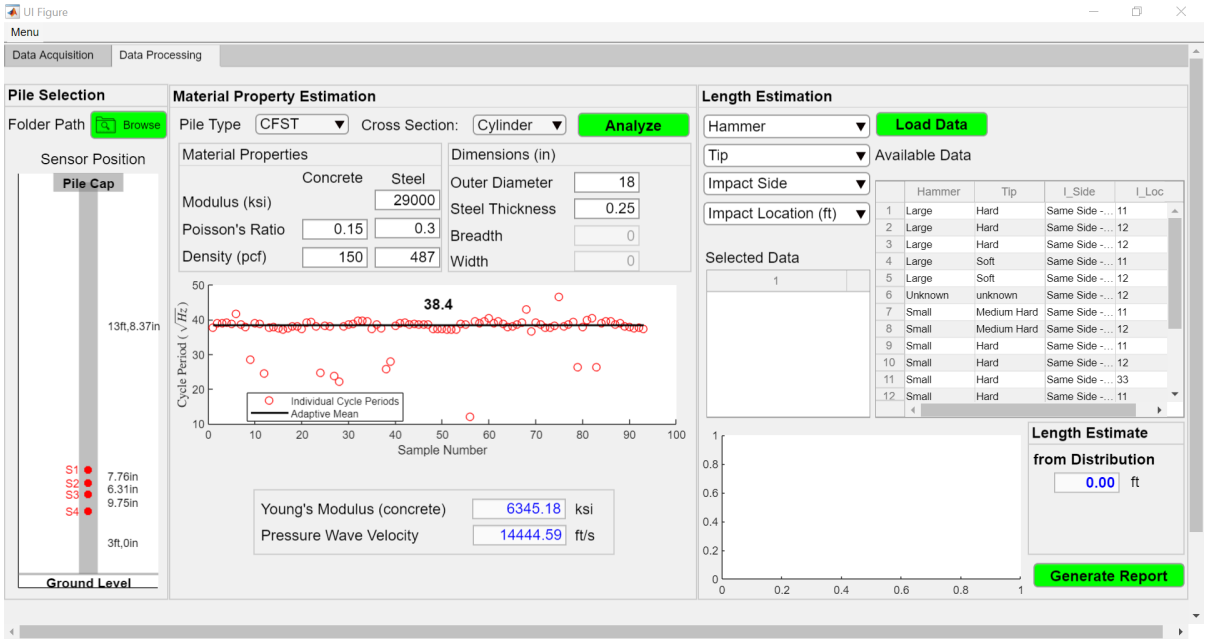

Figure 36: Gold creek data procesing steps 1 and 2

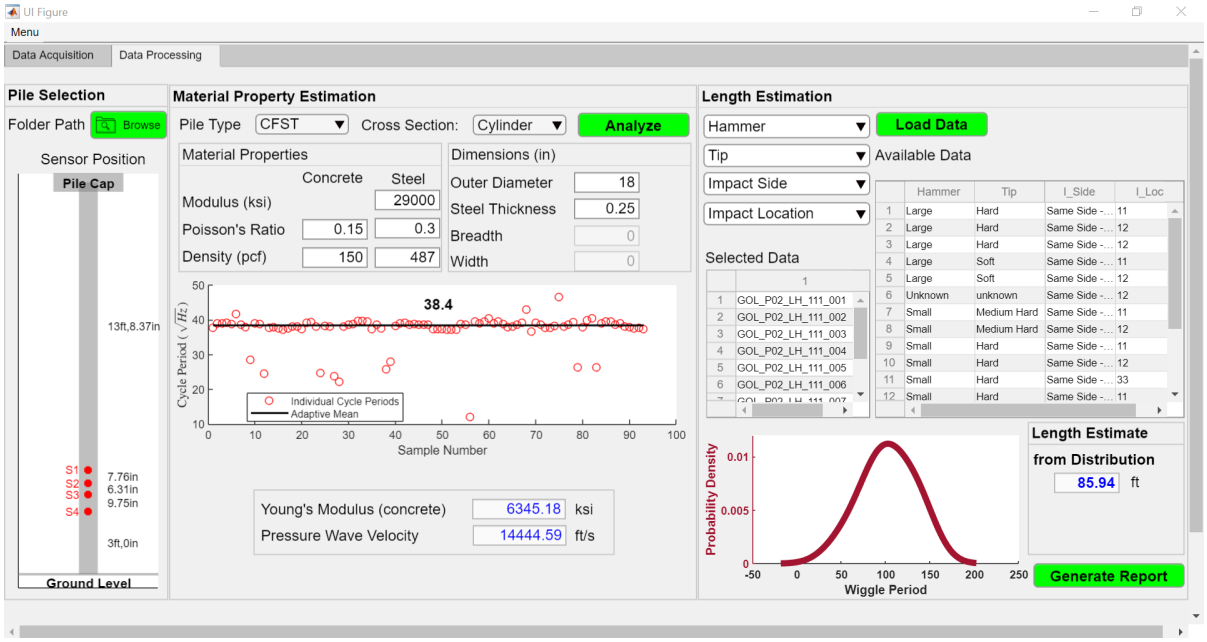

Figure 37: Gold creek length estimate

Chapter 4: Conclusions

Summary

A new methodology called Effective Dispersion Analysis of Reflections to estimate the pile length is developed. EDAR software for data acquisition and processing is developed for seamless application of the EDAR methodology in the field. The method was successfully evaluated in the laboratory conditions with length estimates consistently within 5% error (shown in appendix B). Modifications to the EDAR methodology based on field testing data resulted in length estimates within 10% error margins whenever good data is recorded (see Appendix C for details). In addition to providing length estimates, EDAR also estimates some of the material properties of the pile, e.g. modulus of the concrete inside a CFST pile.

Instructions for EDAR software along with example analyses are presented in this report. Currently, successful application of EDAR methodology is dependent on pile, site and impact characteristics. EDAR was used to successfully estimate pile lengths at many sites but failed to provide reliable length estimates at two sites. Even though it is known that impact characteristics influence the data collected, specific conclusions have not been established. But due to the ease of conducting the test, and portable nature of equipment, data is collected for a variety of impact characteristics to maximize the success percentage of the methodology. The methodology requires user intervention to obtain accurate length estimates.

Current Limitations and Future Work

EDAR technology has been tested for CFST piles, and some concrete piles in North Carolina. EDAR has been tested only in unfrozen soil conditions. It should not be used in frozen conditions without further research into the effect of the interaction between the pile and frozen soil on wave reflections. While the methodology is applicable in theory to other pile types, we do not recommend using it until further research is conducted. Specifically, the interaction between the soil and pile may need to be investigated for both H and timber piles, due to complicated geometry and impedance differences respectively. Given that timber deteriorates differently from concrete, timber piles may require further investigation to ensure that EDAR is adjusted as needed before routine application.

While EDAR was successful for driven piles with diameter less than two feet and depth less than 90 ft, further research is needed before it can be applied to drilled piles, especially with larger diameters and longer depths.

Finally, current EDAR software requires expert user intervention to pick the frequency range for analysis of wiggles. It is recommended that automation of the methodology be explored using advanced techniques such as statistical machine learning to not only eliminate the need for expert user, but also improve the objectivity and confidence of the length estimates, while providing reliability estimates that would help in informed decision making related decommissioning, repair or retrofit.

Appendix A: Testing Equipment

The main components required for the accurate measurement of pile response are, accelerometers, data acquisition system (DAQ), processing center (computer or tablet), accessories to connect the systems and a hammer to impact the pile and generate a response in the desired frequency range. A typical setup with all the components is shown in Figure 27. A windows-based tablet computer is used to acquire and power the equipment for testing. Thus, the entire system is very portable and does not require any external power, which makes it easier to test in the field. Extensive research was conducted on the available data acquisition system technology and accelerometers and the following were chosen based on the key aspects described.

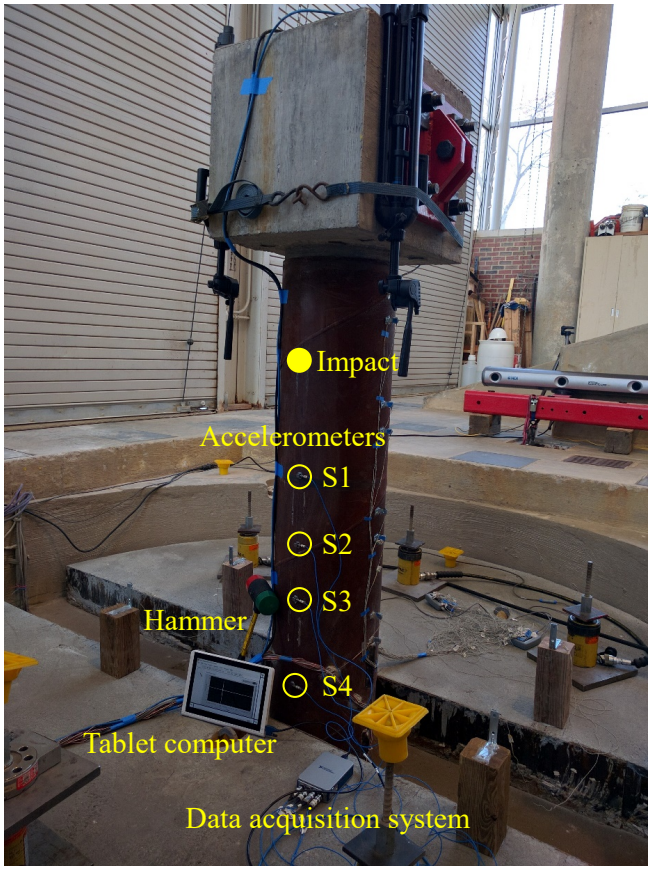

Figure 38: Typical setup and equipment (S#= sensor site)

Accelerometers

The sensors used to measure the response of the pile to the hammer impact were piezoelectric accelerometers. When stress is applied on the piezoelectric crystal, a high impedance electric charge is produced proportional to the stress applied, which is caused by the acceleration. The main characteristics that need to be considered before selecting an accelerometer are sensitivity, bandwidth and mounting, which are described below.

Sensitivity of an accelerometer is given at a specific reference frequency and is the factor that is used to convert voltage into acceleration. It is generally given in units of mV/g and the output voltage of the accelerometer is given by the product of acceleration and sensitivity. Sensitivity has an inverse relationship with the acceleration measurement range of the sensor. Thus, typically, lower sensitivity accelerometers are used to measure high amplitude and vice versa. Further, sensors must be selected based on the amplitude of the acceleration that will be generated from a hammer impact in order to avoid them from overloading.

Bandwidth is the range of frequency that can be measured with high accuracy using a specific accelerometer. This is important as the sensors need to be selected based on the application under consideration and the frequencies excited. In the context of EDAR, one needs to ensure that the bandwidth should include the range of frequencies where wiggles are expected. In many laboratory and field tests performed as a part of this research, this range is typically between 500 Hz and 3000 Hz.

Proper mounting of the sensors is critical to acquire accurate pile response in the entire range of frequencies where wiggles are expected. Several mounting methods are considered, e.g. handheld, magnetic or adhesive, can be used. Handheld can measure only specific frequency ranges generally between 500Hz and 1000Hz and is mostly used in hard to mount application and initially identify potential location where the sensor can be permanently mounted. Magnetic mounting is a convenient means of attaching the sensor, but the choice of magnet and mounting surface are critical for reliable measurements. Adhesives can provide both temporary and permanent mount based on the choice of adhesive (wax, hot glue and super glue) and generally provide better high-frequency response. These require minimum preparation of the surface and often provide reliable connection to the structure. Based on these advantages, adhesive mounting was chosen for EDAR application. Hot glue was used in laboratory setting and sensors with stud mounts were used in field setting with super glue.

Single-axis accelerometer shown in Figure 28 were used after taking into consideration all the above characteristics and its specifications are shown in Table 11. 353C33 can be stud mounted which makes it convenient to be used with super glue adhesive mounting. The accelerometers are connected to the DAQ using low-noise coaxial plug to BNC plug cables (PCB 003C10) which come bundled with the sensors.

Figure 39: PCB 353C33 Accelerometer

Table 6: Accelerometer specifications

Property	353C33
Sensitivity	100mV/g
Measurement Range	50 g
Frequency Range	0.5 to 10000 Hz
Broadband resolution	0.00015 g rms
Transverse Sensitivity	≤ 5%

Data Acquisition System (DAQ)

The main purpose of a data acquisition is to covert the analog signal from the sensors into digital data which is done with the help of an analog to digital converter (ADC). Four channel DAQ, NI9234 from National Instruments with a 24 bit ADC resolution and 51.2 KS/s sampling rate was selected for this application. These DAQs are directly compatible with accelerometers and powered through USB connection to the computer. LabVIEW software is used to control the DAQ in the computer. Based on the sensors used and experimental requirements, the maximum frequency of interest was around 10 kHz. Based on the Nyquist theorem, a minimum of 20 kHz sampling rate is required. Using NI9234 the response was oversampled at the maximum rate of 51.2 kHz which reduces the signal-to-noise ratio of the signal.

Signal Processing: One of the important aspect for obtaining better results is the handling of noise in the system. Every system will encounter noise of different origins, which cannot be avoided. One way to overcome this is to improve the signal to noise ratio (SNR). This can be done by oversampling during the test or later using specific noise filtering techniques. Pile response is measured only for a short time, typically 2 to 4 seconds, and the waves might not be attenuate completely within this time. Since, the data is predominantly processed in the frequency domain, an exponential window [1] is applied which reduces the noise in the frequency domain. Further, once the EDAR plot is obtained, it can be smoothed to facilitate easy peak picking for estimating the wiggle periods. All this is done internally in the application.

Hammer

Multiple hammers with different sizes and interchangeable rubber tips of varying hardness, as shown in Figure 29, were used to impact the pile. Several factors such as the hammer weight, tip size (diameter), pile material and tip hardness play a key role in the frequency content generated on impact. Inherently, the process of impacting with a hammer is a nonlinear and localized phenomenon affected by surface interactions. Quantitative understanding of the impact characteristics would require a deeper knowledge of both hammer and structure properties which are often variable and unavailable; characterizing these properties would be more complicated than the main objective of pile NDE [2]–[4].

Thus, a more qualitative approach based on the frequency response obtained from the hammer impact was used to study the effect of different hammer sizes and tips through which the recommendations were specified in the procedure. Six hammer tips have been used during the testing in the laboratory as well as the field tests. These tips include the hard (LH) and soft (LS) tips of the large sledge hammer and Hard (SH), Medium Hard (SC), Medium (SM) and Tough (ST) tips of the small sledge hammer. Specifications about all the hammers used are presented in Table 12.

Table 7: Hammer specifications

Hammer/Specification	Mass (kg)	Head Diameter (cm)	Measurement Range
Large Sledge Hammer	5.5	7.62	±22240 N
Small Sledge Hammer	2	6.35	NA

Figure 40: Different hammers used for testing

Appendix B: Theory and laboratory validation of EDAR Methodology

This appendix represents a publication resulting from the research [5].

Introduction

Even after more than two decades of research and implementation ([6] ,[7]), the National Bridge Inventory reports that the United States has about 28,000 bridges with unknown foundation depths in 2016 that could be potentially susceptible to scour. The scour vulnerability of a bridge cannot be determined until the embedded depth of the foundation is known, and records that contain the total lengths of piles do not always exist. Thus, in order to evaluate the potential for scour, nondestructive evaluation (NDE) techniques are typically needed to estimate the length of embedded piles.

One class of NDE methods for pile foundations is borehole techniques, which include parallel seismic, cross-hole sonic, borehole sonic, borehole radar, and borehole ultrasonic methods as well as induction testing and borehole magnetic testing for steel piles (see [6][8]–[13] for examples). All these tests require either a borehole alongside the pile foundation or a pre-installed test pipe in the pile. They also require expensive equipment along with an experienced user to interpret the results. Even though these techniques are reliable and applicable to a vast number of situations, using borehole methods to test a large group of piles is not practical due to excessive costs and site limitations.

The other class of NDE methods is surface-based techniques, which do not require drilling boreholes. These methods include sonic echo, impulse response, ultra-seismic, and bending wave (short kernel) methods. Levy [14] and Dunn [15] pioneered work that led to the development of the sonic echo and impulse response techniques. Both methods are based on generating a longitudinal wave using a hammer impact on the top of a pile and analyzing the obtained response in the time domain for the sonic echo method and in the frequency domain for the impulse response method. Specifically, in time domain length estimates are obtained by identifying peaks associated with initial and reflected waves. This methodology became more prevalent after the advent of digital signal processing, starting with the work of Rausche et al. [16].Several researchers have continued to use this methodology since then for a variety of situations [17]–[22]. Recent work by Rashidyan [23] investigated sonic echo type of methods for existing timber piles without top access (by vertically impacting on a metal block attached to the pile); however, other researchers determined that this method is not successful when testing steel H piles[13]. An extension of the sonic echo method using multiple sensors on the pile side, known as the ultra-seismic method, also has been established. All these surfaced-based methods rely on producing a wave that is dominated by longitudinal mode. However, due to the inaccessibility of the pile top, this process remains difficult because other types of waves (e.g., flexural waves) can also play a part in the data collected.

In order to try to solve the problems associated with an inaccessible pile top, Holt and Douglas first conceived the idea of using lateral impacts to induce flexural waves rather than using the impact-echo method to induce conventional longitudinal waves [24]. A lateral

impact imparts most of the energy through bending waves that are dispersive in nature thus, it is essential to deal with dispersive flexural waves. To this end, Holt and Douglas [24] introduced the bending wave or short kernel method to process responses from dispersive flexural waves to obtain travel-time information, which attempts to delineate the peaks through convolution, thereby enabling the application of simple travel-time algorithms. Although this idea is innovative, the choice of short kernel and subsequent peak selection is complicated, even for experienced users, resulting in subjective estimates with large errors (see e.g., [25]–[27]). Other techniques, such as Hilbert-Huang transform or continuous wavelet transform have been used by Subhani et al. [27], Farid [28] and Sheng-Hugo et al. [29]. All these techniques are based purely on signal processing and do not explicitly incorporate the underlying dispersion properties of the generated waves that could be utilized constructively to develop pile length estimation techniques.

Given both the advantages of using side impacts and the limitations associated with the existing processing techniques for flexural waves, we propose a new signal processing technique we call 'effective dispersion analysis of reflections' (EDAR). EDAR extracts length information by carefully considering the physics of wave dispersion, which has been ignored thus far in relevant methodologies. The experimental set-up for EDAR is identical to flexural wave testing, but the critical data processing step is fundamentally different and built on robust mathematical analysis that is, in turn, built on the precise dispersion relation that represent wave physics. We verified the proposed methodology using synthetic data and validated it using laboratory experiments.

The outline of the rest of the paper is as follows. Section 2 contains the problem definition and experimental set-up. A detailed derivation of the EDAR technique is given in Section 3, starting from simple longitudinal waves and leading to more complicated flexural waves. Section 4 contains the results from the laboratory validation effort, followed by conclusions in Section 5.

Problem Definition and Experimental Set-up

Pile foundations are made of various materials, such as timber, concrete, steel, or a combination thereof, and are either cast in place or driven deep into the soil. Many bridges have part of the pile exposed above the soil, terminating in the pile cap. The aim of this work is to estimate the embedded length of the pile using nondestructive testing. To achieve this aim, the pile foundation is excited by imparting a sharp strike using a hand-held hammer, and the response is measured at a minimum of two locations in the foundation using sensors such as accelerometers or geophones. Depending on the location and type of excitation imparted to the pile, several types of waves can exist, such as longitudinal, flexural, and high order guided waves. Fig. 1 presents a typical pile subjected to lateral impact, which is also the experimental set-up used in this study.

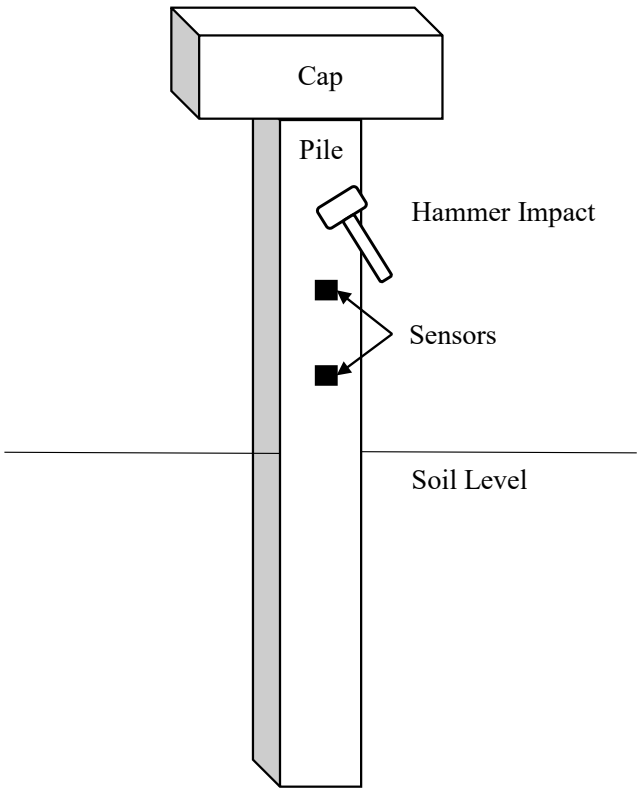

Fig. 1 Pile and experimental set-up schematic

We employed EDAR to process responses measured at two sensor locations along the length of a pile. EDAR can be applied for both longitudinal and flexural waves. Similar to the aforementioned surface-based methods, EDAR requires access to the exposed portion of the pile to record accelerations or velocity from a hammer impact at a minimum of two locations along the length of the pile. The major contribution of this paper (and how it differs from earlier methods) is the way the data are processed to estimate the length of a pile. Section 3 discusses the concept behind processing the data using the EDAR methodology.

Effective Dispersion Analysis of Reflections (EDAR): Theory

The fundamental concept of EDAR is based on the difference of individual phases between the responses measured at the two sensor locations. The basic theory is explained for both longitudinal and flexural waves, followed by verification using synthetic data and validation using laboratory experiments. EDAR presents a unique way to process the same response data that can be obtained from the ultra-seismic or short kernel (bending wave) methods to estimate the length of the pile by incorporating the physical dispersion characteristics of wave propagation.

The (frequency-dependent) phase difference between the responses at the two sensor locations in the frequency domain is given by,

$$P_d = \text{Imag}\left(\log\left(u_2(\omega)\right) - \log\left(u_1(\omega)\right)\right) , \quad (1)$$

where $u_1(\omega)$ and $u_2(\omega)$ are the Fourier transforms of the responses (displacements, velocities or accelerations) obtained at the two sensor locations, respectively. The phase difference between the responses obtained at the two sensor locations in the frequency domain contains the product of theoretical wavenumber (k) and the lengths associated with the pile. Generally, the phase depends on the distance the wave has traveled before and after reflections from the various boundaries in the structure. Section 3.1 explains the characteristics of the phase difference and extraction of the pile length using simple theoretical models: Section 3.1.1 discusses wave propagation without reflections with the help of dispersion analysis, and Section 3.1.2 discusses the effects of the reflections and introduces the concept of EDAR plot.

Longitudinal waves in bar

Propagation without reflections

Longitudinal or axial waves are nondispersive in nature and thus exhibit minimal variation in the initial waveform observed in the time domain. Fig. 2 shows the simplest case of an infinite bar in which a propagating wave traveling from left to right is encountered once by the two sensors.

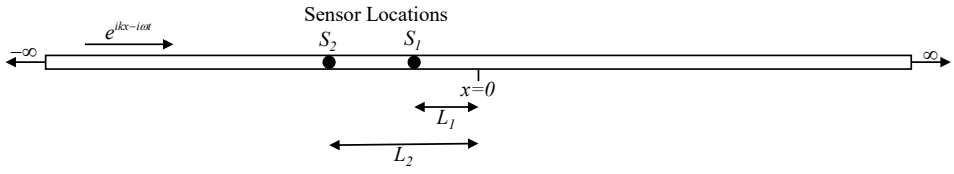

Fig. 2 Schematic of infinite bar

The second order differential equation describing the axial wave propagation in a homogeneous, linearly elastic rod with Young's modulus E and density ρ is given by:

$$-E\frac{\partial^2 u(x,t)}{\partial x^2} + \rho\frac{\partial^2 u(x,t)}{\partial t^2} = 0 . \quad (2)$$

By Fourier transforming in time, the above equation can be written in frequency domain as,

$$-\frac{d^2 u(x,\omega)}{dx^2} - c_b{}^2\omega^2 u(x,\omega) = 0 , \quad (3)$$

where ω is the temporal frequency, c_b is the bar wave velocity and is given by $\sqrt{E/\rho}$, E is Young's modulus, and ρ is density. The solution of the equation in frequency domain takes the form,

$$u(x,\omega) = Ae^{ikx}, \tag{4}$$

where k is the wavenumber . The wavenumber can be determined from the frequency by substituting Equation (4) into Equation (3), which gives the dispersion relation expressed as Equation (5).

$$k = \frac{\omega}{c_b} \tag{5}$$

Substituting Equation (4) in Equation (1) results in the phase difference:

$$P_d = k(L_2 - L_1) = k\Delta L \ . \tag{6}$$

Thus, the phase difference is a product of the theoretical wavenumber (k) and the distance between the sensors (ΔL). Practically, the phase difference that is calculated from the sensor responses results in wrapping between $-\pi$ and π .

An important aspect of this method is to plot the phase as a function of a newly defined quantity called the 'effective wavenumber' (k_e), which is the wavenumber scaled by a material constant. Such scaling eliminates the need for the knowledge of material properties in estimating the length in this particular case (as well as in the more complicated case of Bernoulli-Euler beam theory in Section 3.2). In the specific case of a bar, because the theoretical wavenumber (k) in Equation (5) is directly proportional to the frequency, the effective wavenumber is simply defined as the frequency:

$$k_e^{bar} = \omega \ . \tag{7}$$

For reasons that will become clear after the reflections are analyzed in Section 3.1.2, the plot with the phase difference as the abscissa and the effective wavenumber as the ordinate is called the EDAR plot throughout the rest of the paper. The slope of the EDAR plot is governed by the distance between the sensors (ΔL) and the velocity of the wave propagation (c_b):

$$k_e^{bar} = \left(\frac{c_b}{\Delta L}\right) P_d \ . \tag{8}$$

The slope from Equation (8) would determine the value on the effective wavenumber axis at which the phase gets wrapped. The value at which the first wrapping occurs is called the cycle period (K_1) and is given by

$$K_I^{bar} = \frac{\pi c_b}{\Delta L}. \tag{9}$$

This is the first of the two periods associated with the phase and is a consequence of the initial arrival of the wave. Thus, the cycle is closely related to the time difference between the initial arrivals of the propagating wave at the two sensor locations. As an example, consider a model bar of infinite length with a wave propagation velocity of 1 m/s and lengths $L_1 = 3m$ and $L_2 = 3.5m$, thus making the distance between the sensors $0.5m$. Fig. 3 presents the effective dispersion plot that is obtained using the solution form in equation 3. The first wrapping of phase occurs at 2π, as is expected from Equation (9).

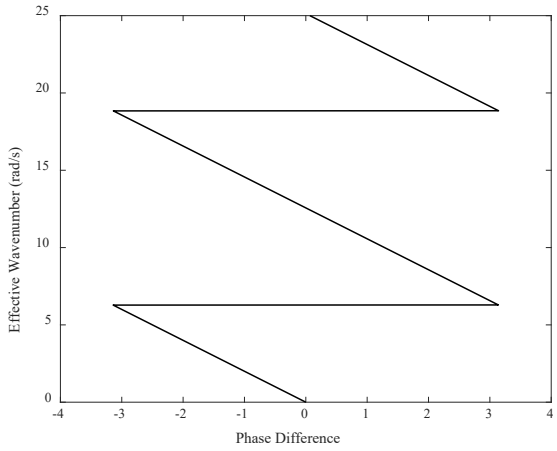

Fig. 3 Effective dispersion plot for infinite bar: phase difference vs. effective wavenumber

Effects of reflections and EDAR plot

Introducing a boundary at $x = 0$ makes the bar semi-infinite and results in a single reflection of the wave from the boundary; see Fig. 4 that assumes a wave traveling from negative infinity towards the boundary where it gets reflected.

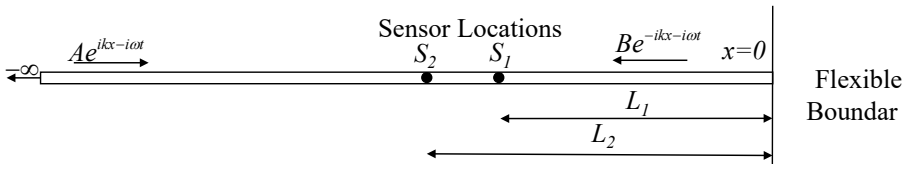

Fig. 4 Semi-infinite bar: single reflection

Without loss of generality, the displacement in the frequency domain anywhere in the bar can be assumed to be

$$u(x) = Ae^{ikx} + Be^{-ikx} \ , \tag{10}$$

where the first term on the right-hand side represents a forward propagating wave and the second term represents the reflected wave. Similar to the infinite case, a model bar with the same parameters are considered for a semi-infinite bar, but the displacement form in equation (10) is used to account for the reflection from the boundary (reflection coefficient of 0.5) that is introduced; Fig. 5 presents the resultant EDAR plot that is computed for a semi-infinite bar. In addition to the cycle oscillations that are similar to those found for the infinite bar, smaller oscillations can be observed with a smaller period in the semi-infinite bar. These small oscillations, called 'wiggles', are a consequence of the wave being reflected at the boundary and can be utilized to estimate the location of the boundary.

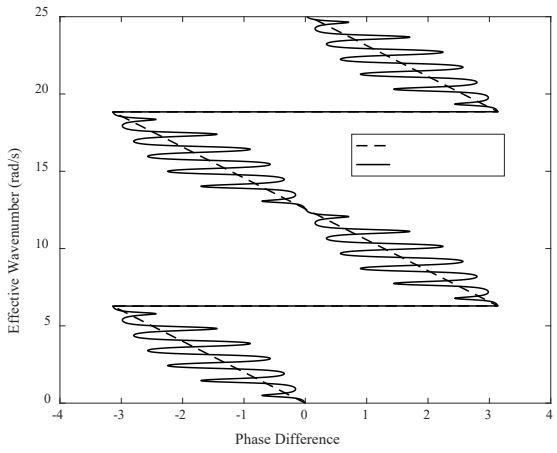

Fig. 5 EDAR plot for semi-infinite bar superimposed on infinite bar

The responses at the accelerometer locations S_1 and S_2 at distances L_1 and L_2, respectively, from the boundary are

$$u_1(L_1) = Ae^{ikL_1} + Be^{-ikL_1} \ , \tag{11}$$

$$u_2(L_2) = Ae^{ikL_2} + Be^{-ikL_2} \ . \tag{12}$$

Using these displacements, the phase difference can be calculated from Equation (1). The steps involved in calculating the phase difference analytically are shown here as Equations (13) through (15).

$$\frac{u_1}{u_2} = \left(\frac{Ae^{2ikL_1} + B}{Ae^{2ikL_2} + B} \right) e^{ik(L_2 - L_1)} \tag{13}$$

Taking the logarithm of the ratio shown in Equation (13) gives

$$log\left(\frac{u_1}{u_2} \right) = ik(L_2 - L_1) + log(Ae^{2ikL_1} + B) - log(Ae^{2ikL_2} + B) \ . \tag{14}$$

The imaginary part of Equation (13) is the phase difference. The imaginary part of the logarithm of a complex number is the argument of the complex number and thus

$$P_d = \underbrace{k(L_2 - L_1)}_{b_1} + \underbrace{\tan^{-1}\left(\frac{A\sin(2kL_1)}{B + A\cos(2kL_1)} \right)}_{b_2} - \underbrace{\tan^{-1}\left(\frac{A\sin(2kL_2)}{B + A\cos(2kL_2)} \right)}_{b_3} . \tag{15}$$

The periodic nature of P_d can be explained from the three terms b_1, b_2, and b_3. The first term is exactly the same as the one obtained for the infinite bar and, along with phase wrapping, gives rise to the cycles shown in the EDAR plot in Fig. 3. The terms b_2 and b_3 are responsible for the smaller oscillations or wiggles observed in Fig. 5. The trigonometric functions b_2 and b_3 can be shown to have a period of π/L_1 and π/L_2, respectively. Because the distance between the sensors is small compared to the length of the pile [L_1 is approximately equal to L_2 that is approximately equal to L^e], L^e is the distance between the midpoints of the sensors to the boundary. Thus, the period of the last two terms in Equation (14) in the theoretical wavenumber (k) space is given by

$$K_R^{bar} = \frac{\pi c_b}{L^e} \ . \tag{16}$$

One of the main practical concerns here is obtaining an accurate estimate of the wave velocity for the system under consideration. Often, pile foundations are old and deteriorated and knowledge about the construction material is hard to obtain. Examining the ratio of the cycle and wiggle periods helps resolve this issue. The ratio of the cycle and wiggle periods is

$$\frac{K_I^{bar}}{K_R^{bar}} = \frac{\pi c_b / \Delta L}{\pi c_b / L^e} = \frac{L^e}{\Delta L} \ . \tag{17}$$

Once the cycle and wiggle periods are calculated from the EDAR plot, the only unknown is length L^e, which can be computed without need for any other information about the pile. Because the plot effectively captures (a) the effect of the dispersion relation (simple in this case but can be more complicated for beams) and (b) the effect of reflections from the boundary, the plot and the ensuing analysis that result in Equation (16) are referred to as the 'effective dispersion analysis of reflections', hence, 'EDAR'.

The proposed EDAR technique is similar to the travel-time approach for nondispersive systems, where the travel time between sensors can be used to compute the wave velocity, which in turn can be used to compute the unknown boundary locations based on the arrival times of the reflections. The key advantage of the proposed EDAR method is that it can be extended to dispersive wave propagation, where travel-time approaches fail due to the significant distortion of the waves that is caused by dispersion. Section 3.2 provides details regarding this extension of EDAR.

Flexural waves in beams

Bending waves can be generated by a lateral impact to the pile. The test set-up for bending waves is exactly the same as for longitudinal waves and the responses are likewise measured at a minimum of two sensor locations. There are two main differences between the waves propagating in a bar and a beam. Firstly, along with the propagating waves, there exists evanescent waves, which decay exponentially. Due to this decaying nature, the effect of evanescent waves on measured reflections is negligible and does not have a significant effect on EDAR processing. Secondly, the propagating waves are dispersive in nature as explained Equations (18) through (20) which is a critical for the formulation of the EDAR procedure.

The governing differential equation for a homogeneous, linearly elastic Bernoulli-Euler (BE) beam is given by

$$EI\frac{\partial^4 v}{\partial x^4}+\rho A\frac{\partial^2 v}{\partial t^2}=0, \tag{18}$$

where v is the transverse displacement. Similar to the case for a bar, the general solution for Equation (18) can be given by

$$y=e^{ikx-i\omega t}\ . \tag{19}$$

Substituting Equation (18) in Equation (17) we get the dispersion relation between wavenumber and temporal frequency given by

$$k=\sqrt{\frac{\omega}{c_b r}}\ , \tag{20}$$

where c_b is the bar wave velocity and $r=\sqrt{I/A}$ is the radius of gyration. The phase velocity can be calculated from Equation (20); clearly frequency-dependent, resulting in wave dispersion, which distorts the waveform as it propagates through the length of the beam. This wave distortion makes peak-picking difficult and often impossible, thus making travel-time approaches difficult.

The dispersion relation shown in Equation (20) is the key to defining the effective wavenumber for EDAR, which is obtained by scaling the wavenumber. Specifically, the

material constants and cross-sectional properties are dropped from Equation (20) to define the effective wavenumber:

$$k_e^{BE} = \sqrt{\omega} \ . \tag{21}$$

The above choice facilitates the estimation of length without prior knowledge about the material constants, as discussed below. Equation (21) also makes the relation between the phase difference and effective wavenumber linear, and thus, all the expressions relating to EDAR obtained for a bar become applicable to a beam. The cycle and wiggle periods computed using the above definitions are

$$K_I^{BE} = \frac{\pi\sqrt{c_b r}}{\Delta L} \ , \tag{22}$$

$$K_R^{BE} = \frac{\pi\sqrt{c_b r}}{L^e} \ . \tag{23}$$

Similarly, taking the ratios of the two periods, a length estimate of the pile (L^e) can be obtained as

$$L^e = \frac{K_I^{BE}\Delta L}{K_R^{BE}} \ . \tag{24}$$

Once the responses at the sensor locations are obtained, Equation (23) requires only the cycle period, wiggle period, and the distance between the sensors to obtain an estimate for the length of the member. The important modification is the definition of the effective wavenumber as the square root of the frequency, thus making the wiggle period constant and facilitating the extension of the bar length estimation shown in Equation (16) to the beam length estimation shown in Equation (23).

This method pertains specifically to BE beam theory. BE beam theory is simple, but not accurate for higher frequencies where the wavelength is of the same order as the beam thickness. However, the EDAR methodology can be extended to more sophisticated models, such as Timoshenko beam theory. The governing equation for a Timoshenko beam with Young's modulus E, density ρ, shear modulus G, area A, moment of inertia I, and Timoshenko shear coefficient κ is

$$\frac{EI}{\rho A}\frac{\partial^4 y}{\partial x^4} - \left(\frac{I}{A} + \frac{EI}{GA\kappa}\right)\frac{\partial^4 y}{\partial x^2 \partial t^2} + \frac{\partial^2 y}{\partial t^2} + \frac{\rho I}{GA\kappa}\frac{\partial^4 y}{\partial t^4} = 0 \ . \tag{25}$$

The corresponding dispersion relation is

$$\frac{EI}{\rho A}k^4 - \left(\frac{I}{A} + \frac{EI}{GA\kappa}\right)\omega^2 k^2 - \omega^2 + \frac{\rho I}{GA\kappa}\omega^4 = 0 \ . \tag{26}$$

EDAR can be used with any model for which the dispersion relation can be obtained either theoretically (Timoshenko) or numerically (guided wave propagation) by defining the effective wavenumber as the actual wavenumber obtained from the respective models. As models become more sophisticated, they more closely represent actual wave physics but at the same time lack the simplicity of the bar or BE beam model. Different material properties regarding structure might be needed as opposed to not requiring any material properties as is the case with the simpler BE beam model. The EDAR procedure must be used cautiously, paying utmost attention to the frequency content under consideration and the validity of the underlying models. At lower frequencies, use of BE beam theory might be justified, but at higher frequencies, more robust models, such as Timoshenko beam theory or even more sophisticated models based on guided wave theory, may be required.

Synthetic examples for EDAR verification

In this study, a finite BE beam, with square cross section, was modeled with half spaces (HS) on the top and bottom with variable material properties to control the reflection coefficients and to treat reflections from different boundaries separately. Material damping was introduced by using complex values for the modulus of the pile (imaginary part was taken to be 5% of the Young's modulus). Table 1 presents the model BE beam properties and Fig. 6 presents a schematic of the BE beam model with lengths.

Table 8 Model Bernoulli-Euler Beam Properties

Property	Value
Young's Modulus	35 GPa
Density	2400 kg m/s^2
Poisson's Ratio	0.1
Cross section (square)	0.3048 m x 0.3048 m

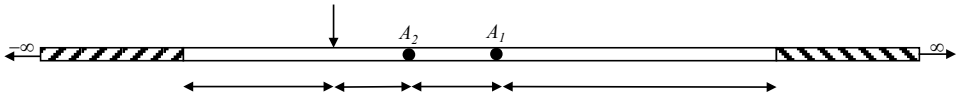

Fig. 6 Schematic of Bernoulli-Euler beam model

Example 1: The top HS is modeled such that it matches the beam to prevent reflections from the top. The bottom HS modulus is a large value to simulate a fixed end. Fig. 7 presents the EDAR plot obtained from the BE model and Table 2 presents the BE model beam length estimates.

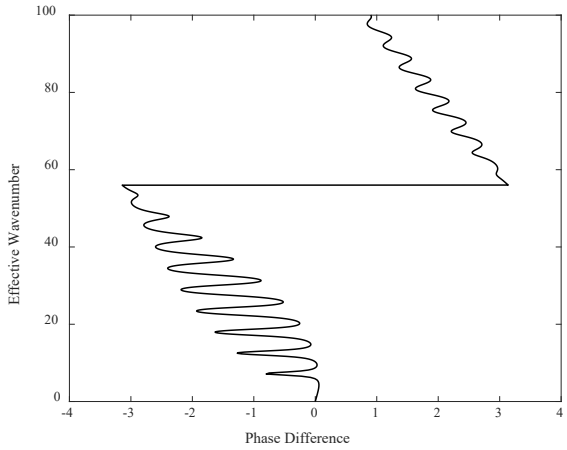

Fig. 7 EDAR plot for synthetic Bernoulli-Euler beam experiment involving bottom reflections

Table 9 Bernoulli-Euler Beam Model Length Estimate

Cycle Period	Wiggle Period	Distance between sensors	Estimated Length (m)	Actual Length (m)	Error
64.49	6.2	0.4	5.66	5.7	-0.7%

Example 2: Both the top and bottom HS moduli are set to a large value to simulate a beam with fixed boundary conditions on both ends. Fig. 8 presents the EDAR plot obtained from the BE beam model.

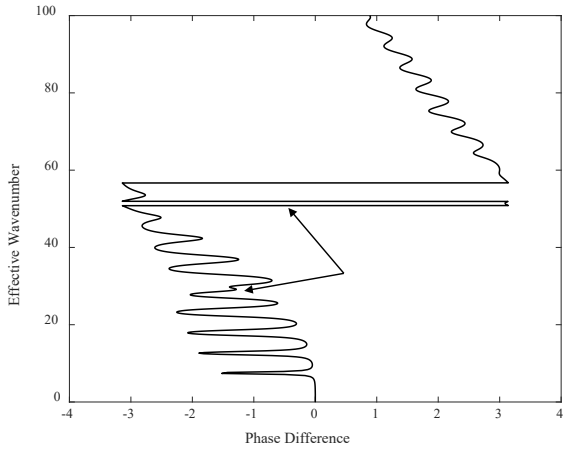

Fig. 8 EDAR plot for Bernoulli-Euler beam model: bottom and top reflections

Fig. 8 shows the effect of the top reflection in the EDAR plot. Even though the top reflections disturbed the wiggle, the important aspect to note is the distinctive characteristics of the disturbances. They do not look similar to wiggles and can be ignored while calculating the wiggle period. This difference between the disturbances shown and wiggles is a consequence of the impact locations and the wave propagation direction. By using the unaffected wiggles in the EDAR plot, similar length estimates, as shown in Table 2, were obtained. Depending on the length to the top of the pile, there can sometimes be interference between the top effect and cycle frequency. This situation can be avoided by using multiple distances between the sensors, which we did during actual experimentation. We used four sensors instead of the two sensors required for EDAR. In this way, we built redundancy into the test and thus the cycle and wiggle periods can be obtained from multiple sensor combinations.

Experimental Validation of EDAR

Following the successful verification of EDAR using synthetic data, we performed experiments at the Constructed Facilities Laboratory at North Carolina State University (NCSU) to validate the proposed EDAR. Fig. 9 shows one of the concrete filled steel tube (CFST) piles, installed as part of a different project at NCSU, which we used for initial testing. Table 3 presents the properties of the CFST.

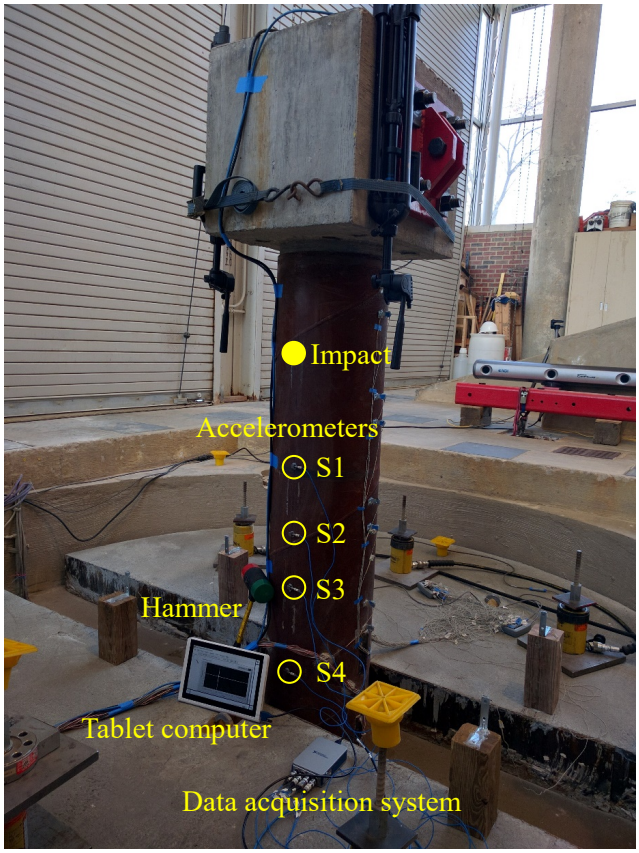

Fig. 9 Concrete filled steel tube tested at NCSU

Table 10 Properties of Concrete Filled Steel Tube

Property	Value (m)
Total Length	5.92
Embedded Length	4.17
Cap Dimensions	0.6096 x 0.4572 x 0.4572
Concrete Diameter	0.292
Steel Thickness	0.0064

Accelerometers from PCB (352C33) and a data acquisition system from National Instruments (NI9232) were used respectively for sensing and recording the responses of CFST to a lateral impact from a small sledge-hammer. The impact is applied between the pile cap and top sensor, maintaining sufficient distance from the top sensor to prevent any overload. Fig. 10 shows the equipment used for laboratory testing and Table 4 provides a summary of the equipment specifications.

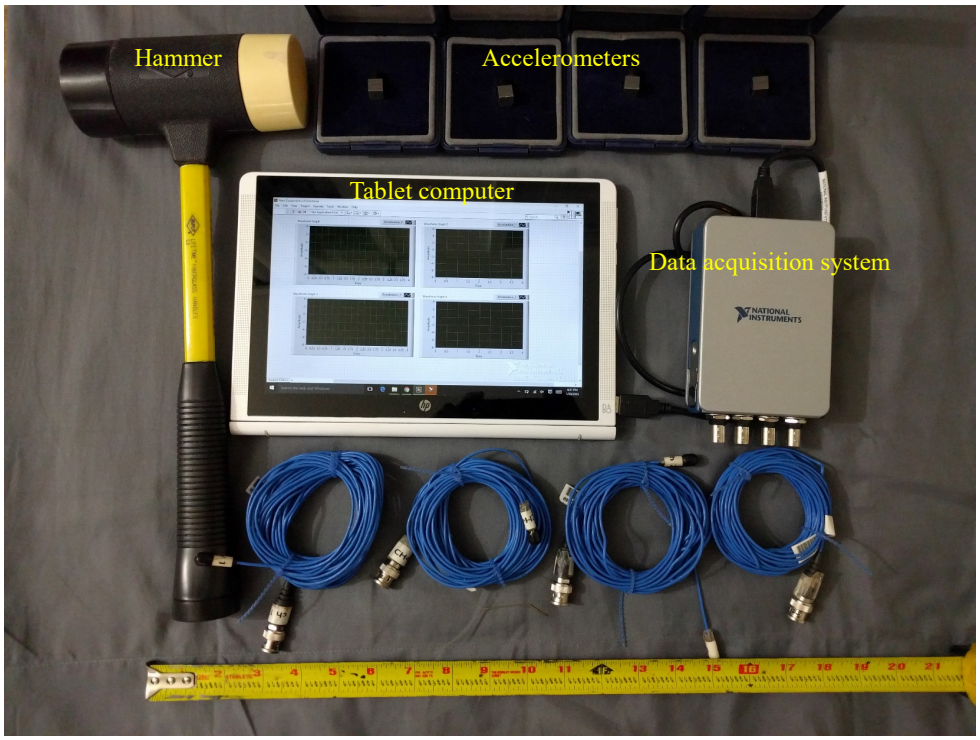

Fig. 10 Equipment used for EDAR testing

Table 11 Equipment Specifications

Equipment type	Model	Important specifications	
		Item	Range
Accelerometer	PCB 352C33	Frequency	0 to 10000 Hz
		Measurement Range	±50 g
		Sensitivity	100 mV/g
DAQ System	NI 9234 with USB chassis	Analog Input Resolution	24 Bits
		Sampling Rate	51.2 KS/s

Four accelerometers were used to build redundancy in the data obtained, giving six two-sensor combinations. The distances between the four sensors were 0.203, 0.152, and 0.254 m and are directly reflected in the cycle periods observed in the EDAR plots. Fig. 11 presents the time domain plots of the accelerations obtained at the four sensor locations. Examining these time histories indicate that there are no clear peaks associated with incident and reflected waves, owing to the dispersion associated with flexural waves.

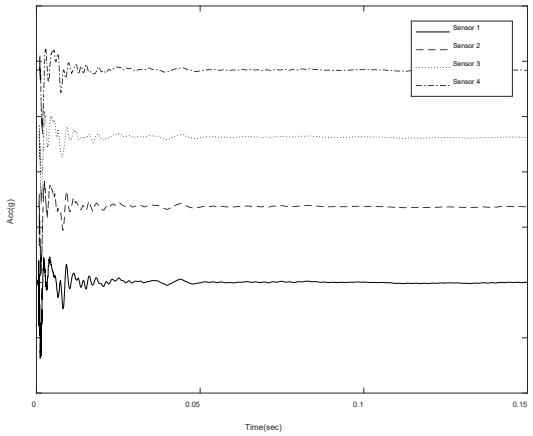

Fig. 11 Experimental response: time domain

Fig. 12(a) presents EDAR plots that clearly show the cycles and wiggles which are as expected from the theory presented earlier in section 3. Raw data from the tests were processed using an exponential window in the time domain to reduce noise effects and to facilitate peak-picking to find the wiggle period. The cycle and wiggle period were obtained as shown in Fig. 12(b).

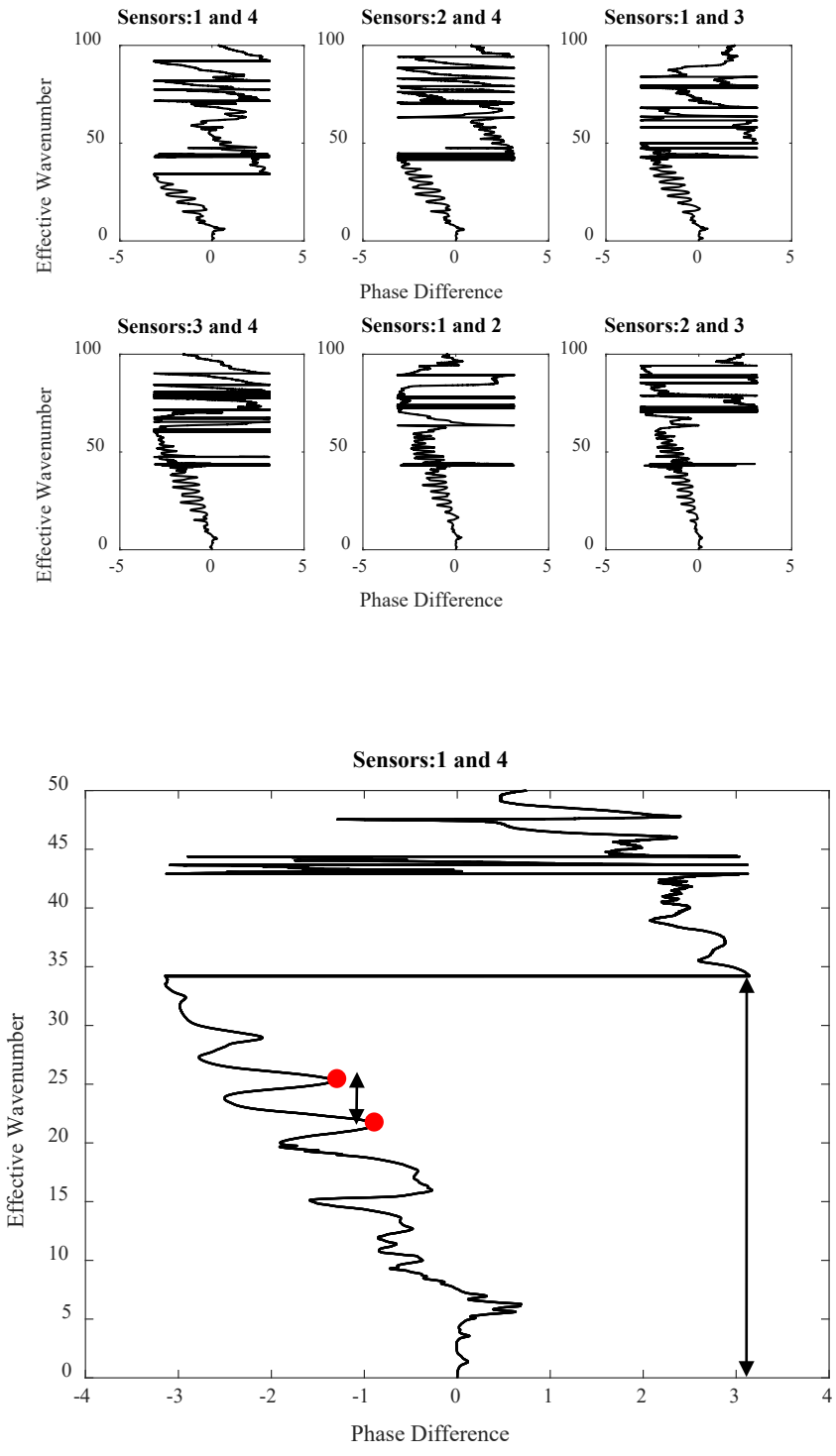

Fig. 12 (a) Representative experimental EDAR plots (b) Finding wiggle and cycle period from EDAR plot

Concrete with density = 2400 kg/m3, Young's modulus = 33.37 GPa, Poisson's ratio = 0.2 and steel with density = 7800 kg/m3, Young's modulus = 210 GPa, Poisson's ratio = 0.3 were used for computing the theoretical dispersion curves [30]. Fig. 13 presents the theoretical dispersion relation computed based on BE and Timoshenko beam theories.

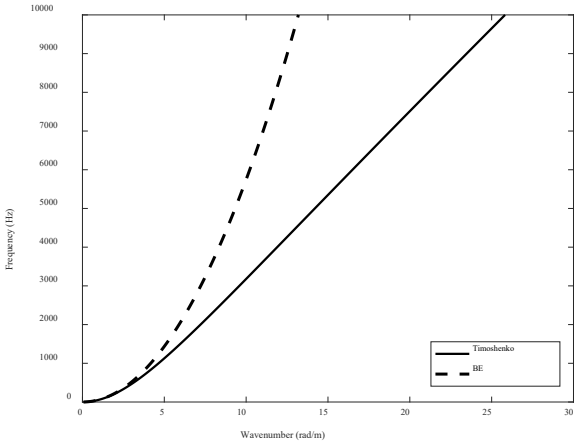

Fig. 13 Theoretical dispersion relation: Bernoulli-Euler vs. Timoshenko beam theories

It is well known that Timoshenko beam theory is more accurate than BE theory for higher frequencies, but at low frequencies the dispersion curves overlap for both models. Thus, using the lowermost wiggle in the frequency axis and cycle period between the farthest two sensors, a length estimate can be obtained.

Table 12 Length Estimate from First Observed Wiggle Using Bernoulli-Euler Beam Theory

Cycle period	Wiggle period from lowermost wiggle	Distance between sensors	Estimated length (m)	Actual length (m)	Error
34.18	3.63	.6096	5.74	5.92	3%

Even though the estimated length presented in Table 5 is close to the actual length, with an error of 3 percent, many wiggles can be observed at different levels on the theoretical wavenumber axis. Each of these wiggles were used to calculate the wiggle period and subsequently used to estimate the length. As explained earlier, the main difference between the BE and Timoshenko beam theories is the theoretical wavenumber axis, and thus, the cycle and wiggle periods are changed, as shown in Fig. 14. In Fig. 15, the length estimates obtained from each observed wiggle are plotted as a function of the frequency at each wiggle. Clearly, the BE beam theory estimates are a function of the frequency and increase as we move up the frequency. This frequency dependence is reduced greatly for estimates obtained using Timoshenko beam theory, and the average error percentage also is reduced significantly (see Table 6).

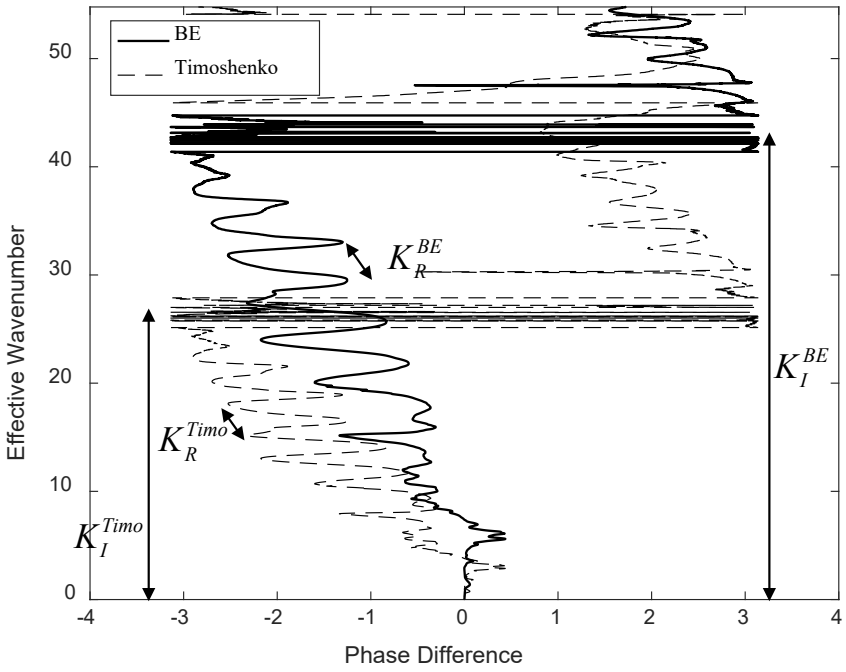

Fig. 14 Comparison of Bernoulli-Euler and Timoshenko EDAR plots

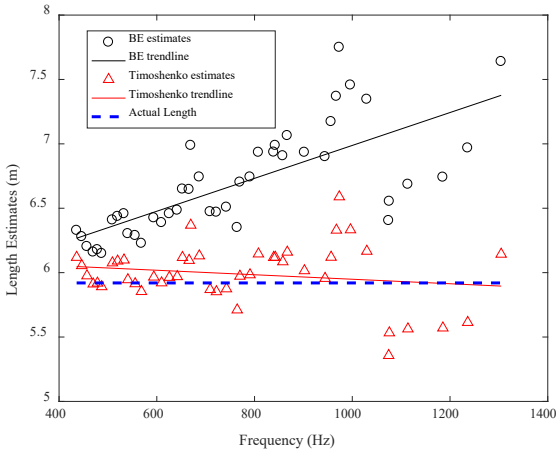

Fig. 15 Length estimates as a function of frequency

Table 13 Average Length Estimates

	Bernoulli-Euler theory	Timoshenko theory	Actual length (m)
Estimate (m)	6.69	5.99	5.92
Error	13%	1.18%	

Unlike Timoshenko beam theory, BE beam theory does not require any information about the pile properties to calculate the effective wavenumber defined in Equation(21). However, BE theory leads to a less accurate representation of the exact physical system, and thus, the resulting estimates are less accurate. Therefore, depending on the availability of material property estimates and location of the wiggles in the frequency axis, one of the two theories can be used to obtain the length. Note that only the relative value of shear stiffness compared to flexural stiffness is needed for Timoshenko beam theory; this value is often a function of Poisson's ratio, which tends not to change much.

In a more general sense, waves that propagate inside a pile are 'guided' waves owing to their three-dimensional nature and reflections from all the boundaries of the pile. Various research efforts conducted at Northwestern University by Finno [31], Hanifah [32], Chao [33], Wang [34], and Lynch [35] have considered the pile as a cylindrical wave guide to obtain the longitudinal, torsional, and flexural modes of vibrations and corresponding dispersion relation. The predominant modes in longitudinal and flexural waves are the first modes, namely L(0,1) and F(1,1), for frequencies excited via hammer impact, which gives us more confidence to use a 1-D wave propagation model.

Conclusion

A newly developed NDE methodology, EDAR, is introduced in this work. EDAR is based on obtaining the phase difference of responses at two different locations on a pile in the frequency domain as a function of a newly defined quantity called the 'effective wavenumber'. The effective wavenumber is a function of the dispersion relation of the model chosen to represent the physical system and the type of impact. The theory behind EDAR is based on longitudinal and flexural waves. We conducted experimental validation and found the pile length estimates to be consistently within a 5 percent error margin. EDAR methodology is based on the underlying physics of wave propagation and thus improves reliability for the results obtained. EDAR is currently being evaluated in the field, following its success in laboratory test conditions. Although we have demonstrated EDAR's effectiveness in estimating the length of a pile, the method should be extensible to other scenarios where the length of a member, e.g., an electricity pole, is to be determined. Future work is aimed at improving the estimates at higher frequencies and potential improvements using sophisticated guided wave models. The piles used in this study, despite being full scale, were relatively short in length compared to typical piles in the field. Also, the soil conditions for the tests were relatively loose, which could potentially have had a minimal effect on the EDAR estimations. Even though the methodology has been experimentally demonstrated to work for CFST piles, it should be applicable to other types of pile foundations as well. Such extension is left for future investigations.

Appendix C: EDAR Improvements for field Conditions

This appendix represents a publication resulting from the research[36].

Introduction

Missing records of bridges has been a longstanding systemic problem in the USA. Engineers have relied on several nondestructive evaluation techniques to obtain the crucial length information about bridge pile foundations, especially when they are classified as scour critical. According to National bridge inventory [37], there are still about 28,000 highway bridges with unknown foundations in 2016 that could be susceptible to scour. Several other bridges over land are also expected to have unknown foundation and missing or incomplete records[38]. Thus, there is a need for an effective nondestructive methodology to estimate the length of pile foundations.

Several pile-length estimation methods have been developed over the years which can be broadly classified into borehole-based methods and surface-based methods (see e.g., [39], [7]). Borehole-based methods include parallel seismic, cross-hole sonic, borehole radar, induction-field and borehole magnetic tests. Although these methods provide reliable results for most foundation types, they are often expensive and time-consuming due to the need for a to drill a borehole near the foundation. In contrast, surface-based methods rely on generating waves through an impact and recording the response at specific sensor locations. Testing is easier, but these methods do not provide the same level of reliability as borehole methods. Surface-based methods for length estimation purposes mainly include sonic echo, impulse response, ultraseismic and bending wave techniques. This paper discusses a newly developed methodology that utilizes multiple types of waves generated through a hammer impact.

One of the most widely used method for length estimation is the sonic echo or pulse echo method, which involves impacting the top of the pile leading to generation of longitudinal waves. This method has been standardized by ASTM (D5882-16) and several researchers have used this methodology in a variety of situations over the years (e.g. [17], [20], [23]). These waves are non-dispersive in nature, i.e. all the frequencies travel at the same velocity. Thus, there is minimal distortion of the initial waveform in the time domain and peak picking can help determine the time of travel and thus the distance of wave propagation. This has been very successful for newly constructed bridges both for length estimation and integrity evaluations but has limitations for existing bridges due to reduced access to the top of the pile. Researchers have tried various methods to induce longitudinal waves without access to the top, but the recorded waveforms tend to be complicated to be able to process. Existing piles have much easier access to the sides of the piles and producing a lateral impact leading to flexural or bending waves is easier from testing perspective. Using lateral excitations for pile length estimation appears to be introduced by Holt and Douglas [24]. Unlike longitudinal waves, flexural waves are dispersive in nature and thus distort as they propagate making any time domain processing of the signals complicated. In order to analyze these complicated signals, the short kernel method was introduced in [24]. This method attempts to extract the peaks through convolution of the signal with a chosen kernel at specific frequency. The choice of kernel frequency and subsequent peak picking is still complicated even for experienced users leading to large errors [27]. Other methods based on signal processing

techniques have also been investigated (e.g. [28], [29]). Major drawback of these methods is that they are purely signal processing based methods and do not explicitly incorporate the underlying physics that causes wave distortion.

A new methodology called Effective Dispersion Analysis of Reflection (EDAR) was introduced recently by the authors [5]. EDAR is based on carefully examining the phase difference between the responses at two locations due to an impact applied to the side of the pile. Specifically, EDAR examines oscillations in EDAR plot, which is the plot of the phase difference plotted as a function of a so-called the effective wavenumber, which is defined based on the physical dispersion of the wave. Given this general definition of effective wavenumber, EDAR can be easily applied to both longitudinal and flexural waves. EDAR methodology was tested in the laboratory resulting in length estimates with less than 5% error. In contrast, preliminary application of EDAR in the field resulted in significant underestimation of the pile depth. A closer look at the physics of waves indicate that there is a significant effect of the compacted soil found in the field, necessitating a revision of the original EDAR methodology. Specifically, through careful analysis, it is shown that the radiation damping into the soil causes differential attenuation of longitudinal and transverse waves. This paper is focused on a detailed discussion of this phenomenon, and a resulting modification to EDAR methodology that results in accurate estimation of embedded pile depths in field settings.

The outline of the paper is as follows. Section 2 contains a brief introduction to the original EDAR methodology and a summary of laboratory validation. Incorrect length estimates obtained from direct application of EDAR to field data are presented Section 3. Section 4 contains the reasons for discrepancies in the initial length estimates, while Section 5 contains the modified EDAR methodology for compacted soils. The paper is concluded with field validation in Section 6, followed by closing remarks in Section 7.

EDAR Preliminaries

Traditionally, surface-based techniques have relied on generating a wave through a hammer strike at various locations on the exposed parts of the pile. The two main types of waves that are generated are the longitudinal and flexural/transverse waves. Depending on the type of hammer impact and the sensor orientation various waves can be recorded (Figure 1). Measuring axial accelerations for a top impact produces clear signals that can be processed by picking peaks in the time-domain, from the initial and reflected wave arrivals. This is a consequence of the nondispersive nature of the longitudinal waves, i.e. the wave does not get distorted as it travels. In contrast, lateral impact produces flexural waves that are dispersive and get distorted as they travel along the pile making any time domain interpretation of the results very complicated (there are no longer clear peaks associated with reflections, since the energy at different frequencies get reflected at different times). To analyze such dispersive reflections, the authors have recently developed Effective Dispersion Analysis of Reflections (EDAR), which can analyze both longitudinal and flexural waves with equal ease to obtain length information.

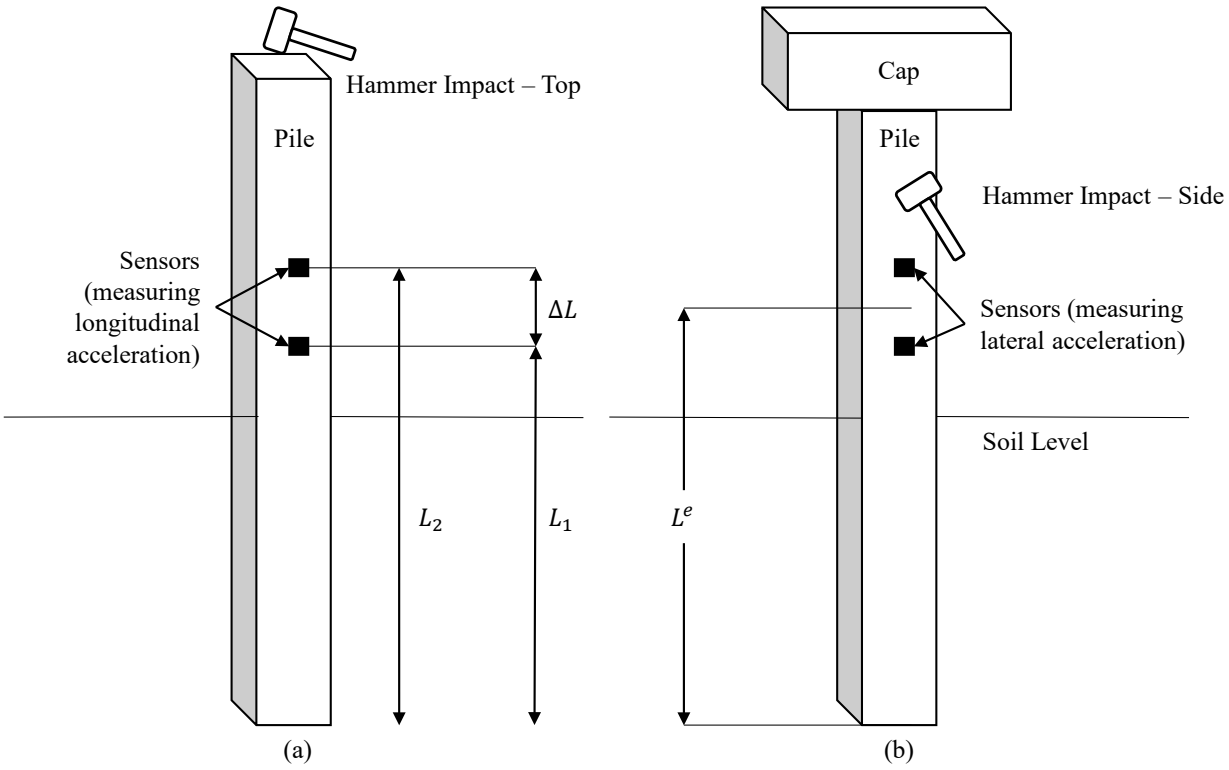

Figure 41*:* Pile setup (a) Top impact (b) Side impact

Theory

EDAR requires two sensors along the length of the exposed region of the pile. Depending on the impact scenario either lateral or longitudinal accelerations are measured. The impact should be above the top sensor and could be in either longitudinal or lateral direction. The phase difference (P_d) is given by,

$$P_d = \text{Imag}\left(\log\left(u_2(\omega)\right) - \log\left(u_1(\omega)\right)\right), \tag{27}$$

where u_1 and u_2 are the frequency-domain representation of responses (accelerations, velocities or displacements) at the two sensor locations. *We introduce the concept of effective wavenumber, which is essentially a scaled wavenumber and is based on the dispersion relation of the propagating waves*. For longitudinal waves, the wavenumber (k) and frequency(ω) have a linear relationship with the bar wave velocity (C_b) as the proportionality constant:

$$k = \frac{\omega}{c_b}. \tag{28}$$

The bar wave velocity (C_b) is defined as

$$C_b = \sqrt{\frac{E}{\rho}}, \tag{29}$$

where, E is the Young's modulus and ρ is the density.

Correspondingly, effective wavenumber is defined as,

$$k_e = \omega, \tag{30}$$

which is proportional to the wavenumber. We emphasize that this is not a real wavenumber, but rather a scaled wavenumber (it does not even have the same dimension of the wavenumber). This specific definition facilitates the estimation of the pile length without the need for the material properties of the pile, as explained below.

The general form of wave propagating in a bar is given by,

$$u(x) = Ae^{ikx} + Be^{-ikx}. \tag{31}$$

Using the Equations (1) and (5), the phase difference can be derived as [5] ,

$$P_d = k\underbrace{(L_2 - L_1)}_{=\Delta L} + \tan^{-1}\left(\frac{A\sin(2kL_1)}{B + A\cos(2kL_1)}\right) - \tan^{-1}\left(\frac{A\sin(2kL_2)}{B + A\cos(2kL_2)}\right). \tag{32}$$

P_d is oscillatory in nature with two periodicities, defined as cycles and wiggles. The first term is the theoretical wavenumber scaled by the distance between the sensors (ΔL) which along with phase wrapping leads to cycle period as shown in Figure 2. The second and third term are responsible for the smaller oscillations called wiggles observed in Figure 2. The trigonometric functions have periods π/L_1 and π/L_2 which can be approximated to π/L^e , where L^e is the distance from midpoint of the sensors to the tip of the pile. To graphically illustrate the concept, wave propagation is simulated in a semi-infinite bar with L_1=3m, L_2=3.5m, c=1m/s. The bar extends towards $-\infty$ with an impedance boundary at the other end with a reflection coefficient of 0.5. The resulting EDAR plot is shown in Figure 2.

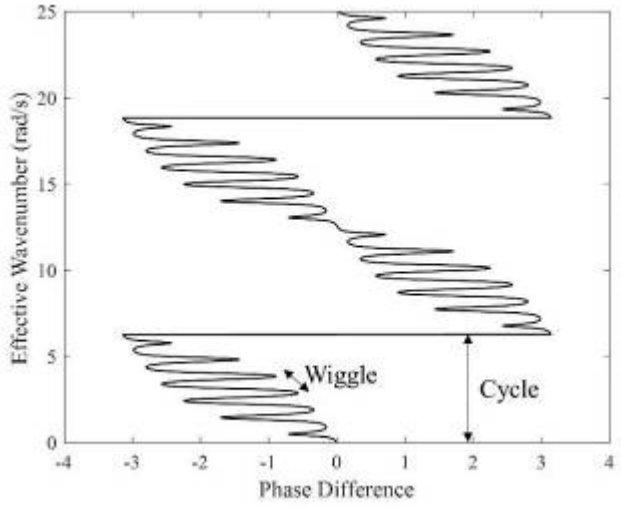

Figure 42: EDAR plots for Semi-Infinite bar with characteristic cycle and wiggle periods

The cycle and wiggle periods shown in Figure 2 are given respectively by

$$K_I^{bar} = \frac{\pi c_b}{\Delta L} \ , \tag{33}$$

$$K_R^{bar} = \frac{\pi c_b}{L^e} \ . \tag{34}$$

Subscript I is used for cycle period and R for the wiggle as they respectively represent the initial arrival and subsequent reflections. The ratio of the cycle and wiggle periods is

$$\frac{K_I^{bar}}{K_R^{bar}} = \frac{L^e}{\Delta L} . \tag{35}$$

Once the cycle and wiggle periods are obtained from the EDAR plot, the only unknown in equation (9) is L^e and can be calculated which is an estimate of the pile length. This is very similar to travel-time approaches where the velocity of wave propagation is calculated based on travel time between sensors and pile length calculated from the travel time of the reflected wave. In addition to providing an easier and alternate analysis methodology for processing non-dispersive waves, the key advantage of EDAR is that it can be extended to dispersive waves in a beam, where the travel time approach fails due to significant distortion in the waves. Similar to the bar, the dispersion relation of a Bernoulli-Euler (BE) beam is given by

$$k = \sqrt{\frac{\omega}{c_b r}} \tag{36}$$

where $r = \sqrt{I/A}$ is the radius of gyration. The phase velocity is frequency-dependent, resulting in wave dispersion, i.e. distortion of the waveform as it propagates through the

length of the beam. We correspondingly define the effective wavenumber as the quantity proportional to the wavenumber but independent of the material and section properties:

$$k_e^{BE} = \sqrt{\omega}\,, \tag{37}$$

The above definition of the effective wavenumber makes the relationship between phase difference and effective wavenumber linear and all the results described earlier for the bar can be applied to the BE beam. The length estimate of the pile can derived based on Equation (9) adapted to Bernoulli-Euler beam:

$$L^e = \frac{K_I^{BE}\Delta L}{K_R^{BE}}\ . \tag{38}$$

More sophisticated models can be used in place of B-E beam theory to more accurately represent the waves propagating in the piles. For example, theoretical wavenumber obtained from Timoshenko beam theory can be used as effective wavenumber to obtain the EDAR plot leading to an improved length estimate. The key in selecting the appropriate definition for effective wavenumber lies in carefully examining the type of waves and the range of frequencies in which the cycle and wiggle periods occur. If the propagating waves are predominantly longitudinal in nature, simple bar model can be used. If the waves are predominantly transverse in nature and the wavelengths are significantly larger than the cross-sectional dimensions, use of BE beam theory can be justified (since the slenderness ratio would be large). For shorter wavelengths, Timoshenko beam theory or even more sophisticated guided wave modelling, would lead to more accurate length estimates.

Laboratory testing

Two sensors are required for EDAR methodology but to build redundancy a four-channel USB-based data acquisition (DAQ) system and four accelerometers (PCB352C33) were chosen. Thus, a single impact produces six different EDAR plots from six sensor-pair combinations. The accelerometers were aligned such that they measure the lateral acceleration. Large sledge hammer (PCB 086D50) with hard and soft tips and a small sledge hammer (0.45 Kg) with hard, medium hard, medium and tough tips were used to impact the piles in between the cap and top sensor. The results for the hard tip of the large (LH) and small sledge hammers (SH) are presented here.

The tested piles are concrete filled steel tubes (CFST). Total length of the pile was 6.33 m with 4.22 m embedment. The concrete diameter was 0.292 m with a steel thickness of 0.00635 m. Four sensors, numbered one to four from top to bottom, were used with spacing of 0.2, 0.16, and 0.25 m. The distance from the midpoint of the sensors to the bottom of the cap is 1.1 m. Further details of the laboratory test can be found in references [5] and [30]. Typical EDAR plots for two pairs of sensors are shown in Figure 3. The data shown in the time domain on the left Figure 3 (a) and (b) do not immediately provide much information (owing to wave dispersion it is not clear which peaks corresponding to the initial and reflected wave arrivals). On the other hand, the EDAR plots shown in Figure 3 (c) on the

right clearly show cycles and wiggles, which is used to estimate the embedded depth, as described below.

The periodicities explained earlier can be clearly seen in the EDAR plots for which the effective wavenumber was obtained using equation (11). The data were analyzed using Timoshenko beam theory. The dispersion relation for Timoshenko beam with Young's modulus E, density ρ, shear modulus G, area A, moment of inertia I, and Timoshenko shear coefficient κ, is given by:

$$\frac{EI}{\rho A}k^4 - \left(\frac{I}{A} + \frac{EI}{GA\kappa}\right)\omega^2 k^2 - \omega^2 + \frac{\rho I}{GA\kappa}\omega^4 = 0\,. \tag{39}$$

The shear coefficient κ for a rectangular section can be obtained using [40],

$$\kappa = \frac{10(1+\nu)}{12+11\nu}\,. \tag{40}$$

It is important to note that all the required material properties are readily available in the controlled laboratory setting. The cycle period was obtained from EDAR plot using top and bottom sensors. Multiple wiggles are often observed, and only clear wiggles are used and are plotted as function of frequency in Figure 4. A slight trend can be observed as a function of frequency which is also evident from the length estimates obtained from different frequency ranges as shown in Figure 4.

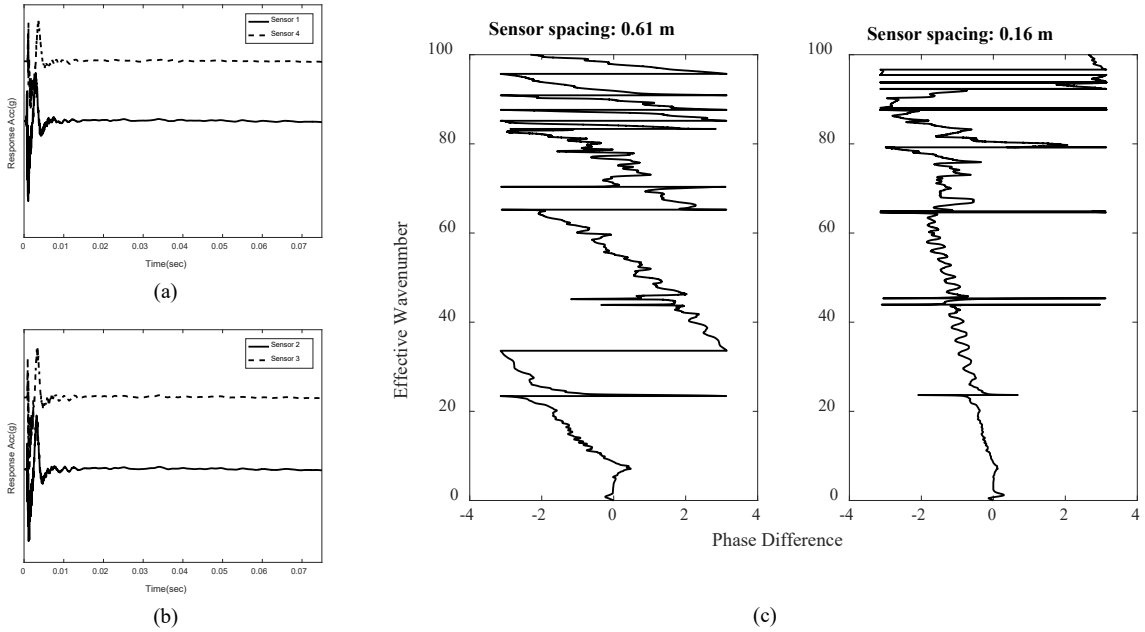

Figure 43: Laboratory pile (a) Time history at accelerometers 1 and 4 (b) Time history at accelerometers 2 and 3 (c) Representative EDAR plots

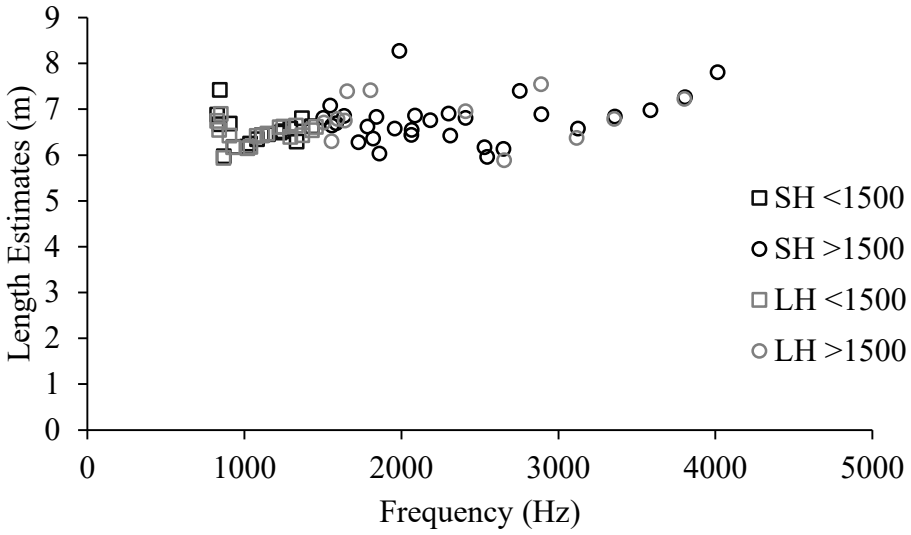

Figure 44: Wiggle period as a function of frequency for large hard tip (LH) and small hard tip (SH) sledge hammers

Estimates at lower frequencies have less error and there is increased scatter at higher frequencies. Nevertheless, the overall trend of the estimates is fairly flat giving us a good average length estimate as shown in Table 1.

Table 14*:* Length Estimates for Laboratory Pile

Actual Length	Frequency Range	Small hammer hard tip		Large hammer hard tip	
		Average Estimate (m)	Error	Average Estimate (m)	Error
6.33	<1500 Hz	6.52	3.0 %	6.46	2.1 %
	>1500 Hz	6.75	6.6 %	6.85	8.2 %
	All	6.67	5.4 %	6.61	4.4 %

Observations from Field Testing

Newly driven solid concrete pile with 16” side and known length in Rodanthe, Outer Banks NC, was used for preliminary field validation of the EDAR methodology. A particular bent with good access to the piles was selected. The piles had their length marked on them, which are used to obtain the length of the exposed and embedded parts of the pile (shown in Table 2). The pile cap was not yet constructed giving us complete access to the entire length of the exposed part of the pile. The site and the pile are shown in Figure 5 (a). A close up of the pile along with the sensor locations and test equipment is shown in Figure 5 (b). Similar to the laboratory testing, four sensors were used to measure the response of the pile to the hammer impact. Cyanoacrylate based super glue is used to mount the studs on which the sensors are attached. This is the glue recommended by the sensor manufacturer to ensure sufficient bonding of the sensors to the pile. Additionally, the studs supplied are grooved at the bottom

for the glue to spread sufficiently and have enough surface area for a good bond. Similar to the laboratory tests, multiple hammers with interchangeable tips (Figure 5 (b)) were used to impact the pile. Not all the hammer tips produced good data with observable wiggles. While multiple hammer tips produced usable data, small hammer with a tough tip was found to be most consistent and results from this hammer tests are presented (effect of hammer type of EDAR is currently under investigation and will be reported in the future).

Table 15: Field Pile Properties

Property	**Value**
Design concrete compressive strength (Fc')	68.9 MPa
Estimated modulus (using AASHTO 5.4.2.4-3)	41.8 GPa
Side of square cross section	0.4064 m
Total length	17.07 m
Top of pile to bottom-most sensor (pile 1)	1.74 m
Top of pile to bottom-most sensor (pile 2)	2.4 m

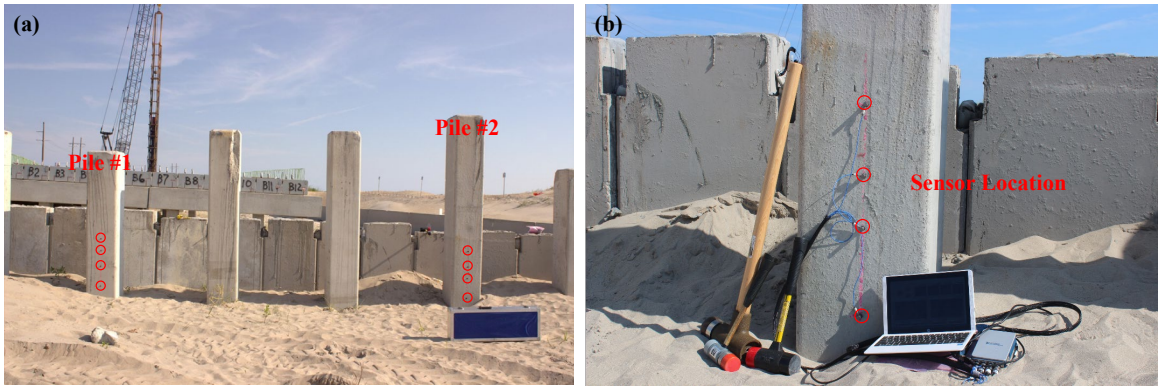

Figure 45: (a) Field piles (b) Equipment and sensor location

Material properties to calculate the Timoshenko wavenumber are in general not readily available in case of unknown foundations. However, in this particular case, the design strength is available from design drawing, which is used to obtain the initial estimates of material properties (a more robust procedure to obtain the material properties is outlined in Section 6.1). The density of concrete was assumed to be 2,400 Kg/m^3 and Young's modulus value was calculated as 41.8 GPa from the 28-day design compressive strength using AASHTO LRFD equation 5.4.2.4-3. Poisson's ratio of concrete is typically between 0.1 to 0.2 and is assumed to be 0.15 for this part of the analysis. Length estimates are obtained by analyzing the data obtained in the field using the same procedure described for the laboratory data. Typical EDAR plot from the field is shown in Figure 6.

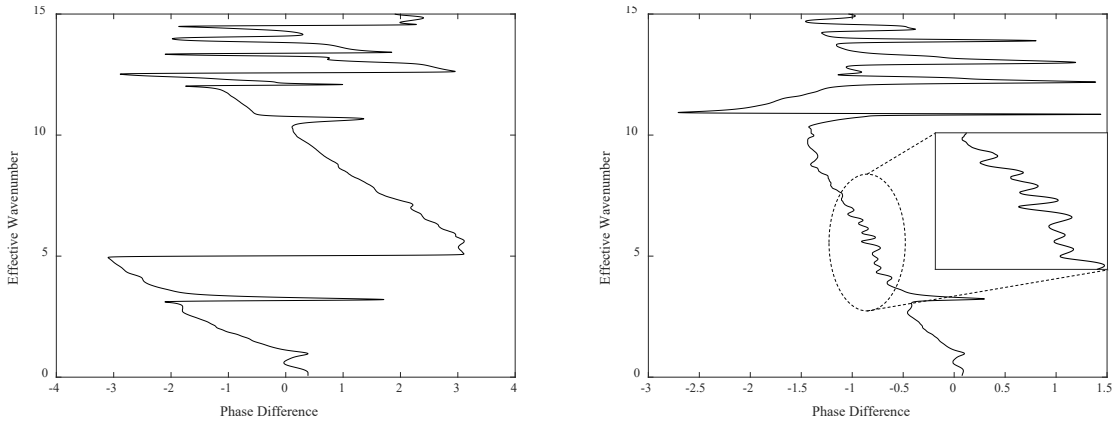

Figure 46: Representative EDAR plots from Pile 2 for (a) Sensor spacing of 0.62 m (b) Sensor spacing of 0.15 m

The cycle period was calculated from the sensor pair with farthest spacing (0.61 m for pile 1 and 0.62 m for pile 2) and wiggles are utilized from the data from all the sensor combinations. Scatter plot of the length estimates is shown in Figure 7. The mean length estimate for pile 1 was 11.2 m which was 34.4% less than the measured length. The mean length estimate for pile 2 was 11.5 m which was 32.6% less than the measured length. Clearly, the length was significantly underestimated in both cases. This led to the further exploration on the effect of consolidated soil, which appears to be the main difference between laboratory and field conditions. This is discussed in the remainder of the paper.

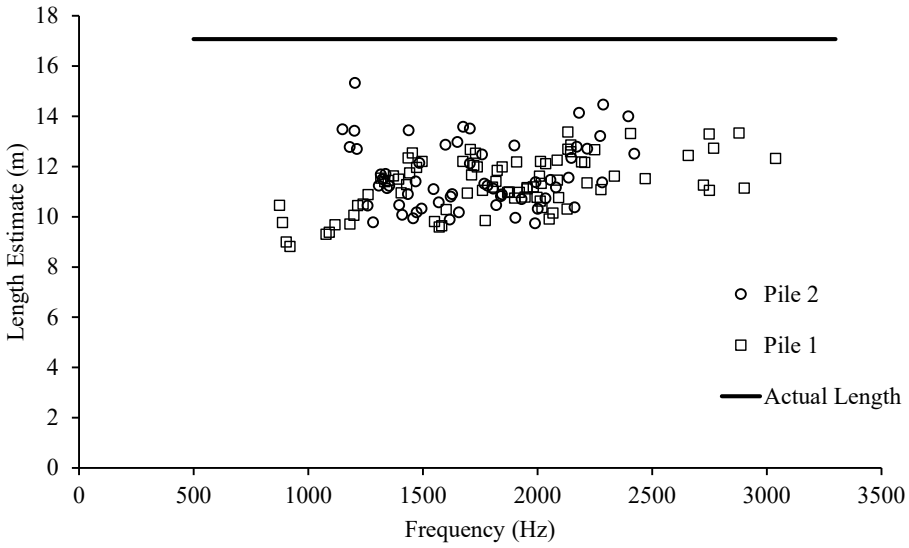

Figure 47: Initial field length estimates (significant underestimation)

Soil boring data and Standard penetration tests conducted near the location of the pile revealed a fairly uniform loose fine sand until a depth of 14.63 m followed by medium to

very dense silty sand up to a depth of 19.2 m. Pile 1 and 2 were embedded to a depth of 15.2 m and 14.5 m respectively and thus the pile tip is expected to have just breached the boundary between the loose and dense sand layers. This eliminates the possibility of any reflections due to embedment into stiff soil layers at the pile depths estimated from EDAR procedure. The other effect is the attenuation of waves due to radiation damping coming from the soil (radiation of energy into unbounded soil). Careful investigation as detailed below in section 4 found that the transverse waves that were the focus of EDAR thus far, get attenuated by the soil. Instead, EDAR appears to capture the effect of reflected longitudinal waves, which are generated due to secondary Poisson's effect from lateral impact. The following sections contain a discussion of the effect of these longitudinal waves on EDAR as well as a modification of EDAR methodology that results in accurate estimates of embedded depths.

The role of longitudinal waves

Even though the pile is impacted laterally, several modes of vibration can be generated based on the frequencies that are excited. In general, the pile acts as a waveguide propagating the waves generated from the hammer impact. To illustrate, example dispersion curves are shown in Figure 8, obtained using guided wave theory [41]. The first three flexural modes (F(1,1), F(1,2) and F(1,3)) and the fundamental longitudinal mode are shown in the figure. The higher modes (F(1,2) and F(1,3) need not be considered as they as they are propagative only at frequencies higher than those exited by hammer impacts. While it is counterintuitive to expect that significant transverse accelerations from longitudinal waves generated from lateral impact, it turns out that these accelerations are not insignificant. This is explained in the following section.

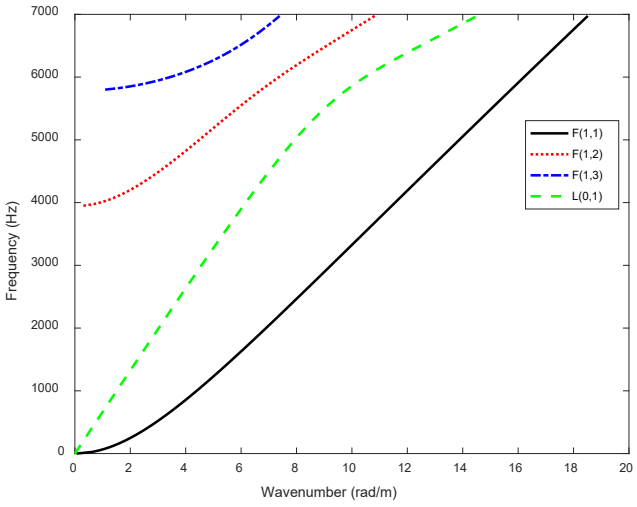

Figure 48: Dispersion curves for cylindrical pile as a waveguide

Existence of secondary longitudinal modes

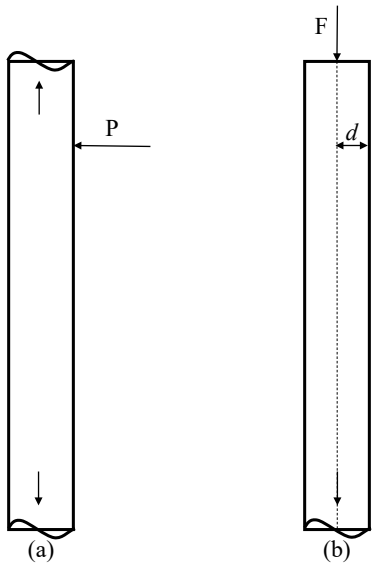

Figure 49: (a) Side impact (b) Top impact on pile

The actual test resembles Figure 9 (a) but as an intermediate step of analysis, an impact at the top center producing symmetric waves in the pile (Figure 9 (b)) is considered. This produces longitudinal waves of the general form

$$u_L = Ae^{ikz-i\omega t} \ . \tag{41}$$

The ratio of longitudinal (ε_L) and transverse (ε_T) strain is given by the Poisson's ratio (υ) and thus

$$\varepsilon_T = \upsilon \varepsilon_L \ . \tag{42}$$

Longitudinal strain can be obtained by taking the spatial derivative of Equation (15),

$$\varepsilon_L = iku_L \, . \tag{43}$$

Due to symmetric displacement field, the transverse displacement (u_L) on the surface of the pile can be obtained as,

$$u_T = d\varepsilon_T \ , \tag{44}$$

where d is half the width of the pile. Thus, the ratio of transverse and longitudinal displacements is be given by

$$\alpha = \left| \frac{u_T}{u_L} \right| = k\upsilon d = \frac{\omega \upsilon d}{c_L} \ , \tag{45}$$

where ω is the frequency and c_L is the longitudinal wave velocity.

For a concrete pile with *d=0.2 m*, $\upsilon = 0.15$, $c_L = 4,200 m/s$ and ω ranging from 1,000 Hz to 2,000 Hz , where wiggles are often observed, α is between 0.05 and 0.09. This gives us the amplitude of lateral acceleration produced from a longitudinal impact.

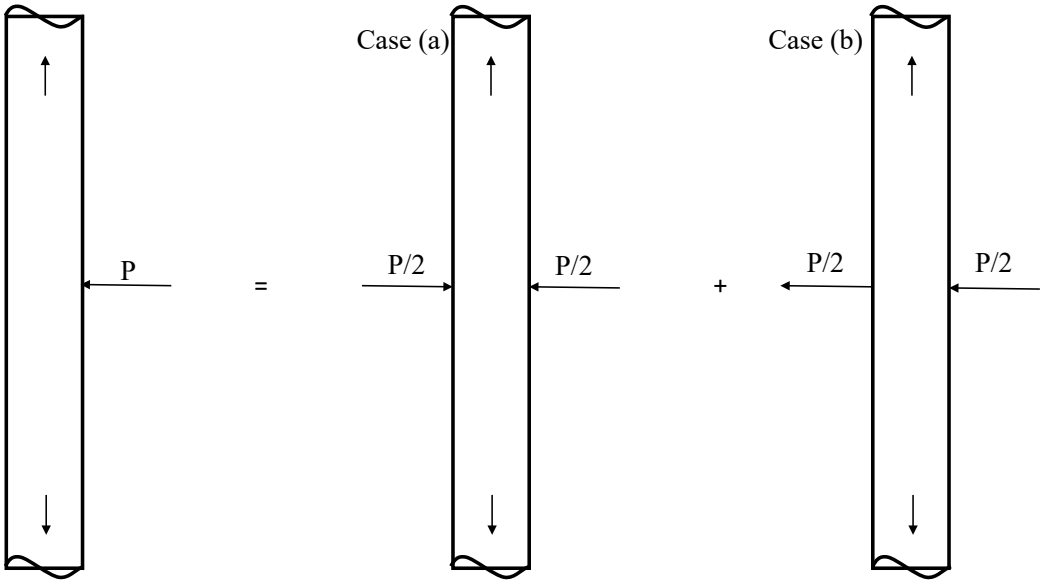

Figure 50: Lateral impact split into symmetric and antisymmetric loading

In reality, a lateral strike is imparted to the pile; to obtain the effect of the longitudinal wave generated from a lateral impact, we utilize the idea of reciprocity. Lateral impact on a pile shown in Figure 9 (a) can be split into the sum of symmetric loading leading to symmetric longitudinal waves and anti-symmetric loading leading to transverse waves as shown in Figure 10. Transverse displacement due to the anti-symmetric loading (case (b)) can be obtained using the corresponding transverse impedance (Z_T) of the beam (Since impedance relates the force and velocity, to obtain displacements velocity is divided by $i\omega$):

$$u_T^b = \frac{P}{2i\omega Z_T} \ . \tag{46}$$

Thus, the load P is given by,

$$P = 2i\omega Z_T u_T^b \ . \tag{47}$$

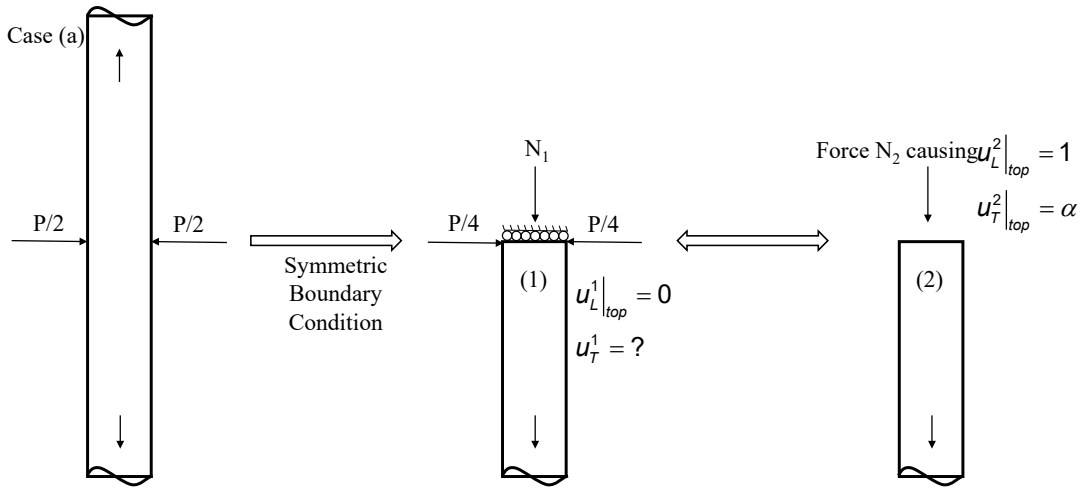

Figure 51: (a) Symmetric loading (b)System 1 by applying symmetric boundary conditions (c) System 2 for application of reciprocity

To obtain the transverse displacement from the symmetric part of loading, the infinite beam is first split into half by horizontal axis of symmetry as shown in Figure 11 (b), with unknown reaction N_1, which can be solved with the help of Maxwell-Betti's reciprocity theorem. Consider two systems, system 1 in Figure 11 (b), and system 2 as shown in Figure 11 (c), which is same as the top impact case considered earlier in Figure 9 (b). According to the reciprocity theorem, work done by forces in system 1 on displacements in system 2 is the same as the work done by forces in system 2 on displacements in system 1. Specifically, work done by forces in system 1 on displacements in system 2 are given by:

$$N_1 \times 1 + 2 \times \frac{P}{4} \times (-\alpha) \tag{48}$$

Since there is no displacement in system 1 in the direction of the only force N_2 in system 2, the work done by forces in system 2 on displacements in system 1 is zero. Thus, equating expression (22) to zero, we get,

$$N_1 = \frac{P\alpha}{2} \tag{49}$$

Longitudinal displacement from the symmetric loading is obtained using the longitudinal impedance (Z_L) and is given by,

$$u_L^a = \frac{N_1}{i\omega Z_L} \ , \tag{50}$$

which can be further simplified using Equation (21) as

$$u_L^a = \frac{\alpha Z_T u_T^b}{Z_L} \ . \tag{51}$$

Combining the above equation with Equation (19) the ratio between the transverse displacements due longitudinal and transverse waves is given by,

$$\frac{u_T^a\big|_L}{u_T^b} = \frac{\alpha^2 Z_T}{Z_L} \ . \tag{52}$$

For purely longitudinal waves, the longitudinal impedance is

$$Z_L = A\sqrt{\rho E} \ , \tag{53}$$

where A is the cross sectional area, ρ is the density and E is the Young's modulus. Transverse impedance is more complicated and frequency dependent. Considering the frequency range of interest, this can be approximated by shear wave equation, but with the effective shear area from Timoshenko beam theory. Thus, the transverse impedance can be approximated as,

$$Z_T = A_S\sqrt{\rho G} \tag{54}$$

where G is the shear modulus and $A_s = \kappa A$ is the effective shear area. Substituting Equations (14), (27), (28) in (26), and noting that the acceleration ratio is the same as the displacement ratio, we obtain,

$$\frac{a_T^L}{a_T^T} = \alpha^2 \frac{10(1+\upsilon)}{(12+11\upsilon)\sqrt{2(1+\upsilon)}} \ , \tag{55}$$

where a_T^L and a_T^T are the transverse accelerations due to longitudinal and transverse waves respectively, and α is given by Equation (19). For a representative Poisson's ratio of 0.15, the acceleration ratio appears to be between 0.0001 and 0.001. On the outset this seems very small to have any noticeable effect on EDAR plot. However, soil plays a significant role in altering the relative content of longitudinal waves making their effect more significant as explained in the next subsection.

Differential attenuation of waves due to presence of soil

Soil surrounding the pile can play a significant role in attenuating the waves generated from the hammer impact. To better understand this phenomenon, a beam-on-elastic foundation model is utilized. Since the hammer impact produces low strain in the pile, effect of soil is included using (frequency-dependent) springs and dampers representing the soil resistance associated with its horizontal cross-section. Although this approach is approximate, it is valid for the frequency range of interest since the associated length scales are larger than the pile diameter. The soil is assumed to be layered and under either plane strain or anti-plane shear (depending on the direction of the waves). The corresponding stiffness for longitudinal and

transverse waves propagating in the pile are obtained separately as a function of the pile radius and soil properties. The pile is considered to be rigid compared to the soil, and always in contact with the soil. Thus, the effective dynamic stiffness from the soil can be obtained by solving the elastodynamic wave equation in soil for full space in 2D, assuming unit displacement boundary condition at the pile-soil boundary [42]. Using such an approach, the stiffness offered by soil for longitudinal waves propagating in the pile is given by

$$K_L = 2\pi G_s \frac{R\omega}{c_s} \frac{H_1^1\left(\frac{R\omega}{c_s}\right)}{H_0^1\left(\frac{R\omega}{c_s}\right)}, \tag{56}$$

where G_s is the shear modulus, R is the radius of the pile, c_s is the shear wave velocity given by $\sqrt{G_s/\rho_s}$, ω is the frequency, and $H_n^1(z)$ is n-th order Hankel function of first kind. It can be seen that the stiffness is complex-valued and frequency dependent. The real part of the stiffness acts like a spring and the imaginary part of the stiffness acts like a damper. Similar, albeit more complicated expression can be obtained for stiffness for transverse waves in the pile ([42], [43]). Figure 12 shows the stiffness variation for representative soft/loose soil and hard/dense soil. The properties of the soft and hard soil cases were adopted from [34] to represent a broad spectrum of soil cases and are shown in Table 3.

Table 16: Properties of soft and hard soil

Soil Type	Density (Kg/m^3)	Young's Modulus (MPa)	Poisson's Ratio	Pressure Wave Velocity (m/s)	Shear Wave Velocity (m/s)
Soft/loose Soil	1800	105	0.3	280	150
Hard/dense Soil	2000	755	0.3	710	380

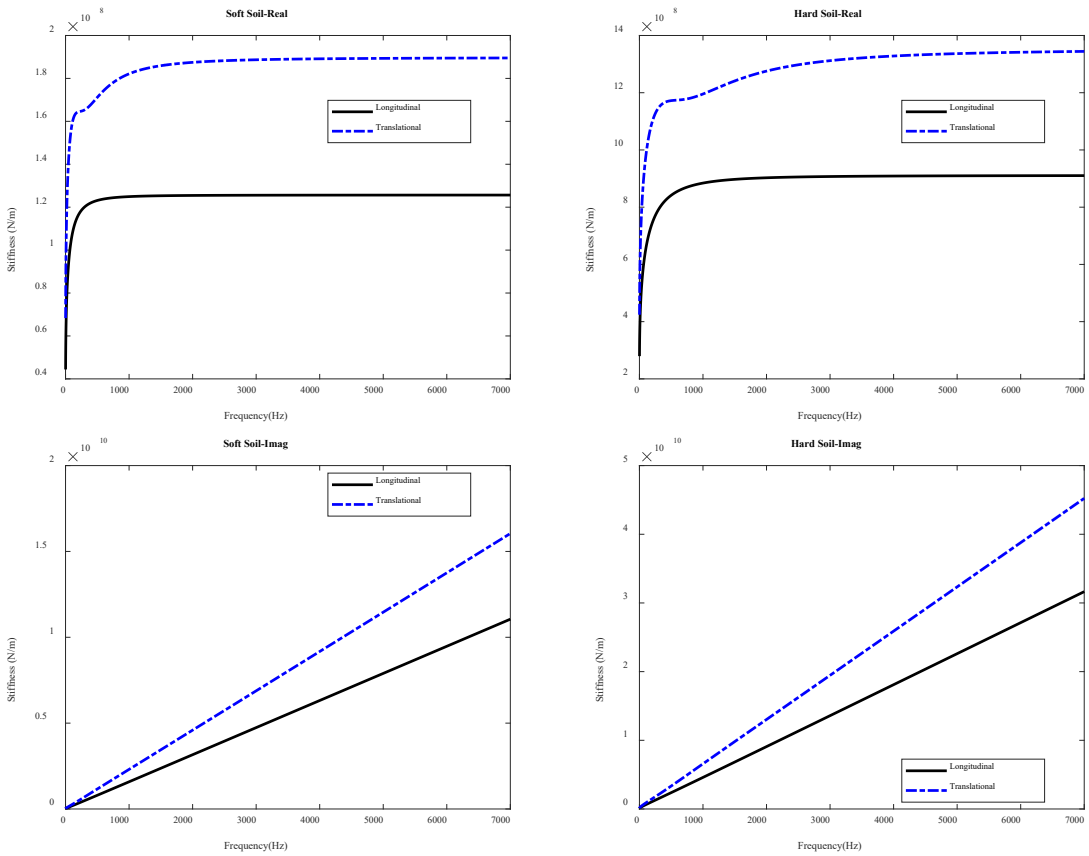

Figure 52: Soil stiffness (a) Soft soil (b) Hard soil

The dynamic soil stiffness values in Figure 12 are used to model the pile for simple 1D shear and longitundinal waves. The resulting wavenumbers are given by,

$$k_L = \sqrt{\frac{\rho_p A_p \omega^2 - K_L^{Soil}}{E_p A_p}}\ , \tag{57}$$

$$k_T = \sqrt{\frac{\rho_p A_p \kappa \omega^2 - K_T^{Soil}}{G_p A_p}}\ , \tag{58}$$

where ρ_p is the density of pile, E_p is the Young's modulus of pile, A_p is pile cross sectional area, K_L^{Soil} is the complex-valued longitudinal soil stiffness, G_p is the shear modulus of pile, K_T^{Soil} is the complex-valued transverse soil stiffness, κ is the Timoshenko shear coefficient and ω is the frequency. The corresponding attenuation coefficient associated with the bottom reflection $\left(e^{2L*imag(k_{L,T})}\right)$ for a fully embedded pile of length 15 m and radius 0.2 m is shown in Figure 13.

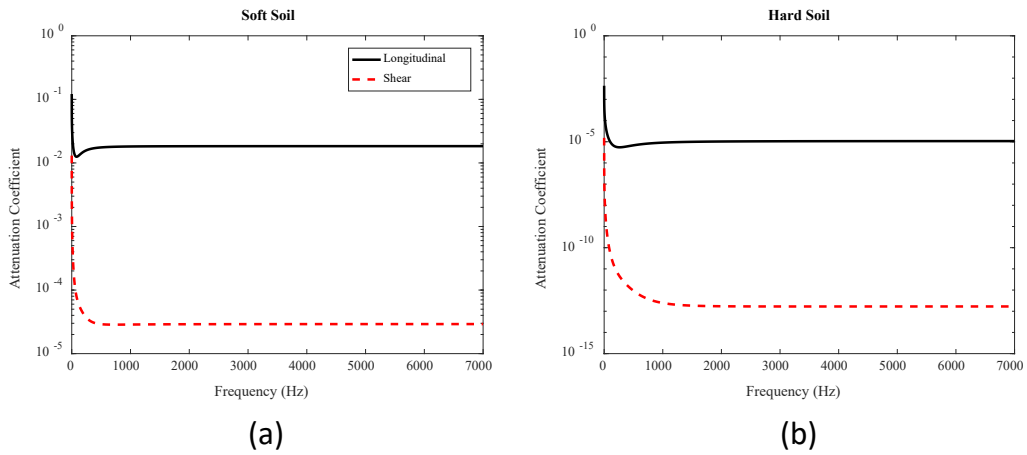

Figure 53: Attenuation coefficient (a) Soft Soil (b) Hard soil

A more detailed guided wave modeling of embedded cylindrical shafts by Wang [34] and Hanifah [32] showed similar results. It is observed that the real part of the complex wavenumber does not change in comparison to non-embedded pile, while there is significant effect of the soil stiffness on the imaginary part of wavenumber; it is higher for hard/dense soils leading to larger attenuation of the waves. This behavior is attributed to the impedance difference between pile and soil. The mismatch between longitudinal wave velocity in pile and shear wave velocity in soil is higher than that between shear/transvers waves in the pile and longitudinal waves in the soil. Due to the smaller impedance contrast, transverse waves in the pile encounter more radiation damping and attenuate much faster than longitudinal waves, as seen in Figure 13. Since the piles were close to the coast, the soil conditions were saturated for a majority of the embedment. Saturation of soil can have a significant effect on the pressure wave velocity and minimal effect on shear wave velocity (since the bulk modulus increases significantly due to saturation, while shear modulus does not). This would only make the attenuation of the transverse waves even more pronounced furthering the dominance by longitudinal waves in the recorded reflections.

In Equation (19), it was established that the ratio of amplitude of longitudinal wave to transverse waves generated from a lateral impact is small. However, as discussed in the previous paragraphs, the transverse waves decay significantly, three to eight orders of magnitude more than longitudinal waves (even for soft soil types without saturation). Thus, the reflections from longitudinal waves dominate the measurements in the field settings, and EDAR analysis should accordingly be modified, as discussed in the next section.

Improved length estimation

EDAR methodology relies on estimating the cycle and wiggle periods from the phase and in doing so already separates the waves into initial arrival and reflections. Based on the analysis in the previous two sections, transverse waves dominate the initial arrival to the sensors, but longitudinal waves dominate the reflections in the field settings. This effect is captured in the modified EDAR methodology that entails the following steps:

1. Obtain average cycle period from a series of impacts for different hammers and sensors combinations (more details can be found in Sections 3.3 and 4 of reference [5]).
2. An infinite Timoshenko beam is used to optimize for Young's modulus of the pile by matching the average cycle period. The cross-sectional area of the pile, distance between the sensors which are measured on site are utilized. The density of pile material and Poisson's ratio are assumed based on pile type.
3. Longitudinal wave velocity is calculated using the estimated Young's modulus and the other assumed material properties and using equation (3).
4. Following the procedure in reference [5], wiggles are identified in the data and corresponding average wiggle periods are calculated as a function of frequency. Wiggle period and longitudinal wave velocities are used along with equation (8) to obtain a length estimate.

Final Field Validation

The data from the tests shown in Section 3 were re-analyzed using the procedure described in Section 5. Detailed analysis of the data by separating the initial arrival (cycle period) and reflections (wiggle period) is presented in this section. Apart from the reflections coming from the pile tip, EDAR plot also contains effects from other reflections (eg. top reflections, as shown in Figure 14). This could affect the cycle and wiggle periods. In order to mitigate these effects, cycle and wiggle periods are obtained by averaging over several impacts and between different sensors combinations.

Material properties from cycle period

EDAR plot for a sensor spacing of 0.62 m for three different impacts are shown in Figure 14. Cycle period, which is primarily a consequence of the initial wave arrival at the two sensors, appears to have some variability. This is attributed to factors such as the reflection from the top, near field effects and wiggle interference at the location of cycle period. Nevertheless, the average cycle period, from different sensor combinations, is utilized to obtain the Young's modulus of the pile as described in the previous section. Cross-sectional properties are measured at the field and the exact distance between the sensors is known. The density of concrete is assumed to be the typical value of 2400 Kg/m^3, and the Poisson's ration is assumed to be three different values, 0.1, 0.15 and 0.2, representing the typical range of 0.1 to 0.2. Young's modulus is obtained by optimizing for the cycle period using an infinite Timoshenko beam with measured cross sections and distance between the sensors.

The cycle period for each sensor combination is averaged over a set of five different impacts. It can be observed from Figure 15 (a) and (b) that the cycle period can be estimated with minimal variation from different sensor combinations. The Young's modulus back-calculated from these average cycle periods is used along with the density to estimate the wave velocity using Equation (3) and is shown in Figure 15 (c) and (d), for an assumed Poisson's ratio of 0.15. The estimated Young's modulus from different sensors combinations was within 5% of the Young's modulus estimated from the design strength of concrete. The wave velocities obtained from different sensor combinations for the piles were within 3% variation between the extreme values. Additionally, it can be observed from Figure 15 (e) that the estimated

longitudinal wave velocity is not very sensitive to the value of the Poisson's ratio with less than 5% difference between the extreme values. This average velocity estimate is used along with the wiggle period obtained in the following section to calculate the length of the pile.

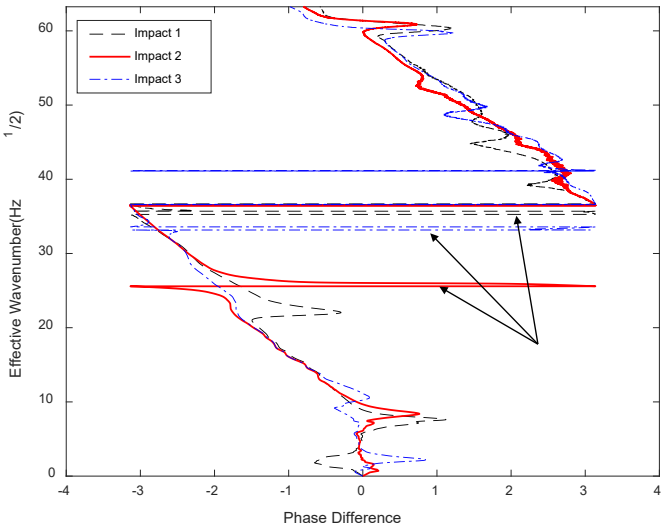

Figure 54: Top effect on EDAR plot and cycle period

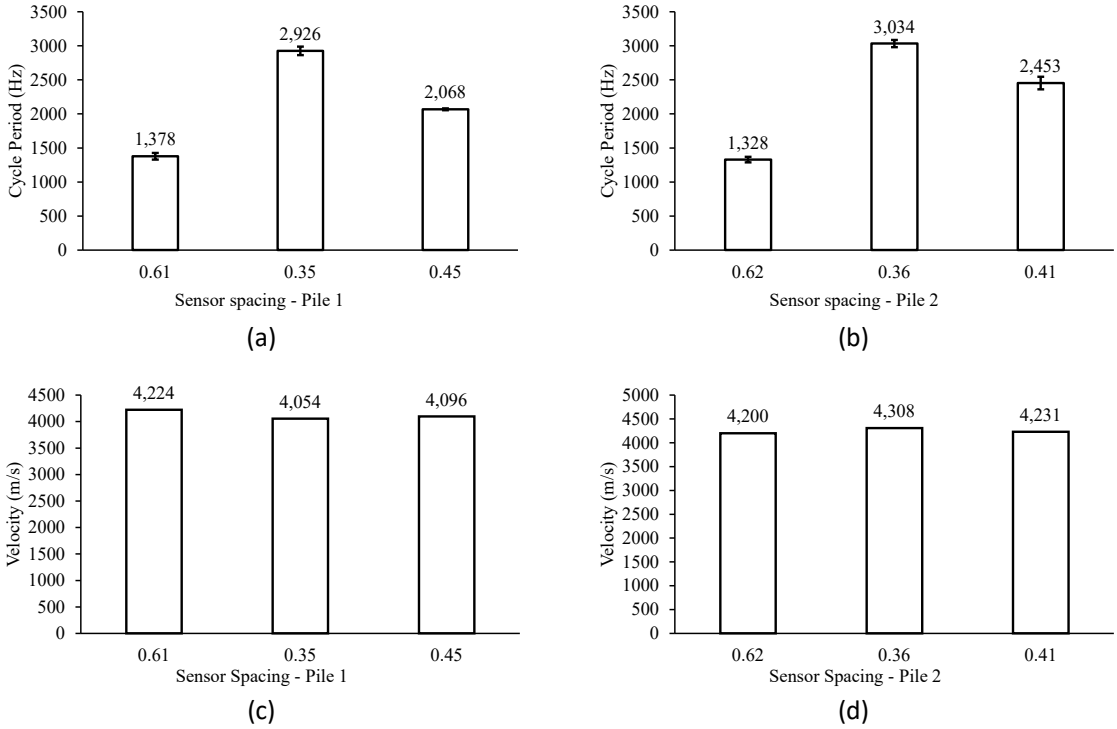

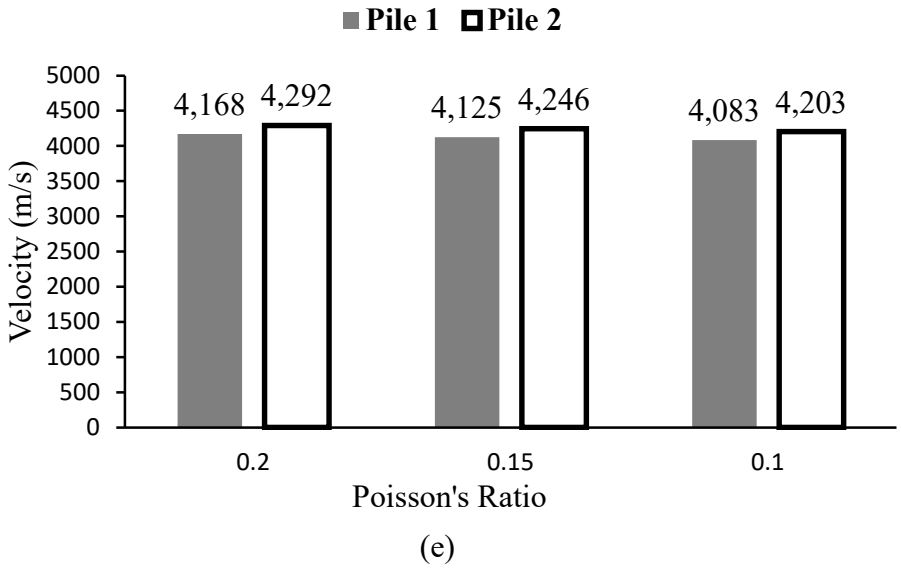

(e)

Figure 55: (a) Variation in cycle period for Pile 1 (b) Variation in cycle period for Pile 2 (c) Variation in velocity for Pile 1 as a function of sensor spacing for Poisson's ratio 0.15 (d) Variation in velocity for Pile 2 as a function of sensor spacing for Poisson's ratio 0.15 (e) Longitudinal wave velocity estimate from cycle period using Timoshenko beam model

Length estimate from wiggle period

The length estimates shown in Figure 16 were calculated from individual wiggles but often these wiggles appear in clusters and thus, instead of individual wiggles, averages were calculated. Doing this reduced the scatter seen in Figure 7, and the overall average of the wiggles is used to obtain the final length estimate. Length estimates obtained using equation (8) with longitudinal wave velocity corresponding to poisons ratio of 0.15, are presented in Table 4. The average length estimates are within 5% error margin and the overall average for both piles have less than 2% error.

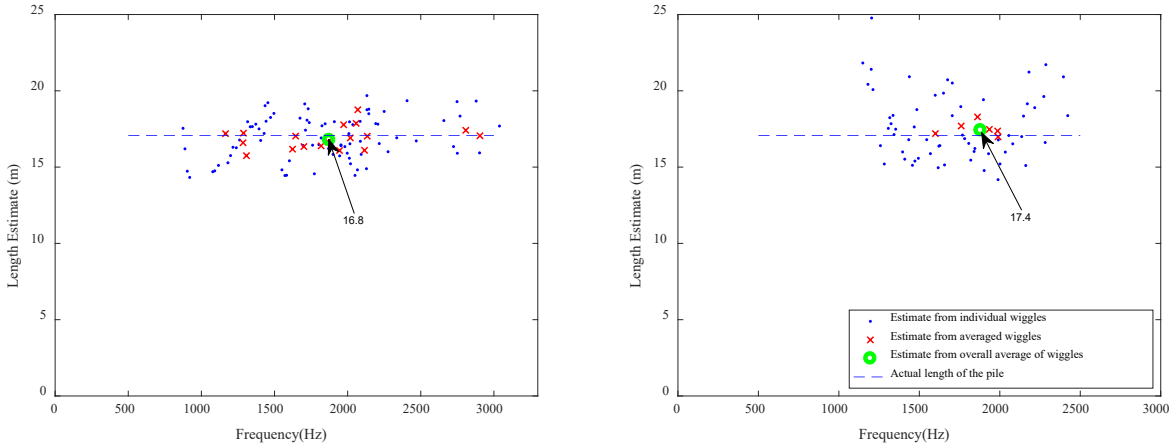

Figure 56: Average length estimate (a) Pile 1 (b) Pile 2

Table 17: Improved length estimates

		Average wiggle (linear frequency)	Length estimate (using wiggle period)	Total length (distance from sensor midpoint to top added)	Error
Overall average	Pile 1	138.5	15.4	16.8	-1.6 %
	Pile 2	135.1	15.3	17.4	2 %
Average (<1500 Hz)	Pile 1	135.2	15.3	16.7	-2.2 %
	Pile 2	133.9	15.7	17.8	4.3 %
Average (>1500 Hz)	Pile 1	140.3	15.4	16.8	-1.6 %
	Pile 2	134.2	15.1	17.2	0.8 %

Summary and Conclusions

EDAR, effective dispersion analysis of reflections, was recently developed to estimate the length of embedded depth of pile foundations. EDAR showed superior accuracy in laboratory settings, but direct application to field conditions resulted in significant errors. This paper presents a modification to EDAR methodology based on a rather counterintuitive observation that the reflected waves captured in field conditions are from longitudinal waves and not from transverse waves (even though the lateral hammer impact creates predominantly transverse waves). This is due to the differential attenuation caused by the radiation damping coming from compacted soil in field conditions. The modified EDAR methodology resulted

in significant improvement in estimated pile depths with errors less than 5%. Ongoing and future enhancements of EDAR include (a) extension to other pile types, e.g. concrete filled steel tubes and timber piles, (b) understanding the influence of hammer characteristics as a function of pile type to increase the likelihood of obtaining good EDAR plots, (c) understanding the effects of top reflections and near field effects to reduce the scatter in material property estimation and thus the estimated pile depth.

References

[1] K. McConnell and P. Varoto, *Vibration testing: theory and practice*. 1995.

[2] W. G. Halvorsen and D. L. Brown, "Impulse Technique for Structural Frequency Resposne Testing," *Sound Vib.*, vol. 11, no. 11, pp. 8–21, 1977.

[3] M. French, "What makes a Good Impact Function?," *Exp. Tech.*, vol. 23, no. 6, pp. 33–35, 1999.

[4] D. L. Brown, R. J. Allemang, and A. W. Phillips, "Forty Years of Use and Abuse of Impact Testing : A Practical Guide to Making Good FRF Measurements," *Exp. Tech. Rotating Mach. Acoust.*, vol. 8, pp. 221–241, 2015.

[5] V. Samu and M. Guddati, "Nondestructive Method for Length Estimation of Pile Foundations Through Effective Dispersion Analysis of Reflections," *J. Nondestruct. Eval.* , vol. 38, no. 45, 2019.

[6] L. D. Olson, F. Jalinoos, and M. F. Aouad, "Determination of Unknown Subsurface Bridge Foundations,(NCHRP 21-5 Interim Report Summary)," *Geotech. Eng. Noteb. Issuance GT-16. Fed. Highw. Adm. Washington, DC*, 1998.

[7] S. Mclemore *et al.*, "Unknown Foundation Bridges Pilot Study," *Fed. Highw. Adm. Florida Dep. Transp.*, 2010.

[8] J.-Y. Zhang, L.-Z. Chen, and J. Zhu, "Theoretical basis and numerical simulation of parallel seismic test for existing piles using flexural wave," 2016.

[9] J. T. Coe and B. Kermani, "Comparison of Borehole Ultrasound and borehole radar in evaluating the length of two unknown bridge foundations," *DFI J. - J. Deep Found. Inst.*, vol. 10, no. 1, pp. 8–24, Jan. 2016.

[10] E. Niederleithinger, "Improvement and extension of the parallel seismic method for foundation depth measurement," *Soils Found.*, vol. 52, pp. 1093–1101, 2013.

[11] K. F. Lo, S. H. Ni, Y. H. Huang, and X. M. Zhou, "Measurement of unknown bridge foundation depth by parallel seismic method," *Exp. Tech.*, vol. 33, no. 1, pp. 23–27, 2009.

[12] D. A. Sack, S. H. Slaughter, and L. D. Olson, "Combined Measurement of Unknown Foundation Depths and Soil Properties with Nondestructive Evaluation Methods," *Transp. Res. Rec. J. Transp. Res. Board*, no. 1868, pp. 76–80, 2004.

[13] M. S. Hossain, ; M S Khan, ; J Hossain, ; G Kibria, and T. Taufiq, "Evaluation of Unknown Foundation Depth Using Different NDT Methods," *J. Perform. Constr. Facil.*, vol. 27, no. 2, pp. 209–214, 2013.

[14] J. F. Levy, "Sonic pulse method of testing Cast-in-Situ concrete piles," *Gr. Eng.*, vol. 3, pp. 17-19., 1970.

[15] A. G. Davis, C. S. Dunn, and CEBTP., "From Theory to Field Experience with the Non-Destructive Vibration Testing of Piles.," *Proc. Inst. Civ. Eng.*, vol. 57, no. 4, pp. 571–593, 1974.

[16] F. Rausche, G. G. Goble, and G. E. Likins, "Dynamic Determination of Pile Capacity," *J. Geotech. Eng.*, vol. 111, no. 3, pp. 367–383, 1985.

[17] H. F. C. Chan, "Non-destructive testing of concrete piles using the sonic echo and transient shock methods," *Diss. Univ. Edinburgh*, 1987.

[18] Y. Lin, M. Sansalone, and N. J. Carino, "Impact-Echo Response of Concrete Shafts," *Geotech. Test. Journal, GTJODJ*, vol. 14, no. 2, pp. 121–137, 1991.

[19] M. Hussein, W. Wright, and B. Edge, "Low Strain Dynamic Testing of Wood Piles Supporting an Existing Pier," *Struct. Congr. XII*, pp. 940–945, 1994.

[20] A. G. Davis, “Nondestructive Evaluation of Existing Deep Foundations,” *J. Perform. Constr. Facil.*, vol. 9, no. 1, pp. 57–74, 1995.
[21] J.-L. Briaud, J.-L. Briaud, M. Ballouz, G. Nasr, and S. J. Buchanan, “Defect And Length Predictions By NDT Methods For Nine Bored Piles,” *Deep Found. 2002 An Int. Perspect. Theory, Des. Constr. Perform.*, pp. 173–192, 2002.
[22] B. Jozi, U. Dackermann, R. Braun, J. Li, and B. Samali, “Application and improvement of conventional stress-wave-based non-destructive testing methods for the condition assessment of in-service timber utility poles,” *Australas. Conf. Mech. Struct. Mater.*, pp. 9–12, 2014.
[23] S. Rashidyan, “Characterization of Unknown Bridge Foundations,” *Diss. Univ. New Mex.*, 2017.
[24] R. A. Douglas and J. D. Holt, “Determining length of installed timber pilings by dispersive wave propagation methods,” *Cent. Transp. Eng. Stud. Dept. Civ. Eng. North Carolina State Univ.*, 1994.
[25] A. Zad, “Determination of Embedded Length and General Condition of Utility Poles Using Non-Destructive Testing Methods,” *Diss. Univ. Technol. Sydney*, 2013.
[26] B. Jozi, “Condition Assessment of In-Service Timber Utility Poles Utilizing Advanced Digital Signal Processing and Multi-Sensors Array,” *Diss. Univ. Technol. Sydney*, no. February, 2015.
[27] M. Subhani, J. Li, B. Samali, and N. Yan, “Determination of the embedded lengths of electricity timber poles utilizing flexural wave generated from impacts,” *Aust. J. Struct. Eng.*, vol. 14, no. 1, pp. 85–96, 2013.
[28] A. T. M. Farid, “Prediction of unknown deep foundation lengths using the Hilbert Huang Transform (HHT),” *HBRC J.*, vol. 8, no. 2, pp. 123–131, 2012.
[29] S.-H. Ni, J.-L. Li, Y.-Z. Yang, and Z.-T. Yang, “An improved approach to evaluating pile length using complex continuous wavelet transform analysis,” *Insight - Non-Destructive Test. Cond. Monit.*, vol. 59, no. 6, pp. 318–324, 2017.
[30] D. A. Realpe, “Seismic Performance and Displacement Capacity of RCFST Drilled Shafts.,” *Diss. North Carolina State Univ.*, 2017.
[31] R. J. Finno, “1-D Wave Propagation Techniques in Foundation Engineering,” in *The Art of Foundation Engineering Practice Congress*, 2010, pp. 260–277.
[32] A. Hanifah, “A theoretical evaluation of guided waves in deep foundations.,” *Diss. Northwest. Univ.*, 2000.
[33] H. C. Chao, “An Experimental Model for Pile Integrity Evaluation using a Guided Wave Approach,” *Diss. Northwest. Univ.*, 2002.
[34] H. Wang, “Theoretical Evaluation of Embedded Plate-Like and Solid Cylindrical Concrete Structures with Guided Waves,” *Diss. Northwest. Univ.*, 2004.
[35] J. J. Lynch, “Experimental verification of flexural guided waves in concrete cylindrical piles,” *Diss. Northwest. Univ.*, 2007.
[36] V. Samu and M. Guddati, “Nondestructive length estimation of an embedded pile through combined analysis of transverse and longitudinal waves,” *NDT E Int.*, p. 102203, Nov. 2019.
[37] “2016 - Download NBI ASCII files - National Bridge Inventory - Bridge Inspection - Safety - Bridges & Structures - Federal Highway Administration.” [Online]. Available: https://www.fhwa.dot.gov/bridge/nbi/ascii2016.cfm.
[38] V. Schaefer R. and Jalinoos Frank, “Characterization of Bridge Foundations

Workshop Report No. FHWA-HRT-13-101," 2013.
[39] L. D. Olson, P. E. Marwan, and F. Aouad, "NCHRP 21-5 Research Results on Determination of Unknown Bridge Foundation Depths," *Int. Water Resour. Eng. Conf.*, 1998.
[40] G. R. Cowper, "The shear coefficient in Timoshenko's beam," *Trans. ASME J. Appl. Mech.*, vol. 33, no. 4, pp. 335–340, 1966.
[41] A. Vaziriastaneh, "On the Forward and Inverse Computational Wave Propagation Problems.," North Carolina State University, 2016.
[42] V. Samu, "Estimation of Embedded Length of Pile Foundation using Flexural Wave Model," 2014.
[43] M. Novak, T. Nogami, and F. Aboul-Ella, "Dynamic Soil Reactions for Plane Strain Case," *Jounal Eng. Mech. Div.* , pp. 953–959, 1978.